Universidade de Aveiro
2018

Departamento de Engenharia Mecânica

Maryam Salimian

Avanços na síntese e caracterização de nanocompositos multifuncionais de níquel / óxido de grafeno reduzido

Advances in multifunctional nickel / reduced graphene oxide nanocomposites, synthesis and characterization

Universidade de Aveiro
2018

Departamento de Engenharia Mecânica

Maryam Salimian

Avanços na síntese e caracterização de nanocompositos multifuncionais de níquel / óxido de grafeno reduzido

Advances in multifunctional nickel / reduced graphene oxide nanocomposites, synthesis and characterization

Tese apresentada à Universidade de Aveiro para cumprimento dos requisitos necessários à obtenção do grau de Doutor em Engenharia Mecânica, realizada sob a orientação científica da Doutora Paula Alexandrina de Aguiar Pereira Marques, equiparada a Investigador Principal do Departamento de Engenharia Mecânica da Universidade de Aveiro e co-orientação do Doutor Gil Alberto Batista Gonçalves investigador no Instituto de Ciência de Materiais de Barcelona (ICMAB), Espanha

Apoio financeiro da FCT (SFRH/BD/98337/2013)

universidade de aveiro
theoria poiesis praxis

FCT Fundação para a Ciência e a Tecnologia

Cofinanciado por:
COMPETE 2020
PORTUGAL 2020
UNIÃO EUROPEIA
Fundo de Coesão

To my beloved parents who always support me

o júri

presidente

Professor Doutor Jose Carlos Esteves Duarte Pedro
Professor Catedrático, Departamento de Engenharia Electrónica e Telecomunicações da Universidade de Aveiro

Doutor Gerard Tobias Rossel
Investigador Coordenador, Instituto de Ciència de Materials de Barcelona, Espanha

Doutor Jérôme Borme
Investigador, International Iberian Nanotechnology Laboratory (INL), Braga, Portugal

Doutor João Carlos Barbas de Oliveira
Investigador Auxiliar, Departamento de Engenharia Mecânica, Faculdade de Ciências da Universidade de Coimbra

Professor Doutor Fernão Domingos de Montenegro Baptista Malheiro de Magalhães
Professor Auxiliar, LEPABE, Departamento de Engenharia Química, Faculdade de Engenharia da Universidade do Porto

Professor Doutor Victor Fernando Santos Neto
Professor Auxiliar Convidado, Departamento de Engenharia Mecânica da Universidade de Aveiro

Doutor Gil Alberto Baptista Gonçalves
Investigador, Institut de Ciència de Materials de Barcelona, Espanha

Agradecimentos

First of all, I would like to express my special thanks to my advisor Dr. Paula Alexandrina de Aguiar Pereira Marques for the continuous support of my Ph.D. study and research, for her motivation and immense knowledge. A very special gratitude goes to my co-advisor Dr. Gil Alberto Batista Gonçalves for his support, great advices and all the useful discussions. My sincere thanks to Professor Jose Gracio who unfortunately is not among us anymore, provided me the opportunity to pursue my PhD study at the University of Aveiro.

I am grateful to Fundação para a Ciência e a Tecnologia (FCT) for my Ph.D. funding under the grant SFRH/BD/98337/2013.

My appreciations extend to all my colleagues, staffs and technicians from TEMA-NRD, mechanical engineering department particularly Dr. Igor Bdikin, Dr. Gonzalo Irurueta, Dr. Maria Hortigüela, Dr. Rahul Krishna, Dr. Olena Okhay, Mrs. Suzana Pinto and Mr. Andre Girao. Special thanks to Dr. Duncan Fagg and his group including Mr. Francisco Loureiro, Dr. Sergey Mikhalev, Dr. Aliaksandr Shaula and Dr. Pukazh Selvan for all their helps, kindness and all the great moments we have had together during my work in mechanical engineering department.

My endless thanks to Dr. Bernd Rellinghaus for giving me the opportunity to work at the institute of solid state and materials research (IFW) in Dresden, Germany, as a visiting PhD student during one year and giving me the access of all needed laboratories and facilities. Also, I would like to thank to all of the members of Institute of metallic materials in IFW including, Dr. Alexander Surrey, Dr. Darius Pohl, Dr. Steffen Oswald and Mrs. Christine Damm for their great help and a friendly atmosphere.

Many thanks to Professor Andrei Kholkin and Dr. Maxim Ivanov from physics department for the AFM measurements and all of the helpful discussions.

I would like to thank our collaboration with Dr. Dmitri Petrovykh and Dr. Francis Deepak at the International Iberian Nanotechnology Laboratory (INL) in Braga.

And the last but the most appreciations go to my lovely parents and my sisters for all of their endless supports, great love, motivation and encouragement. Without their help, I wouldn't be able to reach to this point in my life.

palavras-chave grafeno, óxido de grafeno, níquel, nanocompósito, hidrotermal, solvotermal

resumo

O grafeno é constituído por uma monocamada de átomos de carbono dispostos numa espécie de rede hexagonal perfeita. Devido às suas propriedades extraordinárias, este nanomaterial tem suscitado um grande interesse tanto no setor científico como no industrial. A este respeito, a investigação em torno do grafeno mostrou um aumento exponencial em áreas tão diferentes como a energia, biomedicina, eletrónica, entre outras.

O óxido de grafeno (GO), um dos derivados de grafeno, foi considerado como um substrato interessante para o desenvolvimento de nanocompositos. Isto deve-se fundamentalmente à presença de grupos funcionais de oxigénio na superfície do grafeno, os quais proporcionam locais reativos para a nucleação e o crescimento de outras estruturas.

O níquel (Ni) é um metal de transição muito abundante na terra, possui uma superfície brilhante comum à maioria dos metais e é dúctil e maleável possuindo propriedades magnéticas e catalíticas superiores, condutividade térmica e elétrica razoáveis sendo muito utilizado em diferentes aplicações. As nanopartículas (NPs) de Ni são utilizadas como catalisadores heterogéneos e receberam atenção notável devido ao seu baixo custo, reduzida toxicidade, baixa corrosão, entre outras características. Desta forma, a funcionalização do GO com NPs de Ni pode constituir uma nova família de nanocompósitos com propriedades sinérgicas.

Esta tese está focada no controlo da síntese de nanocompósitos Ni/GO, uma vez que o tamanho, a morfologia e a dispersão de NPs de Ni no grafeno afetam as suas funcionalidades e estão em dependência direta com as metodologias de síntese.

Em primeiro lugar, foi usado um método hidrotérmico de fácil implementação e execução num passo único. Foram estudados vários parâmetros de síntese, incluindo temperatura, tempo de reação e agente redutor. O controlo destes parâmetros influenciou efetivamente o tamanho das NPs de Ni, variando estas de 150 a 900 nm, a morfologia variou de forma esférica a formato em espiga e de partículas finas bem distribuídas para agregados.

Em seguida, o controlo do tamanho das NPs de Ni para valores inferiores a 10 nm e com distribuição de tamanho reduzido no substrato foi conseguido através de um procedimento de síntese em dois passos com base num método solvotérmico seguido por tratamento térmico sob atmosfera redutora de H_2. O tempo de reação mostrou ser um fator chave para controlar a distribuição e o tamanho das NPs de Ni simultaneamente com a redução do GO (rGO). O aquecimento em atmosfera de H_2 foi crucial para formar as NPs de Ni metálicas cristalinas.

A influência de um tratamento térmico adicional em atmosferas redutora e inerte sobre a estrutura do nanocompósito Ni/rGO foi também investigada. Diferentes nanocompósitos apresentaram boa estabilidade térmica sob H_2 até à temperatura de 450 °C durante 2 horas. O tratamento a 900 °C sob o fluxo de árgon alterou a estrutura do Ni/rGO por formação de “sulcos” através da rede de carbono e coalescência das NPs de Ni com formação de partículas maiores. O estudo das propriedades eletrofisicas dos nanocompositos Ni/rGO mostrou que estas são dependentes do tamanho e estrutura das NPs de Ni nas folhas de rGO. Esta é uma potencial vantagem do método de síntese desenvolvido para o design de diferentes nanocompositos de Ni/rGO que poderão ser materiais favoráveis para aplicação em dispositivos eletrónicos integrados.

keywords graphene, graphene oxide, nickel, nanocomposite, hydrothermal, solvothermal

abstract

Graphene, the world thinnest material made of carbon atoms in a dense honeycomb network has captured a great interest in both scientific and industry sectors due to its remarkable properties. In this regard, the graphene research is facing an incredible rise in different areas such as energy, biomedical, sensor and electronic applications, between others.

Graphene oxide (GO), one of the graphene derivatives, has been considered as an interesting substrate to build nanocomposites. This is due to the presence of oxygen functionalities at the graphene surface which provides reactive sites for the nucleation and growth of other structures.

Nickel (Ni) is a transition metal very abundant on earth, it has a shiny surface common to most metals and is both ductile and malleable possessing different properties such as superior magnetic and catalysis properties, a fairly good heat and electrical conductivity and is widely used in different areas of application. Ni nanoparticles (NPs) find use as heterogeneous catalyst and received noteworthy attention because of its inexpensive, non-toxic, low corrosion, waste minimization, between other characteristics. In this way, the functionalization of GO with Ni NPs can establish a new family of nanocomposites with synergic properties.

This thesis is focused on the control of the synthesis of Ni/GO nanocomposites, since the size, morphology and dispersion of Ni NPs on graphene affect their functionalities and are in direct dependence with the synthesis methodologies.

First, a facile one pot hydrothermal method was introduced and various synthesis parameters including temperature, reaction time and reducing agent were investigated. The control of these parameters effectively influenced the Ni size, ranging from 150 to 900 nm, the morphology from spherical to spiky shape and from well distributed fine particles to the big aggregation.

Then, the control of the Ni NPs size to values of less than 10 nm with narrow size distribution on the substrate was achieved via a two-step synthesis procedure based on a solvothermal method followed by a heat treatment under H_2 reducing atmosphere. The reaction time was shown to be a key factor to control the size and size distribution of Ni NPs simultaneously through the reduction of GO (rGO). Heating treatment under H_2 was crucial to form the crystalized metallic Ni NPs.

The influence of further thermal treatment under reducing and inert atmospheres on the structure of Ni/rGO nanocomposite was also investigated. Different nanocomposites showed a good thermal stability under H_2 up to 450°C during 2 hours' treatment. Higher temperature (900°C) under Argon flow changed the structure of Ni/rGO by formation of trenches through the carbon etching and coalescence of Ni NPs to form bigger particles. The study of the electrophysical properties of Ni/rGO showed that these properties are dependent on the size and structure of Ni NPs on rGO nanosheets. This is the potential advantage of the synthesis method developed for designing different matrix of Ni/rGO nanocomposites which could be a favorable material for integrated electronic devices application.

Table of Contents

List of Figures

List of Tables

List of Abbreviation and Acronyms

AC-TEM	aberration corrected transmission electron microscopy
AFM	atomic force microscopy
at. %	atomic percentage
BET	Brunauer–Emmett–Teller (surface area analysis)
CVD	chemical vapor deposition
DFT	density functional theory
DMF	dimethylformamide
EDS	energy dispersive X-ray spectroscopy
EM	electromagnetic
FLG	Few layer graphene
FTIR	Fourier transform infrared spectroscopy
GIC	graphite intercalation compound
GO	graphene oxide
HAADF-STEM	high angle annular dark-field scanning transmission electron microscopy
HH	hydrazine hydrate
HOG	graphene oxide prepared by Hummers' method
HOG^{+}	graphene oxide prepared by modified Hummers' method
HOPG	highly oriented pyrolytic graphite
HRG	highly reduced graphene oxide
HRTEM	high resolution transmission electron microscopy
HSC	hydrogen storage capacity
ICP-OES	inductively coupled plasma optical emission spectroscopy
IGO	graphene oxide prepared by improved Hummers' method
KPFM	kelvin probe force microscopy
MWCNT	Multiwall carbon nanotube
NMR	nuclear magnetic resonance
NPs	nanoparticles
PFM	piezo response force microscopy
PGO	pristine graphite oxide
rGO	reduced graphene oxide

SAED	selected area electron diffraction
SEI	solid electrolyte interface
SEM	scanning electron microscopy
SGH	self-assembled graphene hydrogel
SPM	scanning probe microscopy
SR	spreading resistance
STEM	scanning/transmission electron microscopy
TEGO	thermally exfoliated graphite oxide
TEM	transmission electron microscopy
WF	work function
wt.%	weight percentage
XPS	X-ray photoelectron spectroscopy
XRD	X-ray diffraction

Chapter 1
Introduction

1. Introduction

1.1 Carbon

Carbon is known as one of the most versatile elements, for all known terrestrial life on the earth. It is capable to form many allotropes such as diamond, graphite, lonsdaleite, fullerene and carbon nanotubes, Figure 1.1 [1].

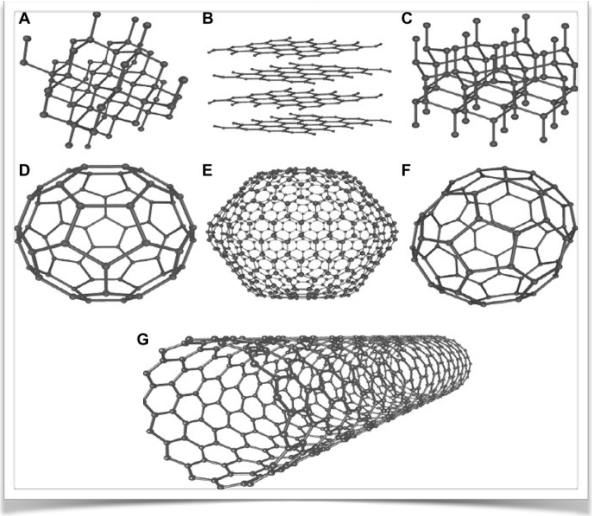

Figure 1.1 carbon allotropes structure A) diamond B) graphite C) lonsdaleite, D-F) fullerene (C60, C540, C70) G) carbon nanotube, adapted from ref [1].

Despite that all carbon allotropes are made entirely out of pure carbon they confer different properties depending on their structure. For example, diamond is a giant tetrahedron structure of carbon atoms. The hardest known material with high transparency which is desirable for both jewelry and use for cutting, grinding or drilling apparatus [2]. Graphite is another allotrope with carbon layered-planar structures. It is greyish- black and opaque, soft and slippery which is used for pencil leads. High electrical conductivity made it a good candidate for electrode materials application. The different fundamental physical properties of different carbon allotropes are the consequence of different molecular configuration.

Carbon atoms have 6 electrons with the configuration of $1s^2\ 2s^2\ 2p^2$. The core electrons with the energy of around -285 eV are strongly bound to the nucleus and don't participate in

atomic bonding. It has only small influence on the physical properties of carbon-based material as a source of dielectric screening for outer shell electrons. The rest 4 electrons in the second shell of orbitals (2s and 2p) have different energy of about 4 eV which is favorable for configuration of 2 electrons in 2s orbital, one electron in $2p_x$ and one in $2p_y$ state.

Carbon can form covalent bonds with other carbon atoms or other elements like hydrogen or oxygen with superposition of quantum states form sp^n (n = 1,2,3) hybridized orbitals which influences molecular geometry and bonding properties.

The sp^2 hybridization forms 3 covalent bonds in-plane with the characteristic angle of 120 degrees known as σ bonds. The additional p_z orbital is perpendicular to these sp^2 hybrid orbitals and stablish π bonds.

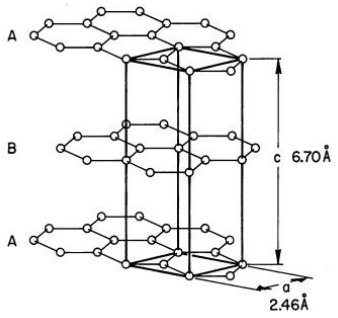

Figure 1.2 The crystal structure of graphite, adapted from reference [3].

Graphite is a typical example of sp^2 hybridized crystal structure. It consists of parallel planes of carbons sheets, which are called graphene, arranged in an ABAB bernal stacking sequence. The carbon atoms are strongly bonded within the graphene layer by σ bonds, the adjacent graphene sheets are weakly bonded by van der Waals interaction caused by π bonds creating the interlayer distance of 0.335 nm between two graphene layers (Figure 1.2) [3]. The C-C σ bonds are the strongest bonds being responsible for the strength of an in plane of graphene and π bonds provide the delocalized electron network which makes the graphene an incredible high electrical conducting material. The π bonds are responsible for the weak bonds between the carbon layers in graphite [4].

1.2 Graphene

Two dimensional materials have been a target for theoretical studies over the 70 years [5], [6]. According to Landau and Peierls, two dimensional materials could not exist due to the thermodynamic instability at room temperature [7],[8]. Several observations in experimental work have been supported this theory. According to this theory the melting temperature of a thin film is thickness dependent. In other words, decreasing the thickness of the thin film leads to decompose or islands segregation when the range of the thickness is about dozens of atomic layers. In this regards the only way to form 2D structure was epitaxial growing it on a 3D monocrystalline lattice structure [9]. Nevertheless, the existence of two dimensional atomic crystals was discovered by easy isolation of exfoliation of graphite under ambition conditions in 2004 by Andre Geim and Constantin Novoselov from Manchester University. These scientists successfully detached a graphene layer from highly oriented pyrolytic graphite (HOPG) using scotch tape. For this discovery, they won the joint Nobel Prize of Physics in 2010 [10].

As referred previously, graphene is a single layer of carbon atoms in a dense honeycomb structure and after its discovery it has been considered as a wonder material. Actually, graphene sheets are considered the building blocks for other carbon materials from different dimensionalities, (Figure 1.3)[9].

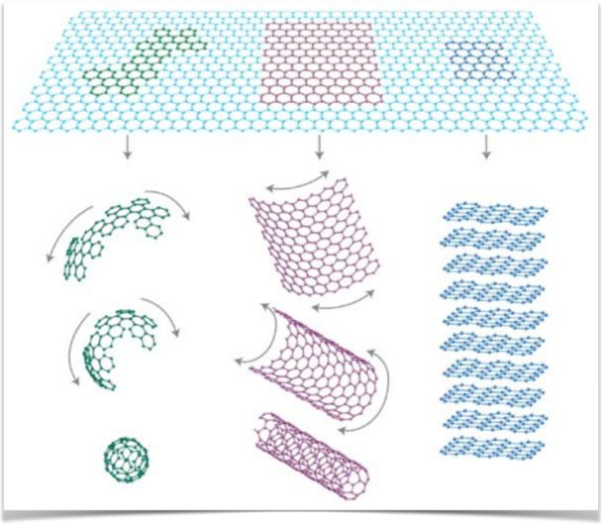

Figure 1.3 Graphene as a building material for other carbon materials [9].

The incredible properties attributed to graphene, such as, high surface area 2630 m^2/g, light weight, high carrier mobility (~10000 $cm^2\ V^{-1}\ s^{-1}$), high thermal conductivity (5300 $W \cdot m^{-1} \cdot K^{-1}$) both at room temperature, high stiffness (1 TPa), high transparency and high mechanical flexibility, opened up a high expectation for different applications in the fields of electronic, energy storage, biomedical, aerospace industry, sensors, between others. These facts about graphene, generated a remarkable research dramatically increasing year by year (Figure 1.4).

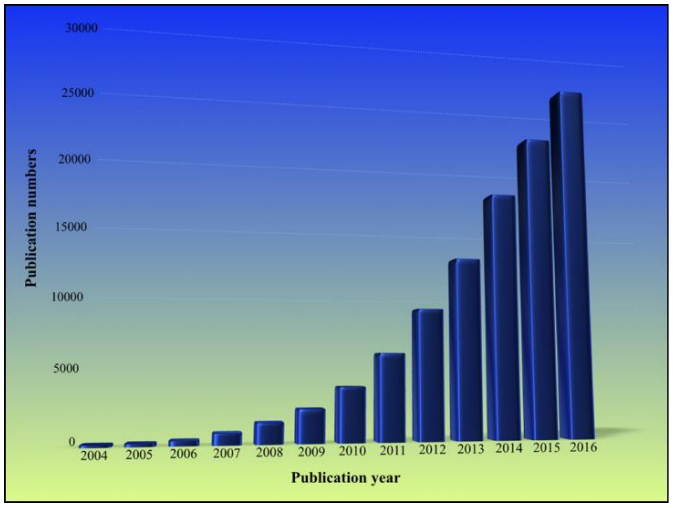

Figure 1.4 Evolution number of publication about graphene during 2004-2016. Obtained by searching key word "Graphene" data source: Web of Science, Date:07/14/2017.

1.3 Graphene fabrication

There are two main routes for graphene fabrication, top-down and bottom-up synthesis (Figure 1.5) [11].

Top down approaches consist on the decoupling of the stacked graphene layers from graphite source including exfoliation of HOPG or natural graphite by mechanical cleavage with scotch tape [10], chemical exfoliation in organic medium [12] and chemical exfoliation involving strong oxidation agents. In the latter case a highly-oxidized form of graphene is obtained called graphene oxide (GO), and due to that a further reduction process needs to be applied by chemical or/and thermal process [13-15].

Bottom up approach is a molecular growth on a substrate from molecular carbon sources including chemical vapor deposition (CVD) [16-18] and epitaxial growth [19-22].

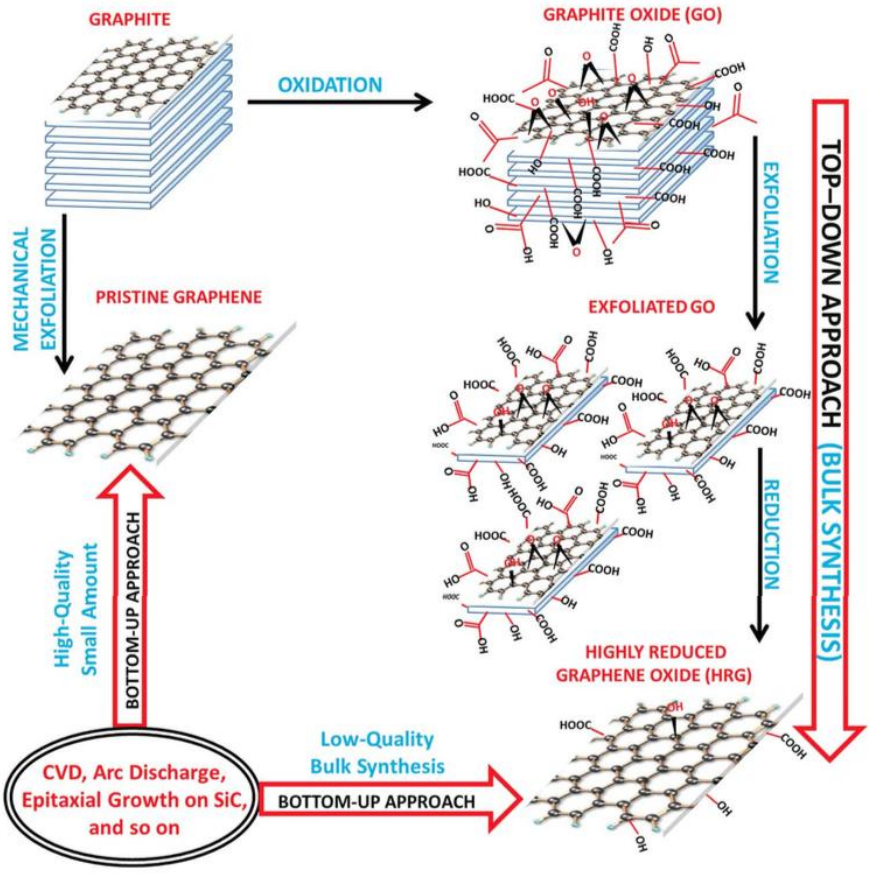

Figure 1.5 Schematic of top down and bottom up approaches for graphene fabrication [11].

1.3.1 Top down approach

Micromechanical cleavage of HOPG is the best-known method for mechanical fabrication of high quality graphene [10]. In this method, a single or few layers graphene can be obtained by peeling off the graphene layers from HOPG on SiO_2 substrate, Figure 1.6 (a) [23]. The obtaining graphene by this method is defect free and has high quality which is competent for electronic characterization; however, this method is not suitable for massive production of graphene.

Liquid based direct exfoliation which contain ultrasonic, electrochemical and shear exfoliation is another method that recently got attention for fabrication of two-dimensional nanomaterials including graphene Figure 1.6 (b) [24]. In this method, a bulk material is exfoliated to a few layers in liquid media either with or without intervention of a chemical reaction. The minimum chemical reaction is looked-for in order to preserve the high crystallinity of the final 2D nanomaterial. One of the important disadvantages of this method is the difficulty of complete removing of dispersants such as the solvent. This method is cheap and scalable and an appropriate way for production of few layered nanomaterials without defects in large volume but not able to form highly uniform single layered structure for electronic application.

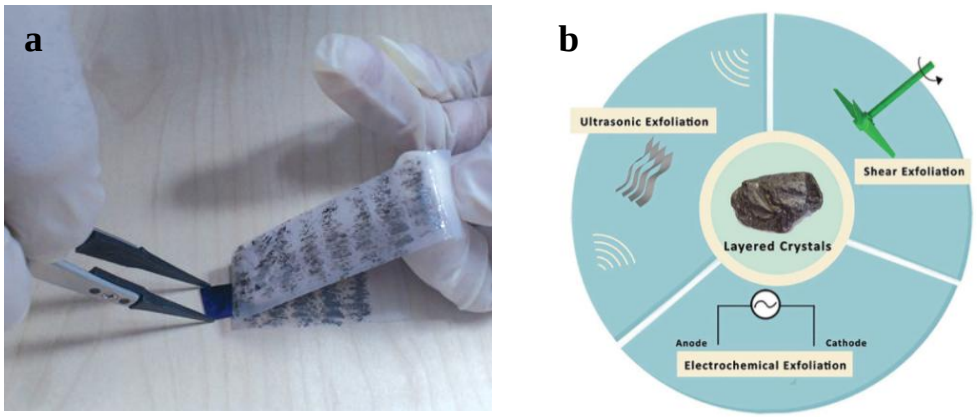

Figure 1.6 Micromechanical exfoliation of graphene (a) [23] and liquid based direct exfoliation (b) [24].

Graphene can be obtained via oxidation of graphite to GO followed by reduction to produce reduced GO (rGO) [25]. In this method, oxygen functional groups like epoxy, hydroxyl, carbonyl and carboxyl groups are introduced in to the layers of graphite by strong acids and oxidants agents. Graphite oxide can be further exfoliated to the individual or few layers GO. The properties of the obtained GO depend on the several factors like the quality of graphite source and the synthetic methods. The obtained rGO by this method is composed of restored pristine graphene areas, together with the defects on the carbon structure like holes and partial content of oxygen functional groups, see Figure 1.7 [26].

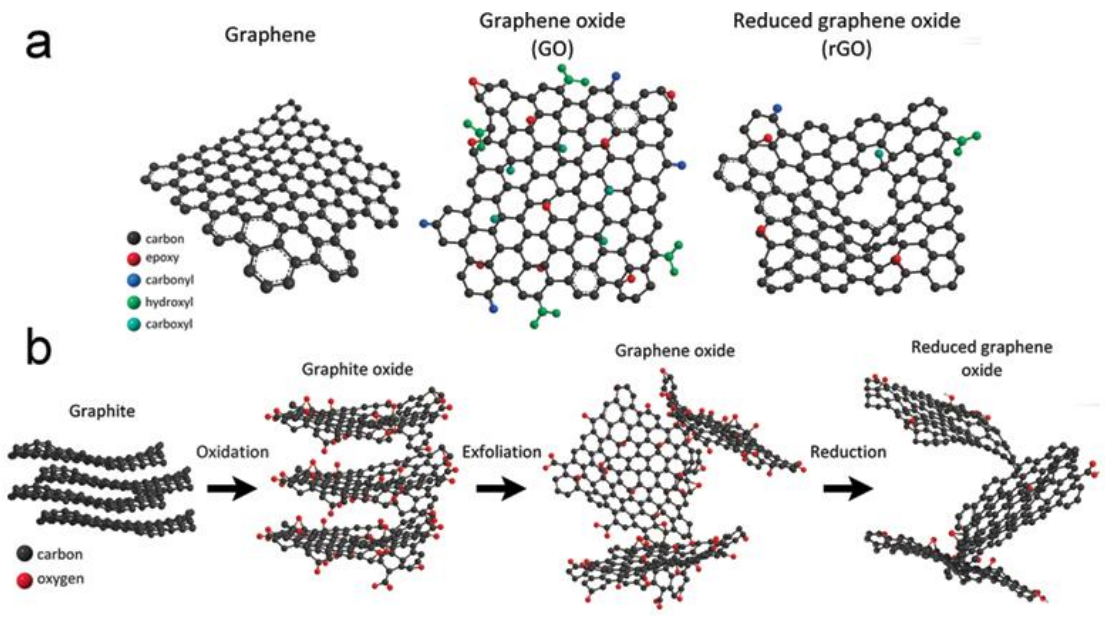

Figure 1.7 Schematic representation of a) pure graphene, individual GO layer with different functional groups and single layer of rGO; b) preparation of rGO via chemical exfoliation of graphite [26].

1.3.2 Bottom-up approach

Chemical vapor deposition (CVD) is the most popular technique for the production of large-area graphene. In CVD method, firstly a thin layer of transition metal like nickel (Ni) or copper (Cu) is deposited on the substrate. Ni has a close lattice match with graphene so it has been suggested as a good candidate for graphene growth on it. This structure is exposed to the carbonaceous environment H_2/CH_4 at high temperature (900-1000 ºC). During the heating process carbon radicals are diffused in to the Ni and precipitate out of it while cooling down forming graphene. After, by chemical etching of Ni, this graphene membrane is detached from the substrate (Figure 1.8) [27]. The graphene grown on Ni contains multilayers regions besides monolayer region which is a drawback of using this substrate. To increase the monolayer graphene region, annealing the Ni substrate in hydrogen atmosphere has been suggested. This treatment reduces the grain boundaries and defects which are responsible for multilayers-graphene growth [28,29].

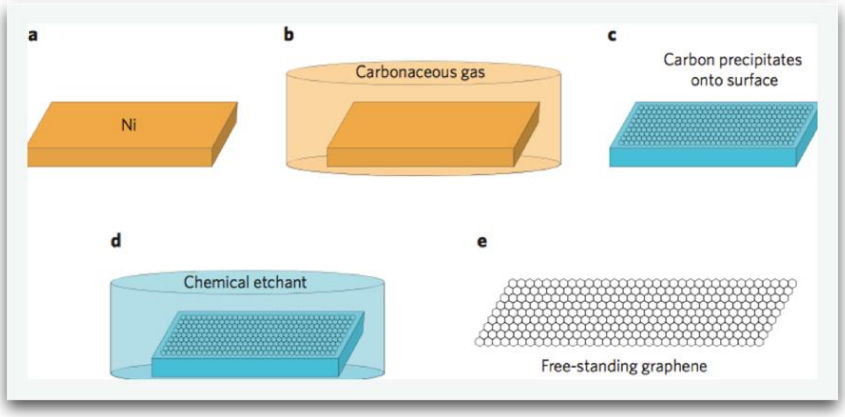

Figure 1.8 Schematic illustration of graphene fabrication via CVD method, orange color resembling high temperature and a gas phase while the blue color related to the cold and etchant [27].

Copper is another interesting element for graphene fabrication in CVD method that was firstly suggested by Ruoff group [30]. The mechanism of graphene formation on Cu is different from Ni in which the former one is based on the carbon segregation or precipitation while the later one is based on the surface adsorption process [31]. Due to the low solubility of carbon in Cu the growth of graphene is limited to the Cu surface even at high temperature leading to the production of predominantly single layer graphene [32]. Different metal substrates have been studied for graphene formation such as Cobalt (Co), Ruthenium (Ru) and Iridium (Ir). The mechanism of growing of graphene on these transition metals is the same as the one was discussed for Ni substrate [33].

Besides the type and crystallinity of metal substrate, the quality of graphene obtained relies also on other factors including growth time, hydrocarbon concentration and the cooling rate. For example, different concentration of hydrocarbon and growth time change the thickness of obtained graphene due to the different amount of carbon radicals diffusing in to the Ni substrate [28].

For the majority of the applications, graphene requires to be on a dielectric substrate removing the catalytic metal and transferring the graphene to a proper substrate, while maintaining the graphene quality. This is another challenge that should be taken in to account for optimization of CVD processes. Reaching the high quality and large scale production of

graphene, CVD technique still requires several studies and investigations to meet the criteria for electronic and optoelectronic application [34].

Epitaxial growth is another bottom up methods for the fabrication of graphene which is based on the decomposition of carbon-containing substrate. Usually single crystal silicon carbide (SiC) is used as a substrate. At ultra-high vacuum and high temperature around 1300 ºC, silicon atoms are sublimated and leave the carbon atoms behind. Rearrangement and graphitization of these carbon atoms produce graphene sheets. The annealing temperature and the time are effective to control the thickness of graphene layers [35]. Epitaxial graphene films can be patterned using nanolithography techniques making it compatible with current semiconductor technology which is in high demand for electronic devices application [36]. However, the epitaxial graphene layers are not uniform on thickness, due to the different polar faces of SiC.

Controlled preparation of monolayered epitaxial graphene can be achieved on silicon terminated surface of SiC substrate by tuning the experimental condition. Nevertheless, the epitaxial graphene obtained on the carbon terminated surface is mostly containing multilayers and is more challenging to be controlled by tuning the experimental conditions [37]. Figure1.9 [38] shows the growth of the epitaxial graphene on SiC substrate and Figure1.10 [38] resembles the differences of epitaxial graphene growth on different surfaces of SiC.

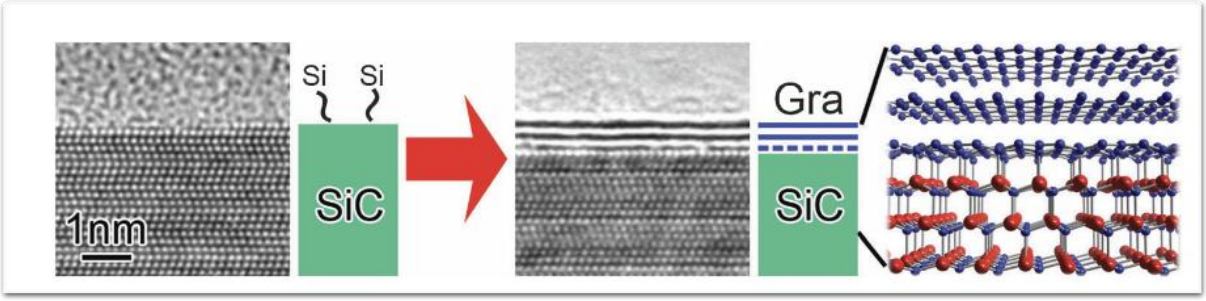

Figure 1.9 The growth of epitaxial bilayer graphene on Si surface of SiC substrate and its structural models. Blue color shows the carbon atom while red is silicon [38].

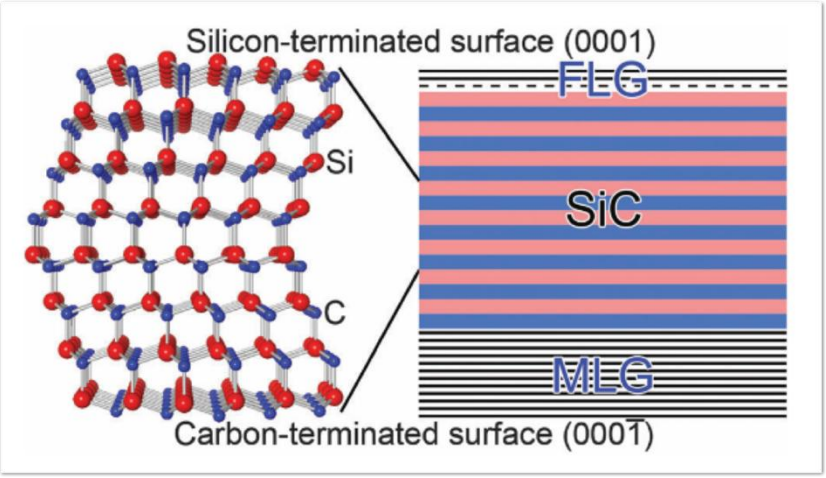

Figure 1.10 Crystal structure of 6H-SiC and corresponding few layers graphene (FLG) on silicon terminated surface and multilayers graphene (MLG) on carbon terminated surface, blue and red shows carbon and silicon atoms respectively [38].

1.4 Graphene Oxide (GO)

1.4.1 History and fabrication methods (Brodie, Staudenmaier and Hummer's method)

The well-known example of oxidizing graphite is the work of the British chemist, B.C. Brodie published in 1859. The oxidation method was based on adding potassium chlorate ($KClO_3$) to graphite in fuming nitric acid (HNO_3). It was reported an increasing of the weight of the final product as a result of the addition of hydrogen and oxygen groups to the carbon structure of the graphite [39].

After 40 years another scientist (L.Staudenmaier, 1898) [40] optimized this preparation method by adding of chlorate to the mixture during the reaction process and also using the concentrated sulfuric acid (H_2SO_4) to the mixture to increase the acidity. The advantage of this method was obtaining highly-oxidized graphite like as Brodie's reported but only in one pot reaction preparation [41]. After 60 years two chemists (W.Hummers and R.Offeman, 1958) [42] used a simple and fast procedure for oxidizing graphite. They prepared a mixture of graphite with concentrated H_2SO_4, potassium permanganate ($KMnO_4$) and sodium nitrate ($NaNO_3$) maintained for few hours to obtain graphitic oxide. In their method, $KClO_3$ was replaced by potassium permanganate ($KMnO_4$) in order to avoid spontaneous explosion during

oxidation process and fuming HNO_3 was replaced by sodium nitrate ($NaNO_3$) to avoid fog acid production [43]. The graphite oxide obtained by Hummers' method always contain nonoxidized graphite, in order to overcome this inequality, modified Hummer's method was proposed for the first time by N.I.Kovtyukhova and her group in 1998 [44]. In this method, a pre-oxidation step was used prior to the Hummers' method. Briefly, the graphite powder was mixed with concentrated H_2SO_4, potassium persulfate ($K_2S_2O_8$) and phosphorus pentoxide (P_2O_5). The mixture was thermally isolated and cooled down to the room temperature over 6 hours. After dilution with distilled water it was washed and filtered and dried in the air. Modified Hummers' method, like the others methods, has the disadvantage of producing toxic gases like NO_2 and N_2O_4. Improved Hummers' method was another process reported by the group of professor M. Tour (by D.C. Marcano, 2010) [45]. In this procedure, instead of $NaNO_3$ that was responsible for toxic gas production they used phosphoric acid (H_3PO_4) and also using higher amount of $KMnO_4$ compared to Hummers' method. In their study, three samples HGO, HGO^+ and IGO were prepared respectively by Hummers method, modified Hummers' method and improved Hummers' method. It was shown that the oxidation degree of the samples is different in the following order, IGO > HGO^+ > HGO. Nevertheless, after reduction of IGO and HGO by hydrazine hydrate both samples showed the same electrical conductivity properties. Figure 1.11 shows the experimental conditions for preparation of GO from graphite flakes in Hummers, modified Hummers and improved Hummers method used by Tour group.

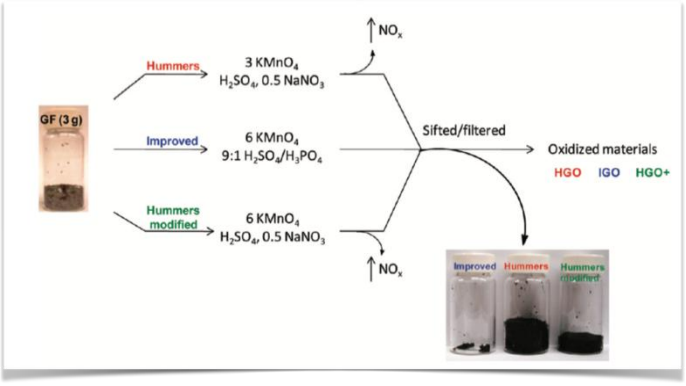

Figure 1.11 Representation of three different methods for oxidizing of graphite flakes (GF). Three bottles showing the hydrophobic carbon materials after purification of HGO, IGO and HGO^+. The IGO has a lower under-oxidized material which proves the efficiency of improved Hummers' method [45].

Currently the modified Hummers' method is the most widely used procedure for GO fabrication. Recently A.M. Dimiev [46] proposed a three steps mechanism to explain the formation of GO by modified Hummers' method (Figure 1.12).

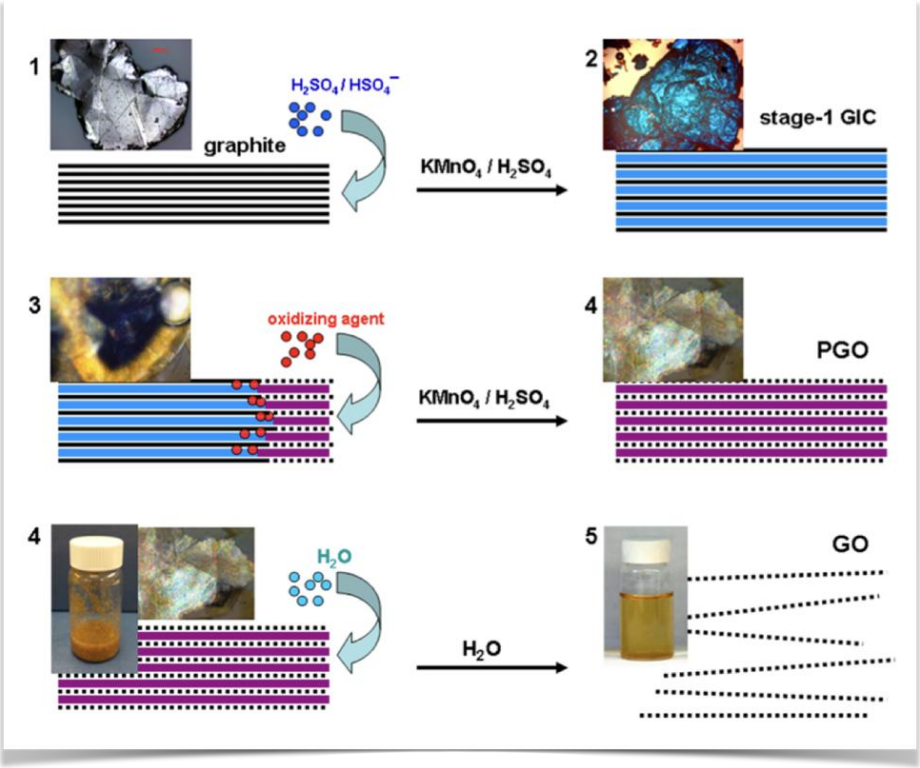

Figure 1.12 Representation of the three steps mechanism of GO formation from graphite flakes with the respective optical images. The black line, blue line, purple line and black dotted line, represents respectively graphene layers, H_2SO_4/HSO_4^- intercalant, a mixture of H_2SO_4/HSO_4^- with reduced oxidizing agent and a GO monolayer [46].

The first step is described as a formation of H_2SO_4– graphite intercalation compound (GIC) and has the characteristic of deep blue color. This product is obtaining during the first 3-5 min of reaction process. The second step which takes quite longer, like several hours or even days, is the formation of pristine graphite oxide (PGO) from GIC. In this step, the progress of oxidation was studied by gradually adding of 1, 2, 3 and 4 wt% $KMnO_4$ to the mixture and studies the sample after each part. Obtained optical images of this step showed the chemical reaction is progressed from edge to the center of the flakes as the blue color was disappearing while appearing the yellow color. It was shown that the percentage of the blue

region which related to the unoxidized area is bigger in big flakes than the smaller ones. This suggests that the oxidizing progress is different for different flake sizes. Small flakes get oxidized faster than the big ones due to the rapid diffusion of oxidizing agent in to the intercalant molecules packed between graphene layers in GIC in small area. The edge to center oxidation process was also confirmed by Raman investigation of different regions of graphite flake.

The last step includes the reaction of PGO with water and conversion into GO. In this step, the water hydrolyses the covalent sulfate which act as protective groups and further oxidation modification leads to the formation of the final GO.

1.4.2 Chemical structure

A simple definition to describe a GO sheet is a graphene layer with both sides bonded to oxygen groups like carboxyl, hydroxyl and epoxy groups [47]. The GO can be synthesized by oxidation of graphite to graphite oxide and then by exfoliation to GO. The interlayer distance between carbon layers in graphite is 0.335 nm which increases to around 0.7 nm after oxidation. The graphite oxide can be easily exfoliated to GO by stirring or mild sonication. Since the graphite oxide is composed of an accumulation of GO sheets, both material exhibit similar structure. Graphene, or more exactly rGO can be obtained by the further reduction of GO by elimination of the oxygen groups. Despite the old history of GO fabrication, this material got heightened interest as a source of graphene production only after the discovery of graphene in 2004 [48]. Unfortunately, due to the nonstoichiometric atomic composition of GO and the lack of characterization techniques until today, the structure of GO is not fully understood and still is on debate. Some of the early proposed schematic structural models for GO are summarized in Figure 1.13. These models are based on those information obtained by exchange reactions, X-ray diffraction (XRD), electron diffraction and infrared spectroscopy [49].

Hofmann and Holst [50] suggested a model in which carbon plane contains epoxy groups on both sides with the C_2O ideal formula. Later on, Ruess [51] proposed another model which contain both epoxy and hydroxyl groups on graphene basal plane [41]. The structure suggested by Scholz and

Boehm [52] considered a flat carbon layer containing regularly C=C bonds and the carbonyl and hydroxyl groups are as the only oxygen functional groups. Nakajima and co-workers used Fourier transform infrared spectroscopy (FTIR) and carbon-13 nuclear magnetic resonance (^{13}C NMR) characterization to study the structure of GO. They also indicated that after fluorination of GO the resultant showed the same C_2F structure by XRD analysis. In this case, they suggested each two carbon layers are linked together by carbon – carbon sp^3 bonds. According to their model the existence of the hydroxyl and carbonyl groups are depends on hydration [53]. Lerf and Klinowski proposed their model in 1998 based on their ^{13}C NMR and ^{1}H NMR studies [54].

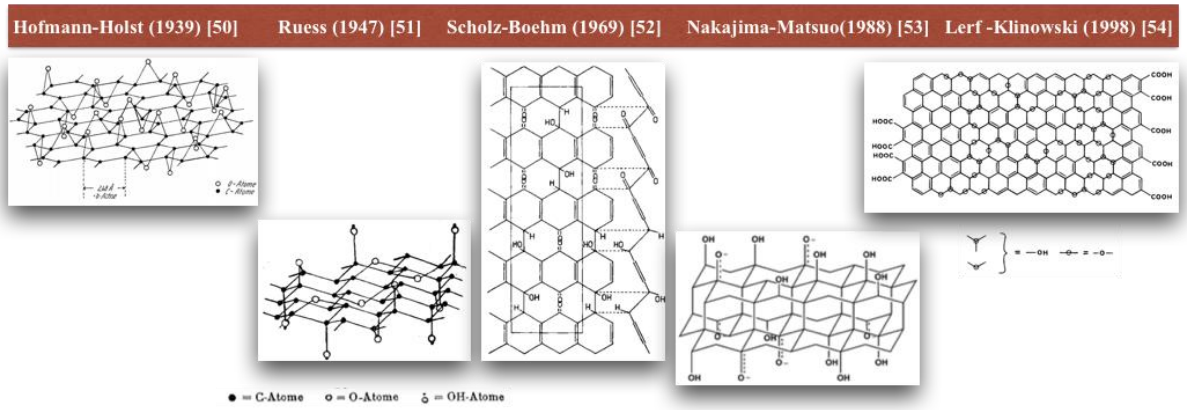

Figure 1.13 Different earliest models for GO structure (Images are adapted from references [50, 51, 52, 53 and 54]).

This model is the most accepted structure for GO. In this model, the oxidized and unoxidized aromatic rings are spread randomly and oxygen functional groups are on the both sides of GO sheets with the GO layers terminated with C-OH and –COOH groups. Those carbon atoms that attach to OH group have slightly disordered arrangement that cause some wrinkles on the GO. It was also suggested the existence of epoxide (1,2-ether) instead of 1,3-ether which was proposed earlier by Mermoux [49]. It was also explained that the negatively configuration of oxygen groups covering both sides of GO is responsible for preventing the carbon from nucleophilic attack. Depending on the oxidation level, GO has different stoichiometry of its elements. Nonetheless the same set of oxygen functional groups are reported for synthesized GO from different methods [55].

Besides of the reported analysis methods that were used for understanding the structure of GO, aberration corrected transmission electron microscopy (AC-TEM) is one powerful technique to study the graphene structure, however in the case of GO it is a challenging technique due to the presence of defects and contaminants that mask the GO surfaces. Another difficulty is the reaction of these contaminants with high energy electron beam resulting changes of GO structure. Kris Erickson [56] studied the local structure of GO using AC-TEM technique. To prepare the proper sample for the macroscopic observation, the GO deposited on a grid was reduced with hydrazine and heated at 550°C in N_2 atmosphere to clean the contaminants. It was shown that the GO consist of three different regions including holes, graphitic regions and disordered areas, see Figure 1.14. The graphitic domains are incomplete oxidation of graphite and disordered areas are continuous containing high contrast resemble the GO region.

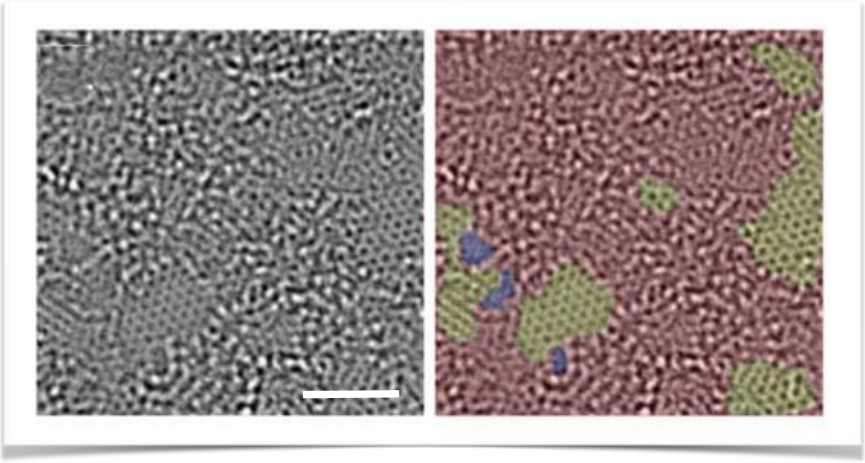

Figure 1.14 Aberration corrected TEM image of a single layer of GO. The blue, yellow and red color indicating the holes, graphitic domain and disordered regions with oxygen groups respectively, scale bar denoting 2 nm, adapted from ref [56].

One of the most recent study of GO with AC-TEM was reported by S. H. Dave in 2016 using in situ heating of sample holder up to 700 ºC [57]. It was mentioned that above 500 ºC the contaminants detached and the crystalline and polycrystalline areas were appeared. The existence of long range sp^2 lattice structure and isolated defects areas in GO was reported.

Figure 1.15 shows closed edges and open edges revealing the disorders in GO which separate the crystalline areas.

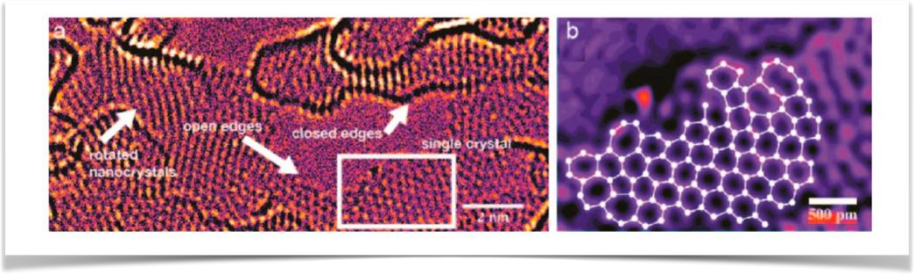

Figure 1.15 a) Atomic structure of GO obtained by (AC-TEM) during the heating process at 700 ºC, b) The structure of only one area in (a) that is shown in white the resolved structure [57].

1.4.3 Preparation of rGO

Different processes are used for elimination of the oxygen functional groups from GO structure and restoration of sp^2 hybridized domain. However, the fully recovering of graphitic domain from GO is not possible due to the formation of stable carbonyl and ether groups, Stone-Wales defects including heptagons and pentagons pairs and the holes that are by-products of carbon releasing from the structure in the form of CO and CO_2 [26]. As a consequence, rGO shows different properties depending on the oxygen reduction level and structural defects. Determination of C/O ratio in rGO is an important factor that can clarify the level of the reduction. X-ray photoelectron spectroscopy (XPS) is the best-known technique for this purpose. The C/O atomic ratio of fully oxidized GO is reported to be about 2:1 , heating it more than 80 °C changes the composition and increases the C/O ratio [58].

On the other hand, the existence of these minor functional groups can be tuned in order to functionalize the GO providing GO with an extraordinary capability for different applications [59-61]. Regardless of the type of methods used for the reduction of GO to rGO, this material goes under several changes. The most visible one is the change of the color from brownish to black in bulk quantity. The hydrophilic characteristic of GO changing to the hydrophobic property. Moreover rGO become more conductive than GO [26]. The efficiency of GO

reduction can be examined by different techniques such as XRD, thermogravimetry and Raman spectroscopy [62].

1.4.3.1 Thermal annealing reduction

Rapid thermal annealing is one strategy to produce bulk quantity of thermally reduced graphene oxide (TRG) from thermal expansion of graphite oxide. Rapid heating (>2000 °C/min) up to 1050 ºC [63] leading to the decomposition of oxygen functional groups in the form of CO and CO_2 yielding high pressure between the stacked layers of the graphite oxide. For exfoliation of graphite oxide, the van der Waals force that keeps the GO layers stacked together should be overcome by this pressure. In other words, the temperature required for this process must exceeds over 550 ºC in order to exfoliation occurrence [64]. The decomposition of oxygen groups produces defects by removing the carbon atoms from basal plane. About 30% weight loss occurring during the thermal annealing of graphite oxide by decomposing of oxygen groups and water evaporation. The need of high temperatures in this method demanding high energy consumption and expensive facilities turns this method not truly practicable. In addition, this procedure is not suitable for some applications, like the preparation of rGO on glass substrate for electronic devices.

Several thermal reduction methods of GO at low temperature has been reported recently. Bin Shen [65] prepared a few layered graphene sheets using HCl at low temperature (130 ºC) and under ambient atmosphere. Obtained graphene sheets were defective with some residual functional sites showing the bulk conductivity of 1200 S m^{-1} for 0.3 g cm^{-3} and the BET surface area of about 500 $m^2g^{-1,}$ which is lower than pristine graphene sheet. A. Kaniyoor [66] synthesized graphene sheets by reduction-exfoliation method at 200 ºC under hydrogen atmosphere. The BET surface area of obtained graphene reported to be 442.9 m^2g^1.

Xianjue Chen [67] reported the possibility of GO thin films reduction in the air by rapid thermal annealing. It was suggested that by increasing the environmental pressure through sandwiching the GO film between two quartz slides, it is possible to decompose the oxygen

groups at temperatures ranging from 100 ºC to 400 ºC in the air while preserving structural integrity.

1.4.3.2 Chemical reduction

rGO can be chemically produced using reducing agents [68] such as hydrazine monohydrate [69,70], sodium borohydride [71,72] and hydroquinone [73]. The basal plane of GO contains different oxygen groups that make it hydrophilic so it can be exfoliated easily in aqueous solution. One effective method for exfoliation and reduction of graphite oxide is to place it in pure hydrazine solution. Although, the complete elimination of oxygen groups is not possible through this method and besides the number of defects created, a significant restoration of sp^2 sites can be achieved [74].

The effect of hydrazine hydrate dosage and reaction time on the reduction of oxygen functional groups were studied by P. Zh [75] using FTIR. Graphite oxide was prepared by Hummer's method and was exfoliated using ultra-sonication. Furtherly, the single layers of GO were isolated by centrifugation. Different doses of hydrazine hydrate 1, 5, 7 and 10 mg were tested for the reduction of GO. It was shown that efficient reduction was achieved for the higher dosage of hydrazine hydrate. These authors also studied the influence of time on the reduction of oxygen groups. FTIR spectra of samples were collected and investigated after five different reaction times (20, 40, 60, 80 and 100 min). After 20min the peaks of oxygen groups were mostly decreased and it was mentioned that the effective complete reduction was achieved after 80min reaction time. It was shown that the reduction degree increases slowly with the time evolution.

The reduction of GO by hydrazine hydrate under different conditions such as different temperatures and reaction time was investigated by P. Gang Ren [76]. The GO was prepared from modified Hummers' method suspended in distilled water and mix with hydrazine hydrate with the weight ratio of (HH/GO=1). The reaction was carried out varying temperature (15, 60, 80, 95 ºC) and time (100h, 24h, 3h). The resultant materials were investigated by different

characterization techniques. It was concluded that the temperature had a higher impact on the reducing process than the reaction time, see Table 1.1.

Table 1.1 The C/O ratio of rGO obtained under different reduction condition, adapted from reference [76].

C/O	GO	15 ℃/100h	60 ℃/100h	80 ℃/24h	95 ℃/3h
	3.0	6.4	10.9	13.1	15.1

On the other hand, a possible reaction mechanism for the reduction of oxygen groups with hydrazine hydrate was suggested by P. Ren [76], see Figure 1.16.

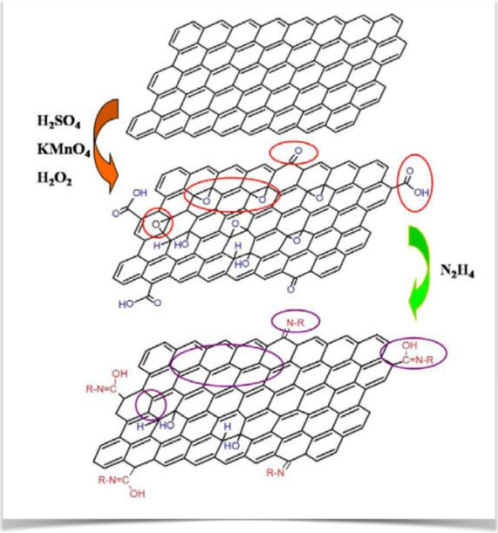

Figure 1.16 Schematic illustration of GO preparation and its reduction with hydrazine hydrate [76].

The majority of oxygen groups are eliminated after chemical reaction but the sp^2 graphene domain is not fully recovered. Some parts of rGO still contain functional groups like C-OH and C-H. Also, the existence of C=N bond with N origin from hydrazine was proved by FTIR and XPS data.

The hydrazine reduction of both graphite oxide and exfoliated GO was reported by the group of R. Ruoff [77]. The graphite oxide was synthesized by modified Hummers' method. For the preparation of the first sample, the graphite oxide was suspended in pure water under ultrasound bath for fully exfoliation of GO. The other sample was graphite oxide that was not further exfoliated like the previous sample. Hydrazine hydrate was added to both suspensions

and the products were characterized. It was shown that the degree of reduction for exfoliated GO (C/O=10.2) was higher than for non-exfoliated graphite oxide (C/O=5). The schematic representation of reduction degrees is shown in Figure 1.17.

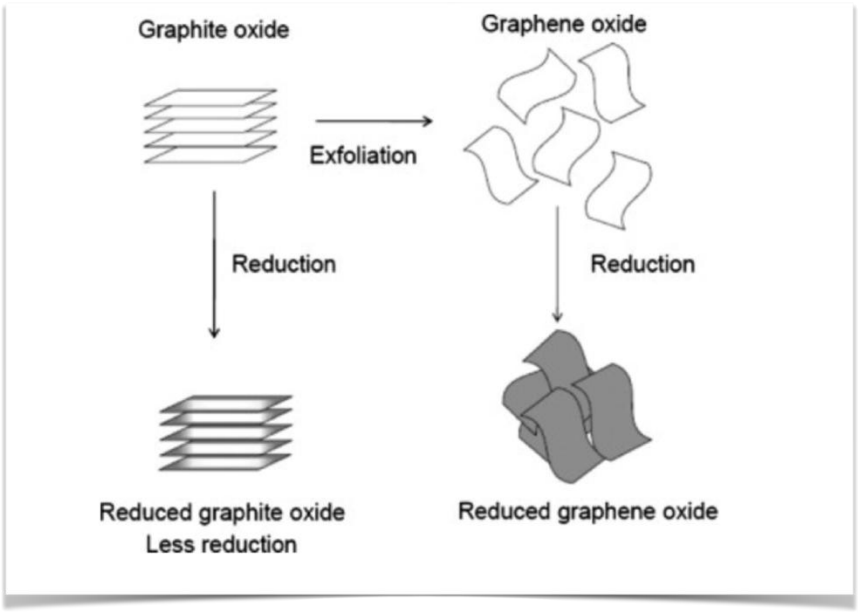

Figure 1.17 The effect of exfoliation of GO on the reduction degrees [77].

1.4.3.3 Hydrothermal and solvothermal reduction

Hydrothermal/solvothermal process is a powerful, facile and environmental friendly method to synthesize nanomaterials. It is a single pot process that is carried out in a closed system at a temperature close to the boiling point or above it in order to provide high pressure for production crystalline nanostructures. These methods are also applied for the reduction of GO. In hydrothermal method, water is used as a solvent and acts as a source of H^+ for protonation of hydroxyl groups [78]. The pH of solution is very important for this method. Highly reduced GO (HRG) is stable in basic solution while in acidic medium the HRG turned to be aggregated.

E.C. Vermisoglou [79] studied the effect of reaction time and alkaline media on the electrochemical properties of rGO obtained from hydrothermal reaction. Modified Staudenmaier's method was used for graphite oxide preparation. Hydrothermal synthesis was performed at 180 ºC for different reaction times of 4, 19, 22 and 24 hours, for pH adjustment K_2CO_3 was used. The higher degree of GO reduction was achieved through the higher reaction times. Moreover, the sample produced under alkaline media showed less defects and higher BET surface area. Highest capacitance performance was obtained for the sample produced under alkaline media for 19 h heating treatment. It was concluded that by manipulation of different factors in hydrothermal synthesis it is possible to tune the electrochemical performance of rGO.

Only water is used in hydrothermal while in solvothermal method different solvents can be used. So the later one is more favorable for the production of nonoxidized products, nonetheless both methods have shown to be successful in nanomaterials production [80].

Reduction of GO through solvothermal route was studied by H. Wang [81]. Graphite oxide was prepared by modified Hummer's method. N,N-dimethylformamide (DMF) was used as a solvent (~0.1mg/mL) and hydrazine monohydrate as a reducing agent and the suspension heated at 180 ºC. The effective reduction achieved by this method is the result of more removal of oxygen groups by hydrazine hydrate at high temperature however, the conductivity was poor due to the presence of structural defects.

1.5 Graphene based nanocomposites

The combination of graphene or graphene related materials with appropriate materials like polymers [82-84], organic molecules [85-87] or NPs [88] can give origin to new materials (nanocomposites) which exhibit different properties that arises from each individual components. For example, it was reported that addition of rGO in a Cu matrix improved the strength and enhanced the mechanical performance[89]. Also, the chemical doping of graphene films by $AuCl_3$ can improve the conductivity of graphene films [90]. Because of this, particular emphasis has been placed on strategies for the optimization of graphene based

nanocomposite properties. The advantages of graphene-based nanocomposites in several applications such as the Li-ion batteries, supercapacitors, fuel cells, photovoltaic devices and photocatalysis are of the huge importance and some examples will be discussed in the following sections.

1.5.1 Graphene nanoparticles nanocomposites

Due to the oxygen functional groups, GO and rGO are good substrates for nucleation and growth of various metals such as Ag [91], Au [92], Pt [93], Pd [94], Ni [95] or metal oxides such as Fe_3O_4 [96] or NiO [97] on their surfaces.

Based on the NPs structural morphology the graphene/NPs nanocomposites can be widely classified in two categories. First, graphene NPs nanocomposites in which NPs are grown on GO or rGO sheet with the size of few nm to hundred nm. The second is graphene-encapsulated NPs in which the big NPs are wrapped by graphene or rGO sheet [98]. There are two different routes for loading or binding metal or metal oxide NPs on GO or rGO known as ex situ hybridization and in situ growth, see Figure 1.18 [78]. In ex situ method, graphene or rGO nanosheets or/and NPs are functionalized and synthesized separately. The functionalization can be non-covalent stacking or can be the covalent C-C coupling reaction. This method is suffering from the low density of NPs and nonhomogeneous distribution of NPs [78]. In situ growth, that is most widely used, is based on using the salts containing metal ions as a source of metal NPs and GO as a substrate for their growth. The advantages of this method are the possibility of preparation the high-density NPs nanocomposite on which NPs are homogenously distributed in the composite matrix. There are different methods for in situ fabrication of rGO/NPs such as reduction procedure, hydrothermal or solvothermal methods [98].

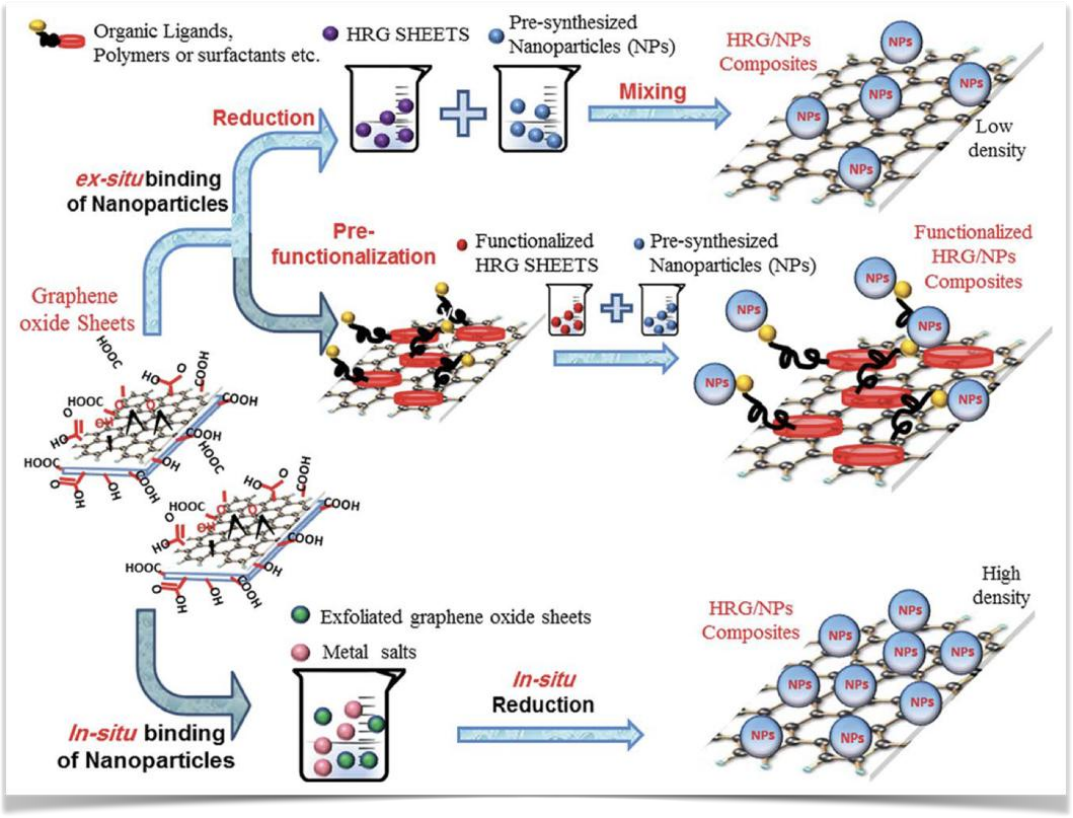

Figure 1.18 Schematic representation of different preparation of graphene/NPs composites [78].

Reduction procedure is a well-known method for the preparation of graphene/noble metal NPs nanocomposites. Noble NPs such as Ag and Au have unique properties such as biocompatibility and optical properties [99]. These NPs are widely used in the field of nanomedicine [100] , imaging [101] and diagnostic [102] ,[98]. Graphene has a high potential to be used as a support for noble metal NPs [103]. The high interaction between functionalized graphene with noble metals leads to high dispersion of catalysts and enhance the catalytic performance [104]. Noble metal NPs also act as a nano spacer and conductor preventing the agglomeration of graphene sheets, making the two sides of the sheets accessible and improving the conductivity [105]. Combining noble metals with graphene also improve the compatibility. For example GO-Ag composites have lower cytotoxicity and better blood compatibility than Ag NPs alone [106].

During the reduction method, the metallic ions present in the salts such as $AgNO_3$ or K_2PtCl_4 are reduced by chemical agents like ethylene glycol, sodium citrate or sodium borohydride. The decoration of rGO taking place in 3 steps: reduction, nucleation and crystal growth. First, the positive charged metal ions are electrostatically attracted by the negatively charged GO, and then by adding the reducing agent it simultaneously reduces the metallic ions and eliminates the oxygen groups. This reduction helps to preserve the 2D structure of rGO. Unlike the easiness and efficiency of the reduction route, this procedure is not promising to control the size and the morphology of NPs which normally present a wide size distribution.

To synthesize inorganic NPs with high crystallinity and narrow size distribution hydrothermal/solvothermal methods are more effective routes. These methodologies are mostly used for synthesizing metal oxide NPs/rGO composites such as Fe_3O_4 [107] ,TiO_2 [108], ZnO [109] , NiO [110]. The high pressure and temperature used in these methods are responsible for the growth of nanocrystals simultaneously with the reduction of GO. The combination of metal oxide with rGO also prevent the restacking of the graphene layers suppressing the agglomeration of particles that enhance the properties of both materials [98].

For example, Fe_3O_4/rGO nanocomposite prepared by the hydrothermal method showed the higher electrochemical performance when compared to bare Fe_3O_4, which could be applicable in lithium batteries [111].The high conductivity of rGO, nano sized and well distributed Fe_3O_4 are the main reasons for these properties enhancement.

S. Bai [112] reported the preparation of rGO supported ferrite (MFe_2O_4, M=Mn, Zn, Co and Ni) hybrids by one pot solvothermal synthesis route and tested their ability for the removal of organic dyes. It was indicated that when the high adsorption property of rGO is combined with the magnetic and photocatalytic properties of magnetic NPs, it brings the aforementioned criteria for environmental application. The size and size-distribution of NPs were adjusted by tuning the metal ion concentration. The high adsorption performance was achieved due to the high rGO surface area and high electrostatic interaction between dyes pollutants and rGO sheets. Considerable saturation magnetization also made possible that the hybrids could be harvested by a magnet after using.

The structure of the NPs obtained by hydrothermal/solvothermal method depends on different reaction parameters such as temperature, reaction time, solvent and reductant effect [113].

For example, the preparation of three different TiO_2/graphene nanosheets structures was reported by Z. He [114]. 12 nm spherical TiO_2 graphene sheets (STG), ultra-small 2 nm TiO_2 graphene nanosheets (USTG), and TiO_2 nanorod–graphene nanosheets (NRTG) were simply synthesized by adjusting the experimental conditions in one pot solvothermal method, see figure 1.19. This example shows the potential of the solvothermal method to control the NPs size by adjusting the reaction parameters.

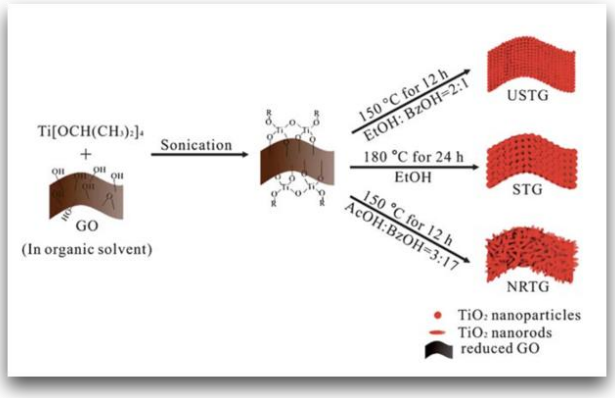

Figure 1.19 Different experimental conditions to synthesize different TiO_2/graphene nanosheets structure [114].

1.5.2 Graphene based nickel compound (nickel hydroxide, nickel oxide, nickel) nanocomposite

Nickel compounds have gained interest due to its multifunctional properties and can be used in different areas such as batteries [115], catalysts [116] and capacitors [117].

1.5.2.1 Reduced graphene oxide/ nickel hydroxide nanocomposite

$Ni(OH)_2$ is a promising anode material for supercapacitors due to its layered structure with large interlayer spacing and well defined electrochemical redox activity. It showed higher specific capacitance than traditional electrode material like RuO_2 related to pseudocapacitive

reaction during the charge and discharge process. The aggregation and restacking of this material during the process diminish the electrochemical performance. It is reported that using graphene not only prevents the aggregation but also enhances the conductivity which is in need for the electrode materials [118].

The properties of $Ni(OH)_2$ are size and morphology dependent. N.A Hoque [119] studied dielectric properties of spherical and nanoplate $Ni(OH)_2$ NPs prepared using hydrothermal process at 150°C for different reaction times. LiOH was used for pH adjustment. It was shown that for higher pH, it is possible to tune the NPs morphology from spherical to nanoplate by changing the reaction time. Also, increasing the reaction time increased the size of nanoplates. Well defined $Ni(OH)_2$ nanoplates sample was obtained under the higher pH and showed a low band gap of around 5.463 eV and a high dielectric constant about 3.12×10^5.

The electrochemical performances of $Ni(OH)_2$/rGO with different size and morphology have been investigated [120,121]. For example, W. Liu [122] reported the preparation of $Ni(OH)_2$ nanowires on rGO synthesized by one step reactable ionic liquid 1-hexadecyl-3-methylimidazolium trifluoroacetate as template assisted hydrothermal method. This nanocomposite showed specific capacitance of ~1875 F g^{-1} at 1 A g^{-1} in 6 M KOH aqueous solution. It was mentioned that the nanowire structure of $Ni(OH)_2$ provide short path length diffusion of electrolyte that enhances the electrochemical performance.

Synthesis of ultra-thin porous $Ni(OH)_2$ nanosheets/rGO was reported by X. Zang [123]. This nanocomposite was prepared through solvothermal method and showed high specific capacitance 1886 F g^{-1} at 5 A g^{-1} and 1362 F g^{-1} at 30 A g^{-1}. The porous structure of $Ni(OH)_2$ nanosheets increases the active sites by increasing the transport and diffusion of electrolyte ions during charge and discharge reaction.

1.5.2.2 Reduced graphene oxide/ nickel oxide nanocomposite

Another nickel compound, NiO, is one of the most important among the transition metal oxides due to its various properties such as low cost, magnetic properties, high theoretical

capacity (2573 F g^{-1}) and high electrochemical performance. Different NiO nanostructures such as NPs [124], nanowires [125], nanoflowers [126], have been mostly studied as electrode materials for supercapacitors. Unfortunately, NiO suffers from low conductivity and easy agglomeration, which inhibit its functionalities. The incorporation of NiO into a flexible, high surface, conductive matrix like graphene could highly increase its capability for extreme performance [127-130].

For example 2D graphene/ 2D NiO structure has been prepared and suggested for gas sensing application[131]. Porous structure of 2D NiO on rGO was prepared using spray coating of GO and Ni-seed solution on a sensing electrode combined with an annealing treatment. This 2D hybrid material showed higher sensitivity toward NO_2, H_2, NH_3 and H_2S when compared to bare NiO nanosheets due to the charge transfer between NiO and rGO. The NiO grown on rGO showed high crystallinity with a specific orientation that might be responsible for NiO hierarchical structure that increases the responsivity towards NO_2. Porous flower like NiO/graphene composite using a combined hydrothermal-annealing methodology was reported by L. Wang [132]. This nanocomposite showed strong microwave absorption properties due to the special structure that provides high surface area for trapping the electromagnetic radiation. A light weight and long-range bandwidth absorption are important criteria for an ideal microwave absorption material.

Tuning the synthesis conditions can result for better performance of rGO/NiO nanocomposites. For instance, the effect of calcination temperature (250 ºC, 300 ºC, 400 ºC, 500 ºC) on the electrochemical performance of NiO/rGO nanocomposite was studied by G. Chen [133]. It was indicated that the nanocomposite calcined at lower temperature has more defects on the surface which improves the surface electrochemical activity. Moreover, smaller NiO NPs obtained at lower temperature boosted the electrochemical performance due to the charge transfer improvement.

1.5.2.3 Reduced graphene oxide/ nickel nanocomposite

Nickel is a ductile and inexpensive metal. It has tremendous potential in different application due to the high catalytic [134] and magnetic properties [135]. Usually it is used as a cathode material for fuel cells and capacitors. Its ferromagnetic property make it recoverable from catalytic processes[136].

The innate properties of Ni can be tuned by manipulation of its size and the structure [137]. For example, nano Ni exhibits high catalytic activity in hydrogenation. This catalytic activity increase with decreasing the size of the NPs [138,139]. Generally, when the NPs size decreases to the less than 10 nm it drastically changes the physical properties, these changes are more pronounced when the size become less than 3nm [137].

Ni can be considered as a promising electromagnetic (EM) absorption materials. Various studies reported on EM absorption potential of different structure of metallic Ni such as ultrafine fiber [140], hierarchical branch like and flower like [141], nanowires [142] and urchin like Ni [143]. Ni NPs are magnetic loss absorbents, if they are integrated with an effective dielectric EM absorber like graphene making better impedance matching between them will enhances the EM absorption properties[144]. Recent urchin like Ni/rGO composite and Ni microspheres/rGO prepared by one pot solvothermal method showed extra ordinary EM absorption properties due to its multiple absorption mechanism [145,146].

Bare Ni NPs are unstable and prone to get oxidized in air; however, in rGO matrix they are more stabilized. This stabilization is due to the existence of free electrons on the surface of rGO that helps metallic Ni remains in its zero-valent state and doesn’t get oxidized to high oxidation state showing a better performance for catalytic applications. rGO/Ni nanocomposite has been reported as a potential catalyst for the reduction of highly toxic aqueous Cr(VI) at room temperature [147].

A facile synthesis of rGO decorated with hexagonal Ni NPs was reported by Zhenyuan [148]. This nanocomposite showed an excellent catalytic property comparing to noble metal catalysts to reduce the p-nitrophenol, a common organic pollutant in agriculture, in the

presence of $NaBH_4$. It also showed the high electrocatalytic activity towards the oxidation of glucose which can be used in biosensing application.

Improvement of hydrogen sorption properties of MgH_2 was investigated in the presence of Ni@rGO nanocomposite. A porous Ni@rGO was synthesized by polyol method and mixed with MgH_2 powder. It was found that the presence of Ni@rGO had a good catalytic effect on de/hydrogenation of MgH_2. It was mentioned the Ni NPs were responsible for the faster sorption kinetic of MgH_2 and rGO was useful preventing the hydride sintering and agglomeration that caused the cyclic stability [149].

Y.J. Mai reported the synthesis of graphene anchored with Ni NPs with the size of 10 nm as a high performance anode material for lithium ion battery [150]. The reversible capacity obtained was 675 mAh g^{-1}, which is a larger reversible capacity when compared to the bare graphene electrode. It was explained that this improvement was achieved due to the thickness optimization of solid electrolyte interface (SEI). Through the synthesis of graphene/Ni hybrid the Ni NPs cover some parts of the active sites of graphene surface which are favorable sites to form SEI. SEI is a layer of mosaic structure which is forming on the surface of negative electrode due to the different electrolyte degradation and lithium salt hydrolysis containing lithium fluoride, lithium oxide and/or lithium carbonate. SEI is one of the important factors for the battery performance which has been a subject for several studies of rechargeable batteries [151,152]. Conductive networks of graphene/Ni NPs is another advantage of this nanocomposite which makes the anode more bearable and tolerant during the high current flow.

Recently Ni NPs decorated rGO sheets has been studied as a solid-state material for hydrogen storage. A. sigal [153] used density functional theory (DFT) for studying the hydrogen storage on graphene/Ni system. It was shown that decoration of graphene with Ni NPs enhances the hydrogen uptake when compared to the bare graphene sheet.

Enhancement of hydrogen adsorption on graphene decorated Ni experimentally was also confirmed by M. Gaboardi [154]. In this study, thermally exfoliated graphite oxide was synthesized and further was chemically functionalized with Ni NPs under oxygen free

condition. The maximum amount of hydrogen uptake by this system was 1.15 mass% at 77K and was reported lesser at elevated temperature. In addition, it was proved that the hydrogen adsorption was fully reversible after several sorption and desorption cycles.

The hydrogen storage capacity (HSC) on rGO doped Ni NPs were also reported by N. Ismail [155]. In this study, the authors compared the HSC and the kinetics of hydrogen up take of the graphene doped with Ni and Pd NPs (5 and 10 wt% Pd or Ni) showing that under the reported experimental conditions, Pd presented a catalytic effect on hydrogen uptake at 80 K and 300 K, while doping with Ni enhanced the HSC only at 80 K but it showed a negative influence on hydrogen adsorption at 300 K. According to the authors, this ambiguous behavior might be because the Ni NPs were in the form of oxide and hydroxide that could hinder the hydrogen uptake at 300 K.

1.6 Thesis outline

This thesis is organized in 5 chapters.

Chapter 1 is this present introduction that contains a literature review and fundamental concepts of graphene, graphene derivatives, graphene based nanocomposites, synthesis and applications.

Chapter 2 is based on a published paper in a peer reviewed journal with addition of some extra supporting data. This chapter refers to the synthesis and characterization of Ni NPs/rGO by hydrothermal method and discuss about the roles of different synthesis parameters on the structure of final products. The role of the reducing agent on the size and morphology of the obtained Ni NPs is discussed in details. Moreover, the electrical properties of nanocomposite with spiky Ni morphology are characterized and its potential application in nanoelectronic area is discussed.

Chapter 3 is under review for submission to a peer reviewed journal. This chapter contains materials describing a solvothermal method for preparation of nanosized Ni decorated rGO. The effect of synthesis parameters on controlling the size of Ni NPs and the structure of rGO is discussed. The effect of the size and structure of Ni NPs on electrophysical properties of Ni/rGO nanocomposite is explored and discussed in details.

Chapter 4 refers to the study of the effect of heating treatment on the structure of Ni NPs and rGO in Ni/rGO nanocomposites obtained through the solvothermal method. The migration of Ni NPs on the rGO surface under intense heating treatment is characterized and discussed.

Chapter 5 is the final chapter that presents the main conclusions of the work of this present thesis and possible outline directions for the future research.

1.7 Bibliography

[1] A. Aqel, K. M. M. A. El-Nour, R. A. A. Ammar, and A. Al-Warthan, "Carbon nanotubes, science and technology part (I) structure, synthesis and characterization," *Arab. J. Chem.*, vol. 5, no. 1, pp. 1–23, 2012.

[2] "Diamond blade having segment type cutting tip for use in cutting, grinding or drilling apparatus," 1999.

[3] T. D. Burchell and J. P. Strizak, "The effect of neutron irradiation on the fracture toughness of graphite," *Nucl. Eng. Des.*, vol. 271, pp. 262–269, 2014.

[4] J. Fuchs and M. Goerbig, "Introduction to the physical properties of graphene," *Lect. Notes*, 2008.

[5] F. D. M. Haldane, "Model for a Quantum Hall Effect without Landau Levels: Condensed-Matter Realization of the "Parity Anomaly&quot," *Phys. Rev. Lett.*, vol. 61, no. 18, pp. 2015–2018, 1988.

[6] P. R. Wallace, "The Band Theory of Graphite," *Phys. Rev.*, vol. 71, no. 9, pp. 622–634, 1947.

[7] L. Landau, "Zur Theorie der Phasenumwandlungen II," *Phys. Z. Sowjet*, vol. 11, pp. 26–35, 1937.

[8] I. D. Vagner, "Thermodynamics of two-dimensional electrons on Landau levels," *HIT J. Sci. Eng. A*, vol. 3, no. 1, pp. 102–152.

[9] A. K. Geim and K. S. Novoselov, "The rise of graphene," *Nat. Mater.*, vol. 6, no. 3, pp. 183–191, 2007.

[10] K. S. Novoselov, A.K. Geim, S.V. Morosov, D. Jiang, Y. Zhang, S.V. Dubonos, I.V. Grigorieva and A.A. Firsov "Electric Field Effect in Atomically Thin Carbon Films," *Science* vol. 306, no. 5696, pp. 666-669, 2004.

[11] M. Khan, M.N. Tahir, S.F. Adil, H.U. Khan, M.R.H. Siddiqui, A.A. Alwarthan and W. Tremel "Graphene based metal and metal oxide nanocomposites: synthesis, properties and their applications," *J. Mater. Chem. A*, vol. 3, no. 37, pp. 18753–18808, 2015.

[12] W. W. Liu and J. N. Wang, "Direct exfoliation of graphene in organic solvents with addition of NaOH," *Chem. Commun. (Camb).*, vol. 47, no. 24, pp. 6888–90, 2011.

[13] S. Stankovich, D.A. Dikin, R.D. Piner, K.A. Kohlhaas, A. Kleinhammes, Y. Jia, Y. Wu, S.T. Nguyen and R.S. Ruoff "Synthesis of graphene-based nanosheets via chemical reduction of exfoliated graphite oxide," *Carbon N. Y.*, vol. 45, no. 7, pp. 1558–1565,

2007.

[14] S. Pei and H. M. Cheng, "The reduction of graphene oxide," *Carbon*, vol. 50, no. 9. Pergamon, pp. 3210–3228, 2012.

[15] S. Abdolhosseinzadeh, H. Asgharzadeh, and H. Seop Kim, "Fast and fully-scalable synthesis of reduced graphene oxide," *Sci. Rep.*, vol. 5, no. 1, p. 10160, 2015.

[16] A. N. Obraztsov, "Chemical vapour deposition: Making graphene on a large scale," *Nat. Nanotechnol.*, vol. 4, no. 4, pp. 212–213, 2009.

[17] A. Reina, X. Jia, J. Ho, D. Nezich, H. Son, V. Bulovic, M.S. Dresselhaus and J. Kong "Large area, few-layer graphene films on arbitrary substrates by chemical vapor deposition," *Nano Lett.*, vol. 9, no. 1, pp. 30–35, 2009.

[18] Y. Zhang, L. Zhang, and C. Zhou, "Review of chemical vapor deposition of graphene and related applications," *Acc. Chem. Res.*, vol. 46, no. 10, pp. 2329–2339, 2013.

[19] K. V. Emtsev, F. Speck, T. Seyller, L. Ley, and J. D. Riley, "Interaction, growth, and ordering of epitaxial graphene on SiC {0001} surfaces: A comparative photoelectron spectroscopy study," *Phys. Rev. B - Condens. Matter Mater. Phys.*, vol. 77, no. 15, p. 155303, 2008.

[20] W. Yang, G. Chen, Z. Shi, C.C. Liu, L. Zhang, G. Xie, M. Cheng, D. Wang "Epitaxial growth of single-domain graphene on hexagonal boron nitride," *Nat. Mater.*, vol. 12, no. 9, pp. 792–797, 2013.

[21] P. W. Sutter, J.-I. Flege, and E. A. Sutter, "Epitaxial graphene on ruthenium," *Nat. Mater.*, vol. 7, no. 5, pp. 406–411, 2008.

[22] J. M. Tour, "Top-Down versus Bottom-Up Fabrication of Graphene-Based Electronics," *Chem. Mater.*, vol. 26, no. 1, pp. 163–171, 2014.

[23] R. Van Noorden, "Production: Beyond sticky tape," *Nature*, vol. 483, no. 7389, pp. S32–S33, 2012.

[24] L. Niu, J. N. Coleman, H. Zhang, H. Shin, M. Chhowalla, and Z. Zheng, "Production of Two-Dimensional Nanomaterials via Liquid-Based Direct Exfoliation," *Small*, vol. 12, no. 3, pp. 272–293, 2016.

[25] J. Low, B. Cheng, J. Yu, and M. Jaroniec, "Carbon-based two-dimensional layered materials for photocatalytic CO2 reduction to solar fuels," *Energy Storage Mater.*, vol. 3, pp. 24–35, 2016.

[26] E. Jimenez, C. Amieva, J. L. Barroso, A. Laura, M. Hernández, and C. V. Santos, "Graphene-Based Materials Functionalization with Natural Polymeric Biomolecules," in *World's largest Science Techonology&Medicine*, InTech, 2016, p. 43.

[27] A. N. Obraztsov, “Chemical vapour deposition: Making graphene on a large scale,” *Nat. Nanotechnol.*, vol. 4, no. 4, pp. 212–213, 2009.

[28] Y. Zhang, L. Zhang, and C. Zhou, “Review of Chemical Vapor Deposition of Graphene and Related Applications,” *Acc. Chem. Res.*, vol. 46, no. 10, pp. 2329–2339, 2013.

[29] Q. Yu, J. Lian, S. Siriponglert, H. Li, Y. P. Chen, and S.-S. Pei, “Graphene segregated on Ni surfaces and transferred to insulators,” *Appl. Phys. Lett.*, vol. 93, no. 11, p. 113103, 2008.

[30] X. Li, W. Cai, J. An, S. Kim, J. Nah, D. Yang, R. Piner and A. Velamakanni “Large-Area Synthesis of High-Quality and Uniform Graphene Films on Copper Foils,” *Science*, vol. 324, no. 5932, pp. 1312-1314, 2009.

[31] X. Li, W. Cai, L. Colombo, and R. S. Ruoff, “Evolution of Graphene Growth on Ni and Cu by Carbon Isotope Labeling,” *Nano Lett.*, vol. 9, no. 12, pp. 4268–4272, 2009.

[32] M. A. Azam, N.N. Zulkaply, N. Dorah, R.N.A.R. Seman, M.H. Ani, M.S. Sirat, E. Ismail, F.B. Fauzi, M.A. Mohamed and B.Y. Majlis “Review—Critical Considerations of High Quality Graphene Synthesized by Plasma-Enhanced Chemical Vapor Deposition for Electronic and Energy Storage Devices,” *ECS J. Solid State Sci. Technol.*, vol. 6, no. 6, pp. 3035–3048, 2017.

[33] R. Muñoz and C. Gómez-Aleixandre, “Review of CVD Synthesis of Graphene,” *Chem. Vap. Depos.*, vol. 19, no. 10-11–12, pp. 297–322, 2013.

[34] X. Li, L. Colombo, and R. S. Ruoff, “Synthesis of Graphene Films on Copper Foils by Chemical Vapor Deposition,” *Adv. Mater.*, vol. 28, no. 29, pp. 6247–6252, 2016.

[35] J.-K. Zheng, Qingbin, Kim, “Synthesis, Structure, and Properties of Graphene and Graphene Oxide,” *Graphene Transparent Conduct.*, pp. 1–220, 2015.

[36] H. Huang, W. Chen, S. Chen, and A. T. S. Wee, “Bottom-up growth of epitaxial graphene on 6H-SiC (0001),” *ACS Nano*, vol. 2, no. 12, pp. 2513–2518, 2008.

[37] B. Sharma, T. Schumann, M. H. Oliveira Jr., and J. M. J. Lopes, “Controlled synthesis and characterization of multilayer graphene films on the C-face of silicon carbide,” *Phys. Status Solidi*, p. 1600721, 2017.

[38] W. Norimatsu and M. Kusunoki, “Epitaxial graphene on SiC {0001}: advances and perspectives,” *Phys. Chem. Chem. Phys.*, vol. 16, no. 16, pp. 3501–3511, 2014.

[39] B. C. Brodie, “On the Atomic Weight of Graphite,” *Philos. Trans. R. Soc. London*, vol. 149, no. 0, pp. 249–259, 1859.

[40] L. Staudenmaier, “Verfahren zur Darstellung der Graphits??ure,” *Berichte der Dtsch. Chem. Gesellschaft*, vol. 31, no. 2, pp. 1481–1487, 1898.

[41] D. R. Dreyer, S. Park, C. W. Bielawski, and R. S. Ruoff, “The chemistry of graphene oxide,” *Chem. Soc. Rev.*, vol. 39, no. 1, pp. 228–240, 2010.

[42] W. S. Hummers and R. E. Offeman, “Preparation of Graphitic Oxide,” *J. Am. Chem. Soc.*, vol. 80, no. 6, pp. 1339–1339, 1958.

[43] N. I. Zaaba, K. L. Foo, U. Hashim, S. J. Tan, W.-W. Liu, and C. H. Voon, “Synthesis of Graphene Oxide using Modified Hummers Method: Solvent Influence,” *Procedia Eng.*, vol. 184, no. 184, pp. 469–477, 2017.

[44] N. I. Kovtyukhova, P.J. Ollivier, B.R. Martin, T.E. Mallouk, S.A. Chizhik, E.V. Buzaneva and A.D. Gorchinskiy “Layer-by-Layer Assembly of Ultrathin Composite Films from Micron-Sized Graphite Oxide Sheets and Polycations,” *Chem. Mater.*, vol. 11, no. 3, pp. 771–778, 1999.

[45] D. C. Marcano, D.V. Cosynkin, J.M. Berlin, A. Sinitskii, Z. Sun, A. Slesarev, L.B. Alemany, W. Lu and J.M. Tour “Improved synthesis of graphene oxide,” *ACS Nano*, vol. 4, no. 8, pp. 4806–4814, 2010.

[46] A. M. Dimiev and J. M. Tour, “Mechanism of graphene oxide formation,” *ACS Nano*, vol. 8, no. 3, pp. 3060–3068, 2014.

[47] K. A. Mkhoyan, A.w. Contryman, J. Silcox, D.A. Stewart, G. Eda, C. Mattevi, C. Miller and M. Chhowalla “Atomic and Electronic Structure of Graphene-Oxide.” *Nano Letter*, Vol. 9, no. 3, pp 1058-1063, 2009.

[48] K. Krishnamoorthy, M. Veerapandian, K. Yun, and S. J. Kim, “The chemical and structural analysis of graphene oxide with different degrees of oxidation,” *Carbon N. Y.*, vol. 53, pp. 38–49, 2013.

[49] M. Mermoux, Y. Chabre, and A. Rousseau, “FTIR and 13C NMR study of graphite oxide,” *Carbon N. Y.*, vol. 29, no. 3, pp. 469–474, 1991.

[50] U. Hofmann and R. Holst, “Über die Säurenatur und die Methylierung von Graphitoxyd,” *Berichte der Dtsch. Chem. Gesellschaft (A B Ser.*, vol. 72, no. 4, pp. 754–771, 1939.

[51] G. Ruess, “Über das Graphitoxyhydroxyd (Graphitoxyd),” *Monatshefte für Chemie*, vol. 76, no. 3–5, pp. 381–417, 1947.

[52] W. Scholz and H. P. Boehm, “Untersuchungen am Graphitoxid. VI. Betrachtungen zur Struktur des Graphitoxids,” *ZAAC J. Inorg. Gen. Chem.*, vol. 369, no. 3–6, pp. 327–340, 1969.

[53] T. Nakajima, A. Mabuchi, and R. Hagiwara, “A new structure model of graphite oxide,” *Carbon N. Y.*, vol. 26, no. 3, pp. 357–361, 1988.

[54] A. Lerf, H. He, M. Forster, and J. Klinowski, “Structure of Graphite Oxide Revisited,” *J. Phys. Chem. B*, vol. 102, no. 23, pp. 4477–4482, 1998.

[55] A. M. Dimiev, L. B. Alemany, and J. M. Tour, “Graphene oxide. Origin of acidity, its instability in water, and a new dynamic structural model,” *ACS Nano*, vol. 7, no. 1, pp. 576–588, 2013.

[56] K. Erickson, R. Erni, Z. Lee, N. Alem, W. Gannett, and A. Zettl, “Determination of the local chemical structure of graphene oxide and reduced graphene oxide,” *Adv. Mater.*, vol. 22, no. 40, pp. 4467–4472, 2010.

[57] S. H. Dave, C. Gong, A. W. Robertson, J. H. Warner, and J. C. Grossman, “Chemistry and Structure of Graphene Oxide via Direct Imaging,” *ACS Nano*, vol. 10, no. 8, pp. 7515–7522, 2016.

[58] J. P. Rourke, P.A. Pandey, J.J. Moore, M. Bates, I.A. Kinloch, R.J. Young and N.R. Wilson “The real graphene oxide revealed: Stripping the oxidative debris from the graphene-like sheets,” *Angew. Chemie - Int. Ed.*, vol. 50, no. 14, pp. 3173–3177, 2011.

[59] G. Goncalves, P. A. A. P. Marques, C. M. Granadeiro, H. I. S. Nogueira, M. K. Singh, and J. Grácio, “Surface modification of graphene nanosheets with gold NPs: The role of oxygen moieties at graphene surface on gold nucleation and growth,” *Chem. Mater.*, vol. 21, no. 20, pp. 4796–4802, 2009.

[60] G. Gonçalves, M. Vila, M. T. Portolés, M. Vallet-Regi, J. Gracio, and P. A. A. P. Marques, “Nano-graphene oxide: A potential multifunctional platform for cancer therapy,” *Adv. Healthc. Mater.*, vol. 2, no. 8, pp. 1072–1090, 2013.

[61] G. Gonçalves, P.A.A.P. Marques, A.B. Timmons, I. Bdkin, N. Emami and J.J. Grácio “Graphene oxide modified with PMMA via ATRP as a reinforcement filler,” *J. Mater. Chem.*, vol. 20, no. 44, p. 9927, 2010.

[62] S. Eigler, S. Grimm, M. Enzelberger-Heim, P. Müller, and A. Hirsch, “Graphene oxide: efficiency of reducing agents,” *Chem. Commun.*, vol. 49, no. 67, p. 7391, 2013.

[63] H. C. Schniepp, J.L. Li, M.J. McAllister, H. Sai, M.H. Alonso, D.H. Adamson, R.K. Prud'homme, R.Car, D.A. Saville and I.A. Aksay “Functionalized single graphene sheets derived from splitting graphite oxide,” *J. Phys. Chem. B*, vol. 110, no. 17, pp. 8535–8539, 2006.

[64] M. J. McAllister, J.L. Li, D.H. Adamson, H.C. Schniepp, A.A. Abdala, J. Liu, M.H. Alonso, D.L. Milius, R. Car, R.K. Prud'homme and I.A. Aksay “Single sheet functionalized graphene by oxidation and thermal expansion of graphite,” *Chem. Mater.*, vol. 19, no. 18, pp. 4396–4404, 2007.

[65] B. Shen, D. Lu, W. Zhai, and W. Zheng, “Synthesis of graphene by low-temperature

exfoliation and reduction of graphite oxide under ambient atmosphere," *J. Mater. Chem. C*, vol. 1, no. 1, pp. 50–53, 2013.

[66] A. Kaniyoor, T. T. Baby, and S. Ramaprabhu, "Graphene synthesis via hydrogen induced low temperature exfoliation of graphite oxide," *J. Mater. Chem.*, vol. 20, no. 39, p. 8467, 2010.

[67] X. Chen, D. Meng, B. Wang, B.W. Li, W. Li, C.W. Bielawski and R.S. Ruoff "Rapid thermal decomposition of confined graphene oxide films in air," *Carbon N. Y.*, vol. 101, pp. 71–76, 2016.

[68] S. Bai and X. Shen, "Graphene–inorganic nanocomposites," *RSC Adv.*, vol. 2, no. 1, pp. 64–98, 2012.

[69] S. Stankovich, D.A. Dikin, R.D. Piner, K.A. Kohlhaas, A. Kleinhammes, Y. Jia, Y. Wu, S.T. Nguyen and R.S. Ruoff "Synthesis of graphene-based nanosheets via chemical reduction of exfoliated graphite oxide," *Carbon N. Y.*, vol. 45, no. 7, pp. 1558–1565, 2007.

[70] O. C. Compton, D. A. Dikin, K. W. Putz, L. C. Brinson, and S. T. Nguyen, "Electrically conductive 'alkylated' graphene paper via chemical reduction of amine-functionalized graphene oxide paper," *Adv. Mater.*, vol. 22, no. 8, pp. 892–896, 2010.

[71] W. Gao, L. B. Alemany, L. Ci, and P. M. Ajayan, "New insights into the structure and reduction of graphite oxide," *Nat. Chem.*, vol. 1, no. 5, pp. 403–408, 2009.

[72] M. R. Muda, M.M. Ramil, S.S. Mat Isa, M.F. Jamlos, S.A.Z. Murad, Z. Norhanisah, M.M. Isa, S.R. Kasjoo, N. Ahmed, N.I.M. Nor and N. Khalid "Fundamental study of reduction graphene oxide by sodium borohydride for gas sensor application," 2017, p. 20034.

[73] G. Wang, J. Young, J. Park, X. Gou, B. Wang, H. Liu and J. Yao "Facile Synthesis and Characterization of Graphene Nanosheets," *J. Phys. Chem. C*, vol. 112, no. 22, pp. 8192–8195, 2008.

[74] M. C. Kim, G. S. Hwang, and R. S. Ruoff, "Epoxide reduction with hydrazine on graphene: A first principles study," *J. Chem. Phys.*, vol. 131, no. 6, p. 64704, 2009.

[75] P. Zhu, M. Shen, S. Xiao, and D. Zhang, "Experimental study on the reducibility of graphene oxide by hydrazine hydrate," *Phys. B Condens. Matter*, vol. 406, no. 3, pp. 498–502, 2011.

[76] P.-G. Ren, D.-X. Yan, X. Ji, T. Chen, and Z.-M. Li, "Temperature dependence of graphene oxide reduced by hydrazine hydrate," *Nanotechnology*, vol. 22, no. 5, p. 55705, 2011.

[77] S. Park, J. An, J. R. Potts, A. Velamakanni, S. Murali, and R. S. Ruoff, "Hydrazine-reduction of graphite- and graphene oxide," *Carbon N. Y.*, vol. 49, no. 9, pp. 3019–3023, 2011.

[78] M. Khan, M.N. Tahir, S.F. Adil, H.U. Khan, M.R.H. Siddiqui, A.A. Alwarthan and W. Tremel "Graphene based metal and metal oxide nanocomposites: synthesis, properties and their applications," *J. Mater. Chem. A*, vol. 3, no. 37, pp. 18753–18808, 2015.

[79] E. C. Vermisoglou, T. Giannakopoulou, G. Giannouri, N. Boukos, C. Lei, C. Lekakou and C. Trapalis "Effect of hydrothermal reaction time and alkaline conditions on the electrochemical properties of reduced graphene oxide," *Applied Surface Science*, 2015, vol. 358, pp. 100–109.

[80] G. Zou, H. Li, Y. Zhang, K. Xiong, and Y. Qian, "Solvothermal/hydrothermal route to semiconductor nanowires," *Nanotechnology*, vol. 17, no. 11, pp. S313–S320, 2006.

[81] H. Wang, J. T. Robinson, X. Li, and H. Dai, "Solvothermal reduction of chemically exfoliated graphene sheets," *J. Am. Chem. Soc.*, vol. 131, no. 29, pp. 9910–9911, 2009.

[82] T. Ramanathan, A.A. Abdala, S. Stankovich, D.A. Dikin, M.H. Alonso, R.D. Piner, D.H. Adamson, H.C. Schniepp, X. Chen, R.S. Ruoff, S.T. Nguyen, I.A. Aksay, R.K. Prud'Homme and L.C. Brinson "Functionalized graphene sheets for polymer nanocomposites," *Nat. Nanotechnol.*, vol. 3, no. 6, pp. 327–331, 2008.

[83] H. Kim, A. A. Abdala, and C. W. MacOsko, "Graphene/polymer nanocomposites," *Macromolecules*, vol. 43, no. 16. American Chemical Society, pp. 6515–6530, 2010.

[84] A. K. Naskar, J. K. Keum, and R. G. Boeman, "Polymer matrix nanocomposites for automotive structural components," *Nat. Nanotechnol.*, vol. 11, no. 12, pp. 1026–1030, 2016.

[85] R. A. Bueno, J.I. Martínes, R.F. Luccas, N.R. Árbol, C. Munuera, I. Palacio, F.J. Palomares, K. Lauwaet, S. Thakur, J.M. Baranowski, W. Strupinski, M.F. López, F. Mompean, M.G. Hernández and J.A.M. Gago "Highly selective covalent organic functionalization of epitaxial graphene," *Nat. Commun.*, vol. 8, no. May, p. 15306, 2017.

[86] A. Wang, W. Yu, Z. Huang, F. Zhou, J. Song, Y. Song, L. Long, M.P. Cifuentes, M.G. Humphrey, L. Zhang, J. Shao, C. Zhang "Covalent functionalization of reduced graphene oxide with porphyrin by means of diazonium chemistry for nonlinear optical performance," *Sci. Rep.*, vol. 6, p. 23325, 2016.

[87] K. Morioku, N. Morimoto, Y. Takeuchi, and Y. Nishina, "Concurrent Formation of Carbon–Carbon Bonds and Functionalized Graphene by Oxidative Carbon-Hydrogen Coupling Reaction," *Sci. Rep.*, vol. 6, p. 25824, 2016.

[88] A. Allain, Z. Han, and V. Bouchiat, "Electrical control of the superconducting-to-insulating transition in graphene–metal hybrids," *Nat. Mater.*, vol. 11, no. 7, pp. 590–594, 2012.

[89] Q. Zhang, Z. Qin, Q. Luo, Z. Wu, L. Liu, B. Shen and W. Hu "Microstructure and nanoindentation behavior of Cu composites reinforced with graphene nanoplatelets by electroless co-deposition technique," *Sci. Rep.*, vol. 7, no. 1, p. 1338, 2017.

[90] K. K. Kim, A. Reina, Y. Shi, H. Park, L.J. Li, Y.H. Lee and J. Kong "Enhancing the conductivity of transparent graphene films via doping," *Nanotechnology*, vol. 21, no. 28, pp. 285205, 2010.

[91] K. Spilarewicz-Stanek, A. Kisielewska, J. Ginter, K. Bałuszyńska, and I. Piwoński, "Elucidation of the function of oxygen moieties on graphene oxide and reduced graphene oxide in the nucleation and growth of silver NPs," *RSC Adv.*, vol. 6, no. 65, pp. 60056–60067, 2016.

[92] X. Dong, W. Huang, and P. Chen, "In Situ Synthesis of Reduced Graphene Oxide and Gold Nanocomposites for Nanoelectronics and Biosensing," *Nanoscale Res. Lett.*, vol. 6, no. 1, pp. 1–6, 2011.

[93] Y. Li, W. Gao, L. Ci, C. Wang, and P. M. Ajayan, "Catalytic performance of Pt NPs on reduced graphene oxide for methanol electro-oxidation," *Carbon N. Y.*, vol. 48, no. 4, pp. 1124–1130, 2010.

[94] A. Krittayavathananon, P. Srimuk, S. Luanwuthi, and M. Sawangphruk, "Palladium NPs decorated on reduced graphene oxide rotating disk electrodes toward ultrasensitive hydrazine detection: Effects of particle size and hydrodynamic diffusion," *Anal. Chem.*, vol. 86, no. 24, pp. 12272–12278, 2014.

[95] Z. Ji, X. Shen, G. Zhu, H. Zhou, and A. Yuan, "Reduced graphene oxide/nickel nanocomposites: facile synthesis, magnetic and catalytic properties," *J. Mater. Chem.*, vol. 22, no. 8, pp. 3471, 2012.

[96] X. Ma, H. Tao, K. Yang, L. Feng, L. Cheng, X. Shi, Y. Li, L. Guo and Z. Liu "A functionalized graphene oxide-iron oxide nanocomposite for magnetically targeted drug delivery, photothermal therapy, and magnetic resonance imaging," *Nano Res.*, vol. 5, no. 3, pp. 199–212, 2012.

[97] X. Zhu, H. Dai, J. Hu, L. Ding, and L. Jiang, "Reduced graphene oxide-nickel oxide composite as high performance electrode materials for supercapacitors," *J. Power Sources*, vol. 203, pp. 243–249, 2012.

[98] P. T. Yin, S. Shah, M. Chhowalla, and K. B. Lee, "Design, synthesis, and characterization of graphene-nanoparticle hybrid materials for bioapplications,"

Chemical Reviews, vol. 115, no. 7. American Chemical Society, pp. 2483–2531, 2015.

[99] S. Eustis and M. A. El-Sayed, "Why gold NPs are more precious than pretty gold: Noble metal surface plasmon resonance and its enhancement of the radiative and nonradiative properties of nanocrystals of different shapes," *Chem. Soc. Rev.*, vol. 35, no. 3, pp. 209–217, 2006.

[100] S. Gurunathan, J.W. Han, J.H. Park, E. Kim, Y.J. Choi, D.N. Kwon and J.H. Kim "Reduced graphene oxide-silver nanoparticle nanocomposite: A potential anticancer nanotherapy," *Int. J. Nanomedicine*, vol. 10, pp. 6257–6276, 2015.

[101] C. Loo, A. Lowery, N. Halas, J. West, and R. Drezek, "Immunotargeted nanoshells for integrated cancer imaging and therapy," *Nano Lett.*, vol. 5, no. 4, pp. 709–711, 2005.

[102] D. P. O'Neal, L. R. Hirsch, N. J. Halas, J. D. Payne, and J. L. West, "Photo-thermal tumor ablation in mice using near infrared-absorbing NPs," *Cancer Lett.*, vol. 209, no. 2, pp. 171–176, 2004.

[103] H. He and C. Gao, "Graphene nanosheets decorated with Pd, Pt, Au, and Ag NPs: Synthesis, characterization, and catalysis applications," *Sci. China Chem.*, vol. 54, no. 2, pp. 397–404, 2011.

[104] Y. Ioni, E. Buslaeva, and S. Gubin, "Synthesis of Graphene with Noble Metals NPs on its Surface," in *Materials Today: Proceedings*, 2016, vol. 3, pp. S209–S213.

[105] I. Khalil, N. M. Julkapli, W. A. Yehye, W. J. Basirun, and S. K. Bhargava, "Graphene-gold NPs hybrid-synthesis, functionalization, and application in an electrochemical and surface-enhanced Raman scattering biosensor," *Materials*, vol. 9, no. 6. 2016.

[106] J. Cui, Y. Yang, M. Zheng, Y. Liu, Y. Xiao, B. Lei and W. Chen "Facile fabrication of graphene oxide loaded with silver NPs as antifungal materials," *Mater. Res. Express*, vol. 1, no. 4, pp. 45007, 2014.

[107] S. Saha, M. Jana, P. Samanta, N.C. Murmu, N.H. Kim, T. Kuila and J.H. Lee "Hydrothermal synthesis of Fe3O4/RGO composites and investigation of electrochemical performances for energy storage applications," *Rsc Adv.*, vol. 4, no. 84, pp. 44777–44785, 2014.

[108] B. Y. Chang, N.M. Huang, M.N. An'amt, A.R. Marlinda, Y. Norazriena, M.R. Muhamad, I. Harrison, H.N. Lim and C.H. Chia "Facile hydrothermal preparation of titanium dioxide decorated reduced graphene oxide nanocomposite," *Int. J. Nanomedicine*, vol. 7, pp. 3379–3387, 2012.

[109] S. Liu, H. Sun, A. Suvorova, and S. Wang, "One-pot hydrothermal synthesis of ZnO-reduced graphene oxide composites using Zn powders for enhanced photocatalysis," *Chem. Eng. J.*, vol. 229, pp. 533–539, 2013.

[110] W. Li, Y. Bu, H. Jin, J. Wang, W. Zhang, S. Wang and J. Wang "The preparation of hierarchical flowerlike NiO/reduced graphene oxide composites for high performance supercapacitor applications," *Energy and Fuels*, vol. 27, no. 10, pp. 6304–6310, Oct. 2013.

[111] Y. Yuan, H. Bi, G. He, J. Zhu, and H. Chen, "A Facile Hydrothermal Synthesis of a MnCo 2 O 4@ Reduced Graphene Oxide Nanocomposite for Application in Supercapacitors," *Chem. Lett.*, vol. 43, no. 1, pp. 83–85, 2014.

[112] S. Bai, X. Shen, X. Zhong, Y. Liu, G. Zhu, X. Xu and K. Chen "One-pot solvothermal preparation of magnetic reduced graphene oxide-ferrite hybrids for organic dye removal," *Carbon N. Y.*, vol. 50, no. 6, pp. 2337–2346, 2012.

[113] J. Lai, W. Niu, R. Luque, and G. Xu, "Solvothermal synthesis of metal nanocrystals and their applications," *Nano Today*, vol. 10, no. 2, pp. 240–267, 2015.

[114] C. M. L. Ziming He, Guanhong Guai, a Jing Liu, Chunxian Guo, Joachim Say Chye Loo and T. T. Y. Tan, "Nanostructure control of graphene-composited TiO2 by a one-step solvothermal approach for high performance dye-sensitized solar cells," *Nanoscale*, vol. 3, no. 11, pp. 4613, 2011.

[115] X. Wang, L. Qiao, X. Sun, X. Li, D. Hu, Q. Zhang and D. He "Mesoporous NiO nanosheet networks as high performance anodes for Li ion batteries," *J. Mater. Chem. A*, vol. 1, no. 13, pp. 4173–4176, 2013.

[116] I. M. Sadiek, A. M. Mohammad, M. E. El-Shakre, and M. S. El-Deab, "Electrocatalytic activity of nickel oxide NPs-modified electrodes: Optimization of the loading level and operating pH towards the oxygen evolution reaction," *Int. J. Hydrogen Energy*, vol. 37, no. 1, pp. 68–77, 2012.

[117] H. Inoue, Y. Namba, and E. Higuchi, "Preparation and characterization of Ni-based positive electrodes for use in aqueous electrochemical capacitors," *J. Power Sources*, vol. 195, no. 18, pp. 6239–6244, 2010.

[118] J. Zhu, S. Chen, H. Zhou, and X. Wang, "Fabrication of a low defect density graphene-nickel hydroxide nanosheet hybrid with enhanced electrochemical performance," *Nano Res.*, vol. 5, no. 1, pp. 11–19, 2012.

[119] N. A. Hoque, P. Thakur, A. Kool, S. Das, and P. P. Ray, "Optical and dielectric properties of hydrothermally synthesized Ni(OH)2 NPs: a morphology and size dependent study," *J. Mater. Sci. Mater. Electron.*, vol. 28, no. 7, pp. 5375–5383, 2017.

[120] Z. Li, J. Han, L. Fan, and R. Guo, "In-situ controllable growth of α-Ni(OH)2 with different morphologies on reduced graphene oxide sheets and capacitive performance for supercapacitors," *Colloid Polym. Sci.*, vol. 294, no. 4, pp. 681–689, 2016.

[121] L. Wang, X. Li, T. Guo, X. Yan, and B. K. Tay, "Three-dimensional Ni(OH)2 nanoflakes/graphene/nickel foam electrode with high rate capability for supercapacitor applications," *Int. J. Hydrogen Energy*, vol. 39, no. 15, pp. 7876–7884, 2014.

[122] W. Liu, C. Ju, D. Jiang, L. Xu, H. Mao, and K. Wang, "Ionic liquid-assisted grown of beta-nickel hydroxide nanowires on reduced graphene oxide for high-performance supercapacitors," *Electrochim. Acta*, vol. 143, pp. 135–142, 2014.

[123] X. Zang, C. Sun, Z. Dai, J. Yang, and X. Dong, "Nickel hydroxide nanosheets supported on reduced graphene oxide for high-performance supercapacitors," *J. Alloys Compd.*, vol. 691, pp. 144–150, 2017.

[124] M. P. Yeager, D. Su, N. S. Marinkovic, and X. Teng, "Pseudocapacitive NiO Fine NPs for Supercapacitor Reactions," *J. Electrochem. Soc.*, vol. 159, no. 10, pp. A1598–A1603, 2012.

[125] B. Vidhyadharan, N.K.M. Zain, I.I. Misnon, R.A. Aziz, J. Ismail, M.M. Yusoff and R. Jose "High performance supercapacitor electrodes from electrospun nickel oxide nanowires," *J. Alloys Compd.*, vol. 610, pp. 143–150, 2014.

[126] S. I. Kim, J. S. Lee, H. J. Ahn, H. K. Song, and J. H. Jang, "Facile route to an efficient nio supercapacitor with a three-dimensional nanonetwork morphology," *ACS Appl. Mater. Interfaces*, vol. 5, no. 5, pp. 1596–1603, 2013.

[127] S. Yang, G. Li, L. Liu, G. Wang, D. Wang, and L. Qu, "Preparation of nickel oxide NPs on N-doped reduced graphene oxide: A two-dimensional hybrid for electrocatalytic sensing of L-cysteine," *J. Alloys Compd.*, vol. 691, pp. 834–840, 2017.

[128] A. Jana, E. Scheer, and S. Polarz, "Synthesis of graphene-transition metal oxide hybrid NPs and their application in various fields," *Beilstein Journal of Nanotechnology*, vol. 8, no. 1. Beilstein-Institut, pp. 688–714, 2017.

[129] Y.-Y. Yang, Z.-A. Hu, Z.-Y. Zhang, F.-H. Zhang, Y.-J. Zhang, P.-J. Liang, H.-Y. Zhang and H.-Y. Wu "Reduced graphene oxide–nickel oxide composites with high electrochemical capacitive performance," *Mater. Chem. Phys.*, vol. 133, no. 1, pp. 363–368, 2012.

[130] F. Gao, Q. Wei, J. Yang, H. Bi, and M. Wang, "Synthesis of graphene/nickel oxide composite with improved electrochemical performance in capacitors."

[131] L. T. Hoa, H. N. Tien, V. H. Luan, J. S. Chung, and S. H. Hur, "Fabrication of a novel 2D-graphene / 2D-NiO nanosheet-based hybrid nanostructure and its use in highly sensitive NO 2 sensors," *Sensors Actuators B. Chem.*, vol. 185, pp. 701–705, 2013.

[132] L. Wang, H. Xing, S. Gao, X. Ji, and Z. Shen, "Porous flower-like NiO@graphene composites with superior microwave absorption properties," *J. Mater. Chem. C*, vol. 5,

no. 8, pp. 2005–2014, 2017.

[133] G. Chen, H. Guan, C. Dong, X. Xiao, and Y. Wang, "Effect of calcination temperatures on the electrochemical performances of nickel oxide/reduction graphene oxide (NiO/RGO) composites synthesized by hydrothermal method," *J. Phys. Chem. Solids*, vol. 98, pp. 209–219, 2016.

[134] J. Montgomery, N. A. Lebel, and J. Montgomery, "Nickel-Catalyzed Reductive Cyclizations and Couplings," *Angew. Chem. Int. Ed*, vol. 43, pp. 3890–3908, 2004.

[135] N. Cordente, M. Respaud, F. Senocq, M-J Casanove, C. Amiens and B. Chaudret "Synthesis and Magnetic Properties of Nickel Nanorods," 2001.

[136] F. W. Campbell and R. G. Compton, "The use of NPs in electroanalysis: an updated review," *Anal. Bioanal. Chem.*, vol. 396, no. 1, pp. 241–259, 2010.

[137] M. R. Knecht, J. C. Garcia-Martinez, and R. M. Crooks, "Synthesis, Characterization, and Magnetic Properties of Dendrimer-Encapsulated Nickel NPs Containing," *chem. Mater*, vol. 18, no. 21, pp. 5039-5044.

[138] Z. Jiang, J. Xie, D. Jiang, X. Wei, and M. Chen, "Modifiers-assisted formation of nickel NPs and their catalytic application to p-nitrophenol reduction," *CrystEngComm*, vol. 15, no. 3, pp. 560–569, 2013.

[139] A. Wang, H. Yin, H. Lu, J. Xue, M. Ren, and T. Jiang, "Catalytic activity of nickel NPs in hydrogenation of p-nitrophenol to p-aminophenol," *Catal. Commun.*, vol. 10, no. 15, pp. 2060–2064, 2009.

[140] C. Gong, J. Zhang, X. Zhang, L. Yu, P. Zhang, Z. Wu and Z. Zhang "Strategy for Ultrafine Ni Fibers and Investigation of the Electromagnetic Characteristics," *J. Phys. Chem. C*, vol. 114, no. 22, pp. 10101–10107, 2010.

[141] Z. Wang, J. Zou, Z. Ding, J. Wu, P. Wang, S. Jin and H. Bi "Magnetic and microwave absorption properties of Ni microcrystals with hierarchical branch-like and flowers-like shapes," *Mater. Chem. Phys.*, vol. 142, no. 1, pp. 119–123, 2013.

[142] L. Qiao, X. Han, B. Gao, J. Wang, F. Wen, and F. Li, "Microwave absorption properties of the hierarchically branched Ni nanowire composites," *J. Appl. Phys.*, vol. 105, no. 5, p. 53911, 2009.

[143] T. Liu, P. H. Zhou, J. L. Xie, and L. J. Deng, "Electromagnetic and absorption properties of urchinlike Ni composites at microwave frequencies," *J. Appl. Phys.*, vol. 111, no. 9, pp. 93905, 2012.

[144] C.-Y. Chen N.-W. Pu, Y.-M. Liu, S.-Y. Huang, C.-H. Wu, M.-D. Ger, Y.-J. Gong and Y.-C. Chou "Remarkable microwave absorption performance of graphene at a very low

loading ratio," *Compos. Part B Eng.*, vol. 114, pp. 395–403, 2017.

[145] G. Liu, W. Jiang, D. Sun, Y. Wang, and F. Li, "One-pot synthesis of urchinlike Ni NPs/RGO composites with extraordinary electromagnetic absorption properties," *Appl. Surf. Sci.*, vol. 314, pp. 523–529, 2014.

[146] Y. Lai, S. Wang, D. Qian, S. Zhong, Y. Wang, S. Han and W. Jiang, "Tunable electromagnetic wave absorption properties of nickel microspheres decorated reduced graphene oxide," *Ceram. Int.*, vol. 43, no. 15, pp. 12904-12914, 2017.

[147] K. Bhowmik, A. Mukherjee, M. K. Mishra, and G. De, "Stable Ni Nanoparticle−Reduced Graphene Oxide Composites for the Reduction of Highly Toxic Aqueous Cr(VI) at Room Temperature," *Langmuir*, vol. 30, pp. 3209-3216, 2014.

[148] Z. Ji, Y. Wang, X. Shen, H. Ma, J. Yang, A. Yuan and H. Zhou "Facile synthesis and enhanced catalytic performance of reduced graphene oxide decorated with hexagonal structure Ni NPs," *J Colloid Interface Sci.*, vol. 487, pp. 223-230, 2017.

[149] G. Liu, Y. Wang, F. Qiu, L. Li, L. Jiao, and H. Yuan, "Synthesis of porous Ni@rGO nanocomposite and its synergetic effect on hydrogen sorption properties of MgH2," *J. Mater. Chem.*, vol. 22, no. 42, pp. 22542, 2012.

[150] Y. J. Mai, J. P. Tu, C. D. Gu, and X. L. Wang, "Graphene anchored with nickel NPs as a high-performance anode material for lithium ion batteries," *J. Power Sources*, vol. 209, pp. 1–6, 2012.

[151] M. Nie, "Anode Solid Electrolyte Interphase (Sei) of Lithium Ion Battery Characterized by Microscopy and Spectroscopy,", open access dissertations, Paper 202, 2014.

[152] S. J. An, J. Li, C. Daniel, D. Mohanty, S. Nagpure, and D. L. Wood, "The state of understanding of the lithium-ion-battery graphite solid electrolyte interphase (SEI) and its relationship to formation cycling," *Carbon N. Y.*, vol. 105, pp. 52–76, 2016.

[153] A. Sigal, M. I. Rojas, and E. P. M. Leiva, "Interferents for hydrogen storage on a graphene sheet decorated with nickel: A DFT study," *Int. J. Hydrogen Energy*, vol. 36, no. 5, pp. 3537–3546, 2011.

[154] M. Gaboardi, A. Bliersbach, G. Bertoni, M. Aramini, G. Vlahopoulou, D. Pontiroli, P. Mauron, G. Magnani, G. Salviati, A. Züttel and M. Riccò "Decoration of graphene with nickel NPs: study of the interaction with hydrogen," *J. Mater. Chem. A*, vol. 2, no. 4, pp. 1039–1046, 2014.

[155] N. Ismail, M. Madian, and M. S. El-Shall, "Reduced graphene oxide doped with Ni/Pd NPs for hydrogen storage application," *J. Ind. Eng. Chem.*, vol. 30, pp. 328–335, 2015.

Chapter 2

Synthesis and characterization of reduced graphene oxide/spiky nickel nanocomposite for nanoelectronic applications

This chapter is based on the following published article:

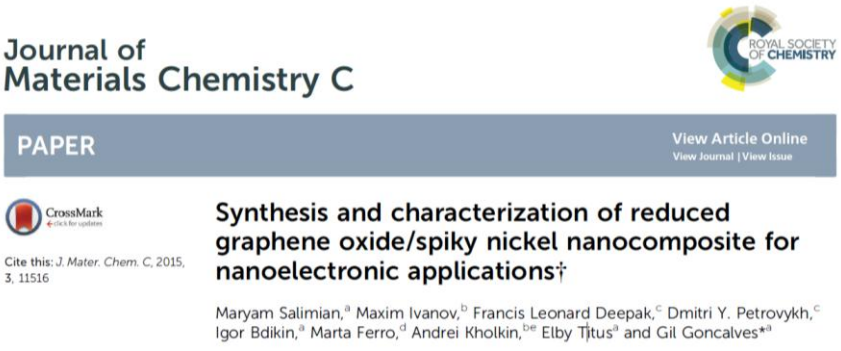

2.1 Scope

The surface modification of graphene oxide (GO) sheets with nickel (Ni) nanoparticles (NPs) has been a subject of intense research in order to develop new preeminent materials with increased performance for different application areas. In this work, we develop a new hydrothermal one-step method for the simple and controllable synthesis of reduced GO/nickel (GO/Ni) nanocomposites. Different reaction parameters have been investigated in order to control the synthetic process: reaction temperature, concentration of Ni precursor and reducing agent. It was observed that the critical parameter for the effective control of Ni particle size, morphology, crystalline structure and distribution at GO surface during the reaction process was the concentration of hydrazine hydrate ($N_2H_4.H_2O$). The results obtained showed that the control of $N_2H_4.H_2O$ concentration allows obtaining crystalline metallic Ni NPs, from spherical to spiky morphologies. For nanocomposites with Ni spiky NPs it was observed that the reaction time allows controlling the growth of the nanothorns. The electrical properties of the reduced graphene Ni nanocomposites containing spikey Ni particles showed a large resistive switching, which is essentially due to the switchable diode effect that can be used as built-in part of graphene-based embedded electronics.

2.2 Introduction

Graphene, a two-dimensional carbon material with the honeycomb structure has received a lot of attention due to its remarkable properties since its discovery in 2004 [1]. The unique structure allows achieving extraordinary properties such as high thermal and electrical conductivity. These properties have been further explored to overcome the forthcoming

thermal problem in electronic circuits and low specific power density in lithium-ion batteries [2-4]. As has been reported, graphene is the strongest material that has been ever examined [5]. Besides these extraordinary properties that arise from the nature of the graphene, new synergetic properties can be achieved by manipulating or decorating its surface with different kinds of biological molecules and materials, macromolecules or NPs. The incorporation of NPs has been one interesting approach to increase the application range of the graphene-based materials.

Graphene nanocomposites can be obtained by methodologies that consists on the direct growth of the NPs on graphene surface or thought processes that allows the self-assembly of NPs at graphene surface [6]. It was observed that the degree of oxidation of graphene [7] and heteroatoms doping of graphene [8] have a strong structural influence on the final nanocomposites. Functionalization of graphene with metal and metal oxide NPs allows the development of new nanocomposite materials for diverse applications such as catalysis, electronics, biological, magnetic and optoelectronics.

In order to develop new graphene nanocomposites with magnetic properties, the most used strategy involves the assembly of magnetic NPs, among which the NPs based on iron [9], nickel [10] and cobalt [11] are the most relevant. Different synthetic routes have been developed in order to create graphene/Ni hybrids in a reproducible and controlled manner. Chen et al. reported preparation of Ni-graphene hybrids using $NaHB_4$ as a reductant and NaOH as an alkaline medium under microwave irradiation for catalytic applications [12]. Choi et al. prepared nanostructured Ni/graphene hybrid using GO in ethylene glycol and Ni(II) nitrate hexahydrate ($Ni(NO_3)_2 \bullet 6H_2O$) as a precursor while reducing reassembled hybrid under

mixed gas of H_2/N_2 (5:95) as an electrochemical hydrogen storage material [13]. Gotoh et al. produced the graphene sheets decorated with metal or metal oxide NPs including Ni NPs using GO, NH_3 solution and $[Ni(NH_3)_6]$ Cl_2 precursor followed by calcination of the Ni complex, at a heating range from room temperature to 673 °K [14]. Koushik et al showed a new multistep method for the synthesis of reduced GO/Ni nanocomposites based on the previous synthesis of $Ni(OH)_2$/GO nanocomposites, followed by the thermal treatment under air at 380 ºC to promote the conversion of NPs into NiO and under H_2 for the final conversion to metallic Ni [15]. Recent studies showed the use of alkali hydroxides for previous pH-adjusted reaction medium with chemicals such as NaOH or KOH for the synthesis of Ni NPs [16-18]. It was also observed that the previous complexation of Ni with urea followed by reduction with $N_2H_4.H_2O$ allows the achievement of reduced GO/Ni nanocomposites [19]. However, one of the most commonly used reducing agents for the synthesis of Ni NPs on the surface of GO nanosheets is $N_2H_4.H_2O$. Wang et al. reported a simple microwave-assisted method for the synthesis of Ni nanospheres in ethylene glycol solution for the development of glucose sensors [20]. Graphene/Ni nanocomposites were also prepared via hydrothermal process through $N_2H_4.H_2O$ reduction of Ni precursors on the surface of GO nanosheets [21,22]. Ji et al. observed that the concentration of Ni ions has an important influence on the morphology of the nanocomposites [21].

In this work, we developed a new approach for the synthesis of GO/Ni nanocomposites by one-step facile, cheap and environmentally friendly hydrothermal route. We investigated the influence of several experimental parameters such as time, temperature and reducing agent concentration of $N_2H_4.H_2O$ on the Ni NPs morphology, crystalline phase and distribution on

the GO surface. The results revealed that the Ni particles size, shape and distribution on GO surface can be simply tailored by adjusting the $N_2H_4.H_2O$ concentration in the reaction medium. For nanocomposites with spiky NPs it was observed that the reaction time can control the growth of the nanothorns. It was observed that $N_2H_4.H_2O$ also promotes the reduction of GO during the synthesis process of the nanocomposites. The electronic characterization showed that spiky Ni particles implanted in rGO matrix enhance conductivity, with the nonlinearity observed in current-voltage dependence if the output electrodes are attached. Via the equilibrium energy band diagrams, we confirmed that all the experimental structure components (Ni particles, rGO, NiO and Pt-tip) are exactly in place, so the NiO plays a role of the gate insulator. In general, this structure works like graphene based transistor switch or a switchable diode embedded in graphene-based matrix, both of these could be very useful for graphene-based embedded nanoelectronics applications.

2.3 Experimental section

2.3.1 Synthesis of graphene oxide

GO was prepared by the chemical exfoliation of graphite (graphite powder, <45 μm, ≥99.99%, Sigma-Aldrich) following a modified Hummers method [16]. Basically, it consists of the cleavage of the interactions of carbon planes in graphite into individual nanosheets under strong acidic (H_2SO_4) and oxidant ($KMnO_4$) conditions. The resultant suspension was extensively washed with distilled water by filtration and the resulting GO was freeze dried in order to avoid agglomeration of the particles.

2.3.2 Synthesis of reduced graphene oxide/nickel nanocomposites

Graphene oxide (10 mg) was dispersed in 10 mL deionized water using ultrasonic bath during 3 hours. A solution of $Ni(NO_3)_2$ (0.07 mol/L) was prepared by dissolving 27 mg into 2 mL of deionized water. The two solutions were mixed together and stirred for two hours, and further sonicated during one hour. After sonication, the desired quantity of $N_2H_4.H_2O$ was added to the solution and stirred for one hour. Then the solution was transferred to 25 mL Teflon autoclave and kept in furnace during different periods of time at 100 ºC. The final nanocomposites were washed out with deionized water and freeze-dried. The $N_2H_4.H_2O$ concentration and reaction time used in this work are summarized in Table 2.1.

Table 2.1 rGO/Ni nanocomposites prepared at different experimental conditions.

Sample	$N_2H_4.H_2O$ conc. (mol/L)	Reaction time (hours)
G/Ni1	0.08	22
G/Ni2	0.17	22
G/Ni3	0.83	5
G/Ni4	0.83	11
G/Ni5	0.83	22
G/Ni6	4.1	22

2.3.3 Characterization

Powder X-ray diffraction data were collected using a Siemens D500 diffractometer with secondary monochromator CuKα radiation in the 5°-85° range with steps of 0.05°, the time for collecting x-rays being 50 s for each measuring point at 30 mA and 40 kV. Morphological

studies were performed using an ultra-high resolution analytical Scanning Electron Microscope HR-FESEM Hitachi SU-70 and a Quanta 650 FEG ESEM (FEI). Transmission Electron Microscopy (TEM), High Resolution Transmission Electron Microscopy (HRTEM), Selected Area Electron Diffraction (SAED) and Scanning/Transmission Electron Microscopy (STEM) analysis, were performed using a Titan ChemiSTEM 80-200 kV probe Cs corrected microscope. Energy dispersive X-ray analysis (EDS) spectra and elemental maps were acquired on a Super-X EDS system. X-ray Photoemission Spectroscopy (XPS) analysis was carried out on an ESCALAB 250 Xi (Thermo Scientific) system equipped with a monochromatic Al Kα X-ray source and sample-charge neutralization system. Fourier transform infrared (FTIR) spectroscopy was carried out using a FTIR spectrometer with the ATR accessory using a Perkin-Elmer Spectrum BX at room temperature. Samples were mixed with KBr then were prepared in the shape of plates for Scanning Probe Microscopy (SPM) measurements. A commercial SPM (Ntegra Aura, NT-MDT, Russia) was used in Atomic Force Microscopy (AFM) mode, Conductive AFM (C-AFM) also known as Spreading Resistance (SR) mode, Kelvin Probe (KPFM) mode and piezoresponse Force Microscopy (PFM) mode in order to perform morphological, conductivity and supposititious piezoeffect analyses of the sample. A conductive Si cantilever coated with Pt (CSG30/Pt, NT-MDT, Russia) with a spring constant of 0.6 N m^{-1} and a resonance frequency of ~48 kHz was used for topography and spreading resistance investigation.

2.4 Results and discussion

2.4.1 Influence of reaction parameters on the G/Ni nanocomposite structure

The synthesis of G/Ni nanocomposites was performed by the chemical interaction of the Ni ions and the GO surface. In the past, it has been reported that the metallic ions can be reduced by the oxygen functional groups at GO surface that can act as nucleation sites for the nucleation and growth of metallic NPs [16]. Besides, our experimental results showed that Ni NPs growth and crystalline phase can be controlled at the GO surface by changing the concentration of $N_2H_4.H_2O$ in the reaction medium, see table 2.2.

Table 2. 2 A description of the crystalline structure, particle size and shape of Ni NPs achieved depending of the experimental conditions.

Sample	Crystalline phase (XRD)	Average particle size (nm)	Particle shape
G/Ni1	$Ni(OH)_2$	-	-
G/Ni2	Ni metallic/$Ni(OH)_2$	145	spherical
G/Ni3	Ni metallic	300	spiky
G/Ni4	Ni metallic	300	spiky
G/Ni5	Ni metallic	300	spiky
G/Ni6	Ni metallic	900	spherical

X-ray diffraction (XRD) patterns of G/Ni nanocomposites are shown in Figure 2.1. The corresponding peak of GO at 10.50° was shifted to 23.4° and broadened according to the effective reduction to rGO [13] during the reaction synthesis of G/Ni nanocomposites. The diffraction profile of the G/Ni1 nanocomposite prepared with the lower concentration of $N_2H_4.H_2O$ (0.08 mol/L) showed the preferential formation of Ni(OH)2, with the presence of

the peaks at 19.38°, 33.32°, 38.78°, 52.13°, 59.38°, 62.98°, 70.23° and 73.07° which are attributed to (001), (100), (101), (102), (110), (111), (200), (103) and (201) planes, respectively [23]. The G/Ni2 nanocomposite prepared with a high concentration of $N_2H_4.H_2O$ (0.17 mol/L) in its reaction medium showed the presence of diffraction peaks corresponding to the metallic Ni phase at 44.7°, 52.0° and 76.5°, which can be attributed to (111), (200) and (220) of Ni planes in a face-centered cubic structure [24]. We also observed the presence of minor peaks that can be attributed to a secondary phase of residual $Ni(OH)_2$. The increase concentration of $N_2H_4.H_2O$ to 0.83 and 4.1 mol/L for samples G/Ni5 and G/Ni6, respectively, showed only the presence of diffraction peaks of metallic Ni without any evidences of $Ni(OH)_2$ phase or other impurities. These results clearly demonstrated that the crystalline phase obtained in Ni graphene nanocomposites through the hydrothermal reaction of $Ni(NO_3)_2$ is dependent on $N_2H_4.H_2O$ concentration. However, it was also observed that the reaction time does not have preponderant effect on the crystalline structure of Ni particles. The XRD showed that for different reaction times from 5 to 11 and to 22 h (samples G/Ni3, G/Ni4 and G/Ni5, respectively,) the crystalline phase obtained in nanocomposite materials is pure metallic Ni.

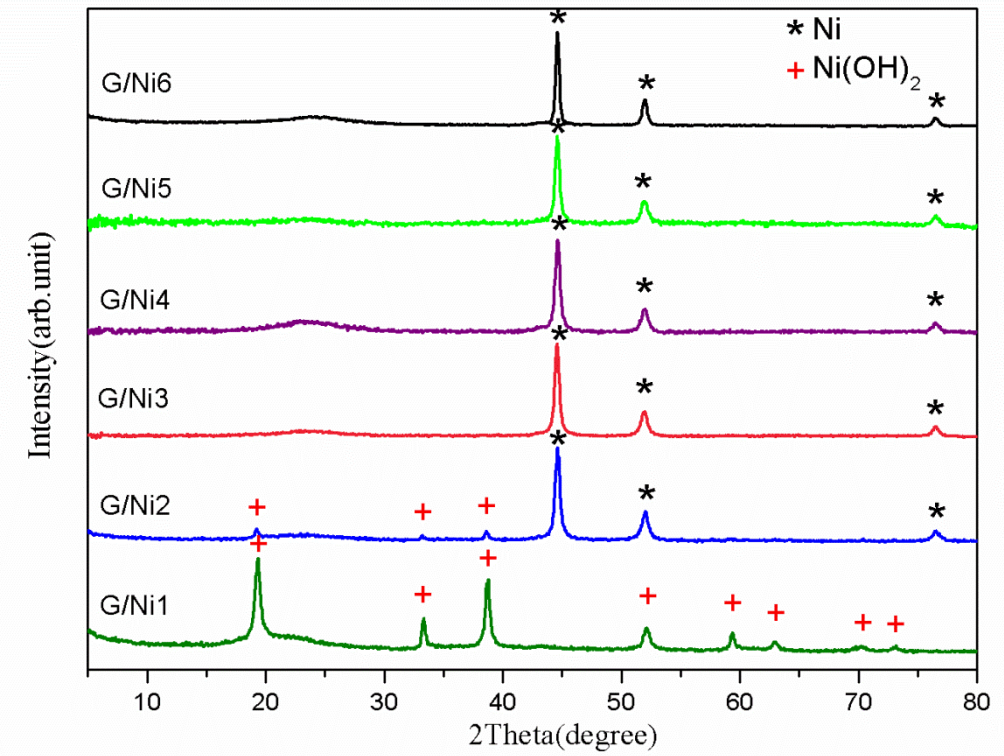

Figure 2.1 XRD profile of G/Ni nanocomposites for different $N_2H_4.H_2O$ concentration (G/Ni1, G/Ni2, G/Ni5, G/Ni6) and different reaction time (G/Ni3, G/Ni4, G/Ni5).

In fact, it was observed that the concentration of $N_2H_4.H_2O$ and reaction time are important experimental parameters for controlling the size and shape of Ni NPs in the studied G/Ni nanocomposites. SEM images of G/Ni nanocomposites (Figure 2.2 and Figure 2.3) showed that the Ni NPs have different particle morphologies and they are really integrated and well dispersed on the surface of GO sheets.

Figure 2.2 showed that the nanocomposites prepared with a lower concentration of $N_2H_4.H_2O$ do not promote the formation of Ni NPs at GO surface (G/Ni1). The increased concentration of $N_2H_4.H_2O$ (G/Ni2) allows the formation of spherical Ni particles with the average size of 145 nm and are distributed homogeneously on the surface of rGO. A further

increase of the $N_2H_4.H_2O$ concentration induced drastic changes to the morphology and the size of Ni NPs. At this stage, spiky Ni particles with the average size of 300 nm (G/Ni5) were obtained homogenously at the rGO surface. For the nanocomposites prepared with the highest concentration of $N_2H_4.H_2O$ (G/Ni6) we observed the presence of agglomerated Ni particles on the surface of rGO with an average size of 900 nm. These results indicated the crucial role of $N_2H_4.H_2O$ concentration in controlling the size, morphology and distribution of Ni particles in G/Ni nanocomposites.

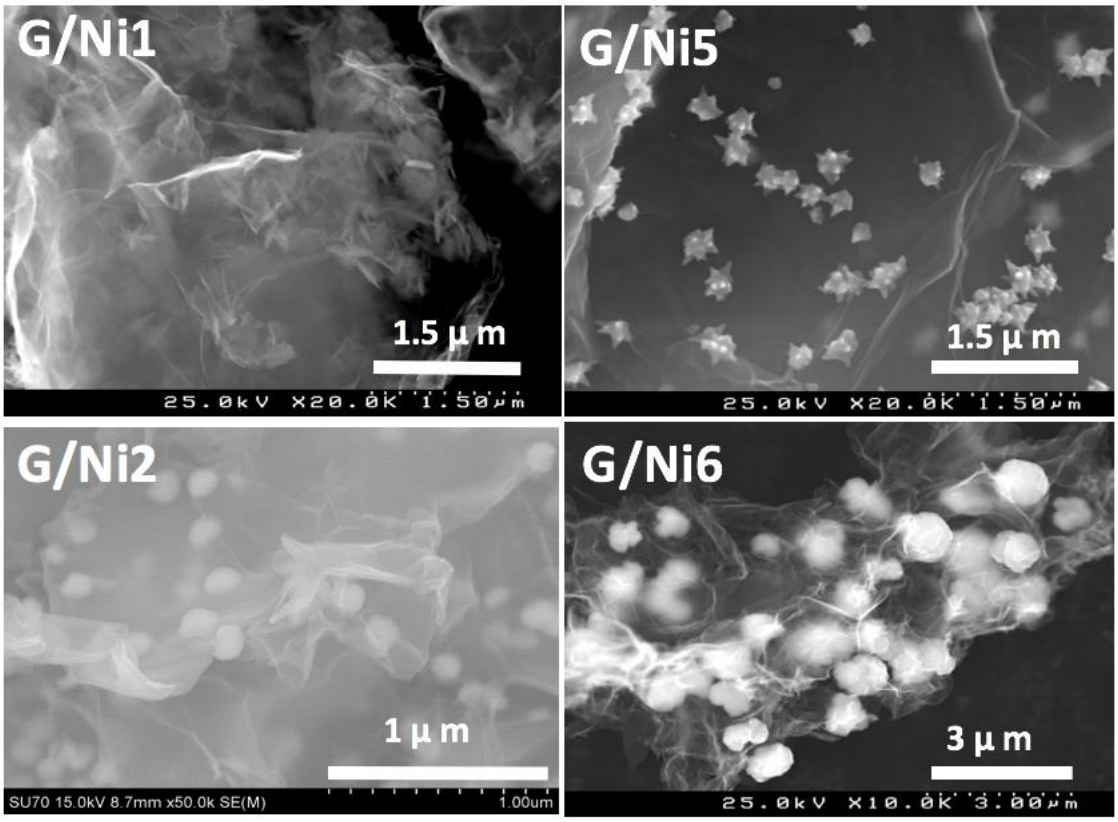

Figure 2.2 SEM images of G/Ni nanocomposites synthesized with different $N_2H_4.H_2O$ concentrations.

Previous studies showed the effect of reaction medium pH on the formation of Ni particles as well [25]. NaOH has been typically used as a basic precursor for controlling the reaction

medium pH during the synthesis of Ni particles [21]. It is well known that the basic medium adjusted by NaOH can change the reaction effects of $N_2H_4.H_2O$. Ni et al. showed that Ni particles morphology can be adjusted under a certain range of base concentration for $N_2H_4.H_2O$ reduction reactions [26]. In fact, it was already observed that other reaction parameters, such as temperature and magnetic field, also play an important role in controlling the morphology of Ni NPs during their reduction by $N_2H_4.H_2O$ [17].

According to our FTIR study of nanocomposites (see Figure A.1.1 in supplementary material section) $N_2H_4.H_2O$ does not only affect the particles morphology but also induces the reduction of GO by elimination of oxygen functional groups during the hydrothermal process. FTIR spectra of G/Ni nanocomposites showed a clear reduction of the bands corresponding to the oxygen functional groups, revealing only the presence of few residual bands of oxygen functional groups [27]. As mentioned above, oxygen functional groups at the GO surface can act as electrophilic agents for the nucleation of Ni ions and the growth of NPs. However, it was observed that the increase of the $N_2H_4.H_2O$ concentration in solution contributes to the particle shape formation by the possible coordination of Ni ions through nitrogen donor groups of $N_2H_4.H_2O$, which acts as a strong reducing agent to form Ni particles. The nanocomposites exhibited different particles morphologies depending on the $N_2H_4.H_2O$ concentration: spherical, spiky and big agglomerates (Figure 2.2).

The growth mechanism of spiky Ni particles can be explained according to Mathew et al [28] There are two main steps in the formation of flower-like structures: first, formation of a core, then, as the reduction reaction continues, the newly formed particles can be adsorbed on the surface of existing particles acting as seeds to form nanothorns on the surface of Ni core. It

was observed that at higher temperature the speed of crystal growth is decreased due to a pronounced movement of Ni ions in solution. Therefore, a longer reaction time is needed to form the flower-like morphology [29].

Although we found that the reaction time does not affect the crystallinity of the Ni particles, it has an important effect on the structure of spiky Ni NPs in G/Ni nanocomposites. SEM images of samples G/Ni3, G/Ni4 and G/Ni5 showed the growth of anisotropic Ni particles on the surface of rGO sheets (Figure 2.3).

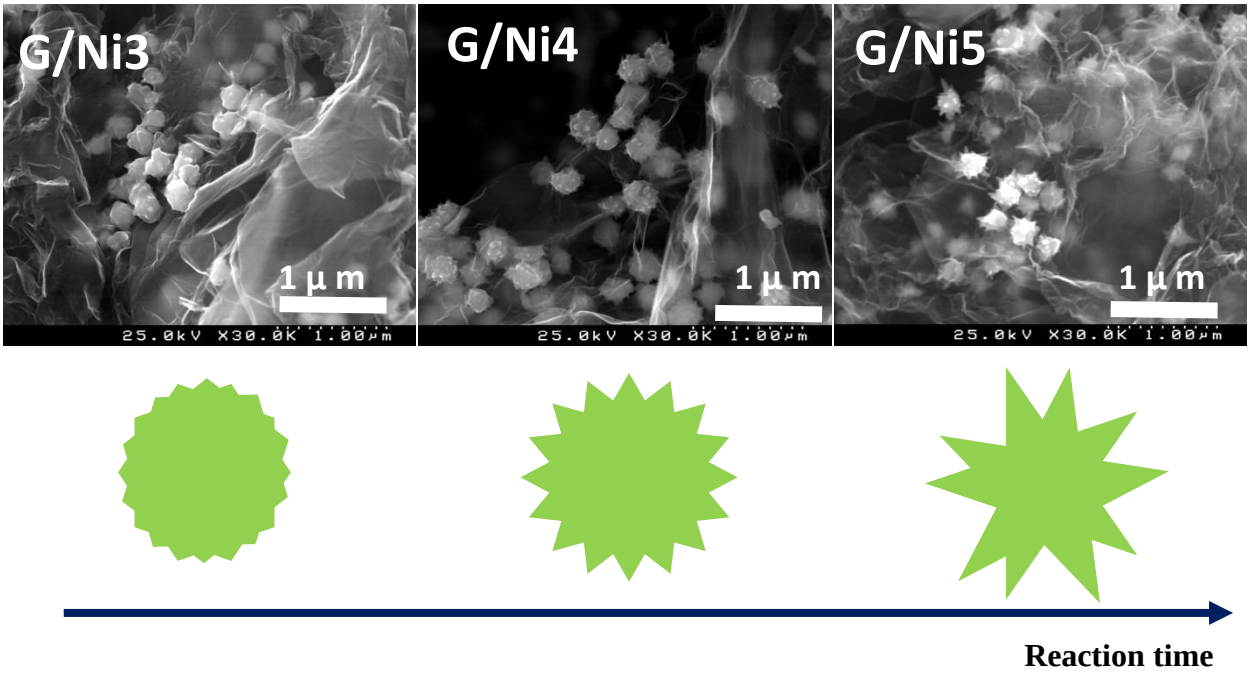

Figure 2.3 SEM images of G/Ni3, G/Ni4 and G/Ni 5 nanocomposites at three different reaction times 5, 11 and 22 hours respectively showing the increase in the growth of spiky Ni NPs and a schematic representation of Ni NPs morphology changes with reaction time.

These images present the dependency of nanothorn size on the reaction time. After 5 hours of hydrothermal treatment, Ni particles showed some anisotropic deformation on their surface

indicating the beginning of the formation of the nanothorns. As the reaction time increased to 11 and 22 hours, the size of the nanothorns also increased.

2.4.2 rGO nanocomposites with spiky nickel nanoparticles

GO sheets homogenously modified with spiky Ni NPs were further explored in this work due to their peculiar structure that can confer novel interesting properties to the composite materials. TEM analysis of individual spiky Ni particle at the surface of the rGO sheet (Figure 2.4) showed that its peculiar structure is composed of two different regions, a core (1) surrounded by nanothorn (2). Statistical analysis of Ni NPs showed that the size of nanothorns varies from 40 nanometers to 100 nanometers and the core is about 200 nm. The selected area diffraction pattern (SAED) of the regions (1 and 2 in Figure 2.4) proved the presence of a thin layer of Ni oxide.

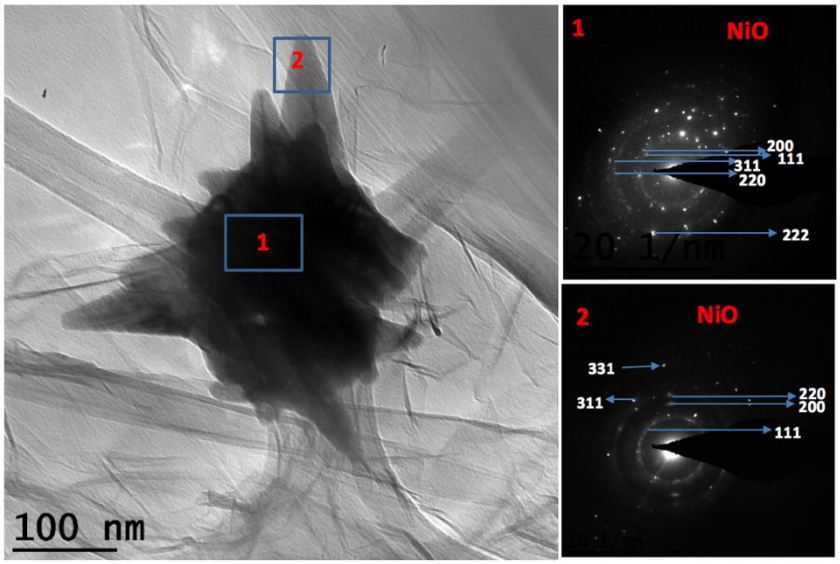

Figure 2.4 TEM image of one single spiky Ni particle at the surface of rGO sheet. Diffraction pattern (SAED) on the core (1) and on a single nonothorn (2) with the respective crystalline planes of NiO.

HRTEM images of a single nanothorn, including a magnified close-up of a selected area, are shown in Figure 2.5. The lattice planes with the spacing of 2.089 Å which correspond to (200) lattice planes (NiO SG: Fm3m Cubic 00-047-1049ICDD Database) confirmed the presence of NiO layer structure on the nanothorn. The surface oxidation of Ni NPs was not detected by XRD measurement, which indicates they are very small fraction compared with the metallic phase.

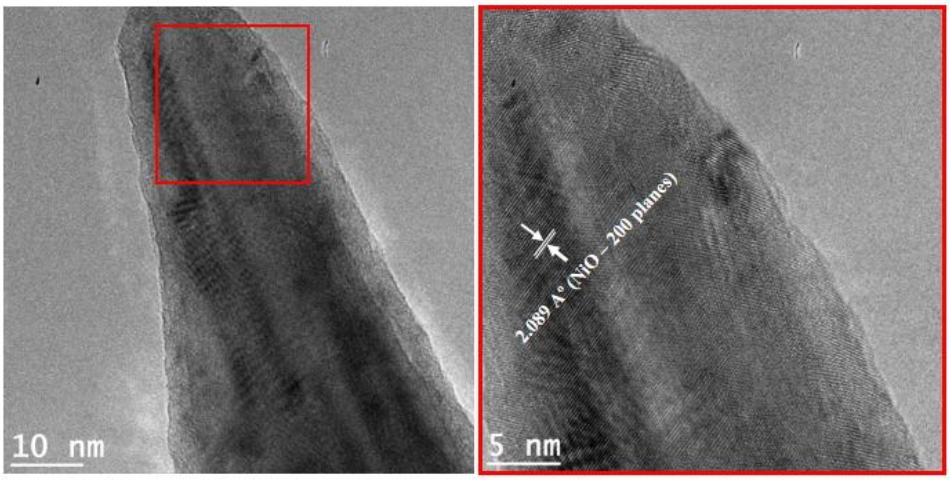

Figure 2.5 HRTEM images of single nanothorn (on the left) and its selected area with high resolution (on the right) showing the lattice structure of NiO.

The presence of an oxidized surface has been further confirmed by X-ray Photoelectron Spectroscopy (XPS) measurements carried out for samples G/Ni3, G/Ni4 and G/Ni5 (Figure 2.6) [30].

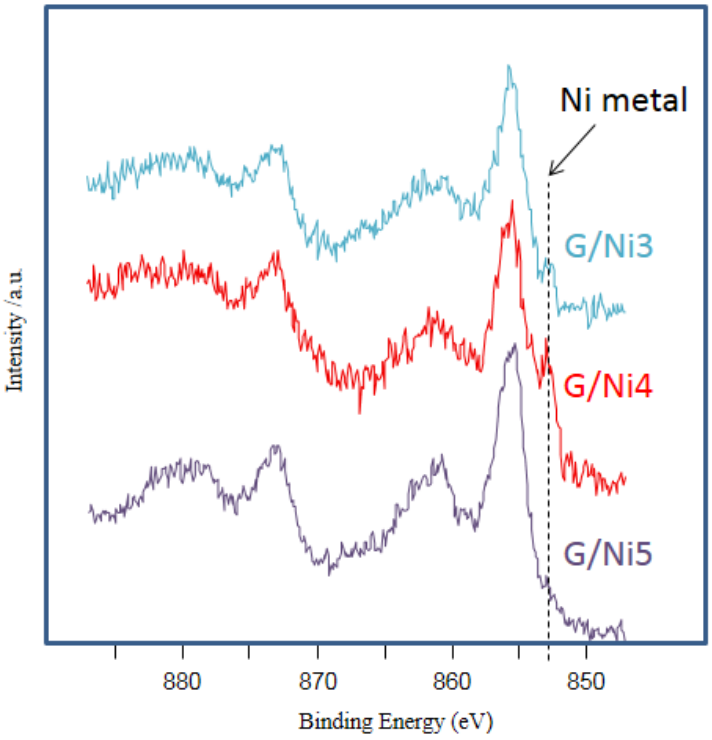

Figure 2. 6 Ni 2p XPS spectra of G/Ni3, G/Ni4, G/Ni5 samples.

For all three samples, the C 1s spectra (data are not shown) have the asymmetric lineshape characteristic of graphitic materials, as would be expected for rGO with $N_2H_4.H_2O$ [30]. The Ni 2p spectra for these materials are qualitatively similar to those previously reported for NiO on rGO [31]. The binding energy (BE) of the strongest Ni $2p_{3/2}$ component is above 855 eV for all the samples in Figure 2.6 While BE>855 eV is occasionally reported for NiO samples, in the NIST XPS Database [32], the majority of BE values are below 855 eV for NiO, so based on the BE values it is more likely to assign the material in the oxidized surface layer of these samples as $Ni(OH)_2$. The small shoulders observed at BE of ca. 853 eV indicate the presence of metallic Ni within the sampling depth of XPS (which is ca. 5 nm at this BE).

For materials with complex nanostructured morphology, an unambiguous interpretation of surface layer composition is difficult, however, the data in Figure 2.6 are consistent with a thin (<5 nm at least in some areas) oxidized surface layer covering a metallic Ni particle. Given the nanoscale size and spikey morphology of the nanothorns, the XPS data indicate that nanothorns are not primarily composed of metallic Ni, as they would represent a large fraction of the overall NPs volume sampled by XPS. Finally, compared to G/Ni3 and G/Ni4 samples, only a minimal amount of metallic Ni is detected in G/Ni5 sample, suggesting that longer reaction times not only increase the nanothorn size but also the degree of the surface oxidation.

Figure 2.7 shows the high-angle annular dark-field scanning transmission electron microscopy (HAADF-STEM) image of G/Ni5 nanocomposite and the corresponding elemental mapping of Ni (green) and oxygen (red). These data further proved the oxidation of Ni particles surface, which is in agreement with the SAED and TEM data. Accordingly, a local EDS spectra of a single Ni particle confirmed the presence of a very thin oxidation layer covering the core and the nanothorns (see Figure A.1.2 and A.1.3 in supplementary material section and discussion therein).

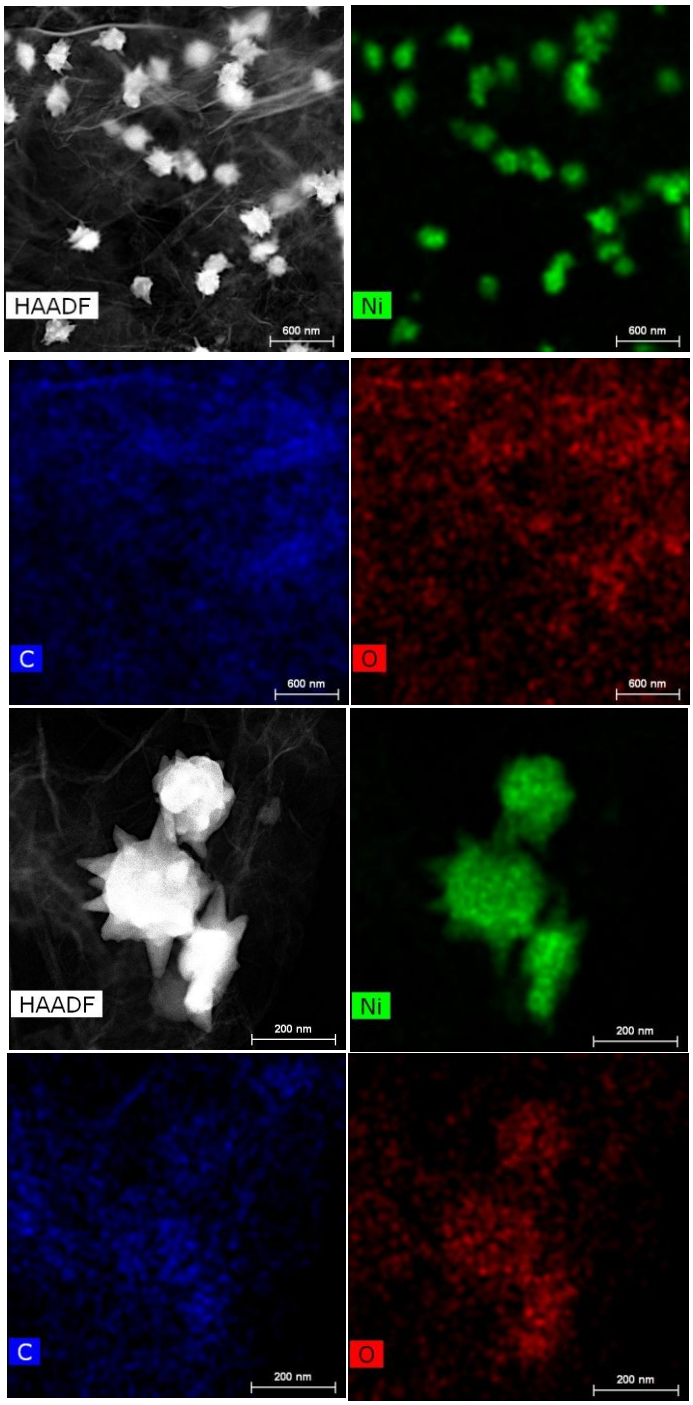

Figure 2.7 High-angle annular dark-field scanning transmission electron microscopy (HAADF-STEM) image of G/Ni5 nanocomposite and the corresponding elemental mapping of nickel (Ni) and oxygen (O).

2.4.3 SPM measurements of Ni/GO nanocomposites

SPM measurements performed to acquire simultaneously topography and spreading resistance images showed a clear manifestation of the presence of Ni particles in rGO matrix (Figure 2.8).

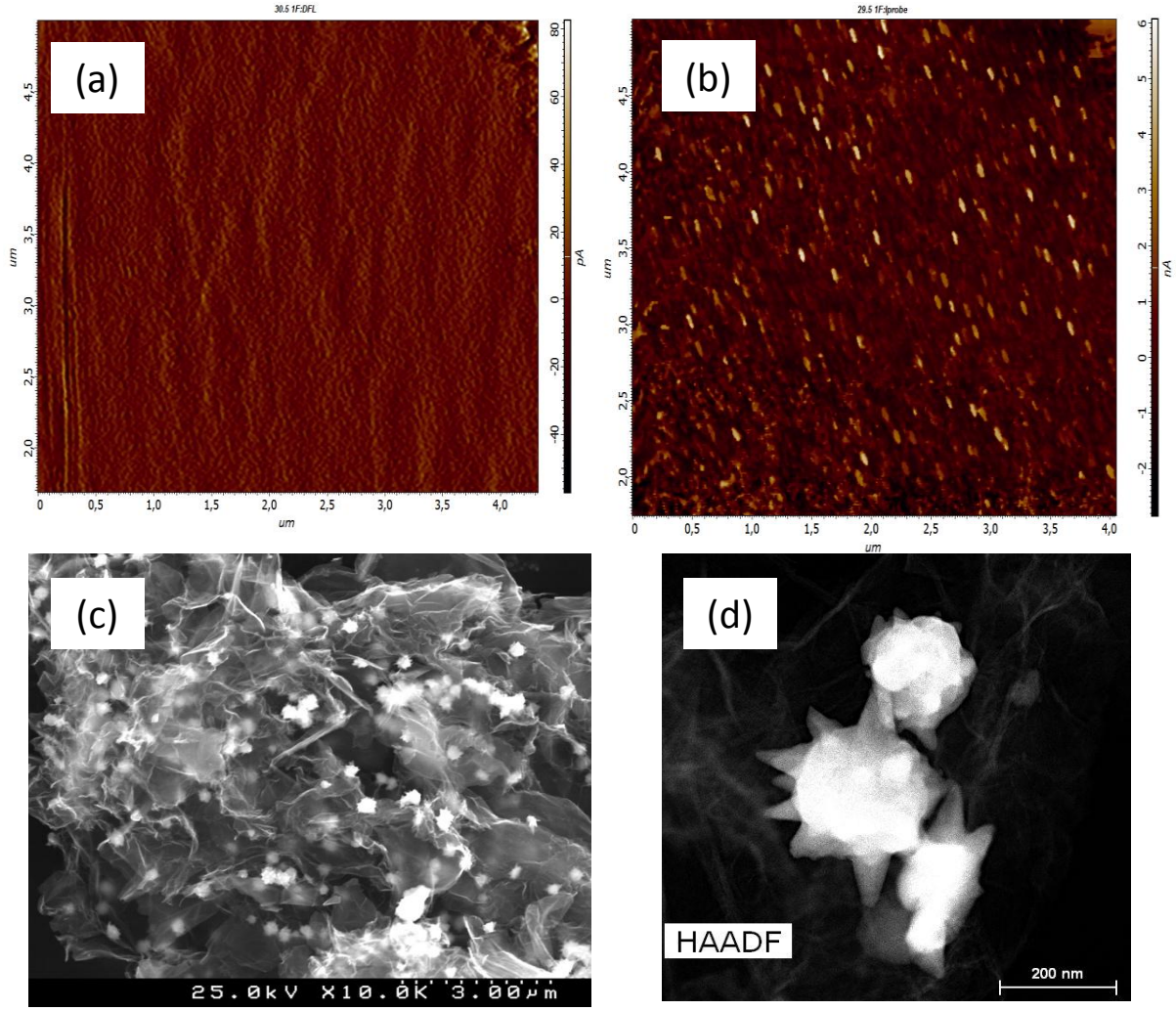

Figure 2.8 Images of the rGO matrix with Ni particles in a) SPM microscopy mode b) spreading resistance SPM mode, c) SEM mode and d) a single spiky Ni particle.

The topography analysis confirmed that the sample surface is sufficiently smooth with the RMS roughness less than 1nm (Figure 2.8 (a)) and did not influence the measured current distribution.SR images represent a real mapping of the sample conductivity (Figure 2.8 (b)). Moreover, this distribution demonstrated a good correlation with SEM images (Figure 2.8 (c)) with the Ni particles dispersed in the rGO matrix within the equal apportionment statistics. By means of comparison of both SPM and SEM methods we could mark the Ni shell (Figure 2.8 (d)) and its response on SR and on SEM scans, respectively.

Kelvin Probe Force Microscopy (KPFM) mode showed a distribution of electric potential on the samples surface (Figure 2.9 (a)), where the Ni particles exhibit higher potential as compared to the rGO matrix, and Ni particle cores and spiky shells could be distinguished, as they have maximum potential due to electric field concentrated on the point of shells (insert to Figure 2.9 (a)).

This resulted in white dots with a maximum KPFM signal around the Ni particles. The contact SR mode reveals the conductive regions that are related to the Ni particle core and shell conglomerates as confirmed by KPFM results (Figure 2.9 (b)). The current voltage dependence has been then studied in two steps based on the most conductive (green circle) and least conductive (yellow circle) points, which are related to Ni particles and rGO, respectively. The I-V behavior, showed a nonlinear and highly reproducible current hysteresis behavior, indicating a large resistive switching, which can be described as the switchable diode effect (Figure 2.9 (c)) [33]. The measurements were performed with 20 cycles by sweeping the bias voltage of the cantilever tip from -5 to 5 V and back to -5 V, repeatedly. Moreover, the forward and backward curves showed an obvious diode-like rectifying I-V characteristic, indicating a forward pass for backward pass diode behavior and a reverse diode behavior for a

forward sweep. It can be seen that during the measuring cycle the diode polarity can be switched at around 2 V.

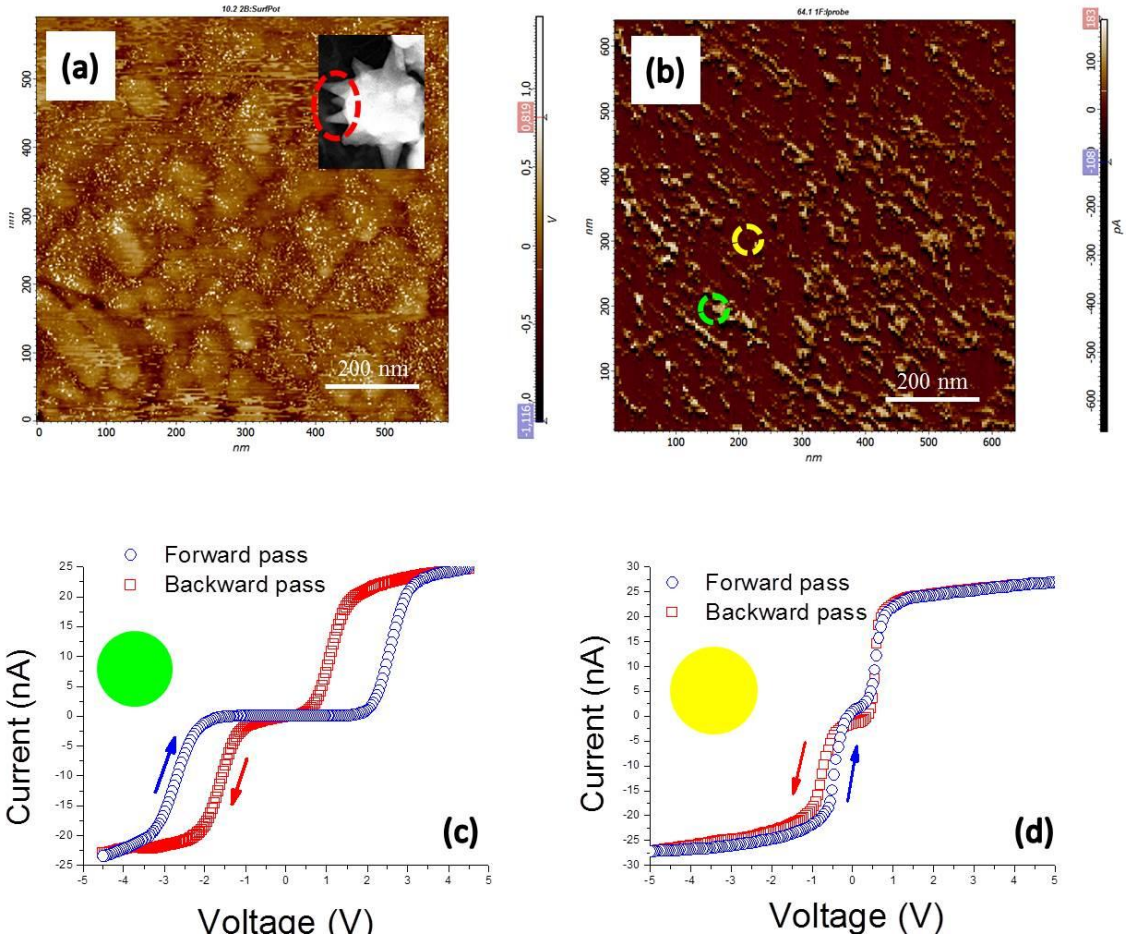

Figure 2.9 SPM images of rGO matrix with Ni particles in a) Kelvin Probe Force Microscopy mode and b) Spreading resistance mode. Current-voltage dependence on the c) most conductive (Ni particle) and d) less conductive (rGO matrix) areas.

In order to exclude the supposititious ferroelectric polarization effect, the relation between the current hysteresis and PFM response has been determined by increasing the voltage sweep range step by step [34]. During all the experiments the PFM response was absent and signal fluctuation were at the noise level. The current-voltage behavior of the rGO point also shows nonlinearity similar to the Schottky effect but does not have any hysteresis behavior (Figure

2.9 (d)). This could be due to the effect of Ni particle on current-voltage behavior of the sample that mainly leads to the switchable diode effect [35].

Based on the analysis of our results, the switchable diode behavior in the sample can be explained qualitatively by the Ni particles modulation of Schottky-like barriers at both bottom and top (cantilever's tip) electrodes. The ideal Schottky barrier at a metal-semiconductor interface is determined by the difference of the metal work function and the semiconductor electron affinity. The work function of rGO is taken as 4.4 eV [36], the work function of Ni is 4.6 eV [37] and the work function of Pt is about 5.3 eV [33]. The NiO layers should also be taken into account because oxygen contributes significantly to the electronic state of Ni particle shells, as confirmed by XPS and HAADF-STEM methods. The NiO band gap energy is 3.6 eV and the electron affinity is 5.3 eV [38]. When rGO, Ni and Pt are joined together in a diode-like structure during the C-AFM experiment, it is obvious that the electrons move faster from Pt to rGO due to the higher work function of Pt than that of rGO leaving behind positive charges in NiO. Then current depletion regions are formed by the differences in charge carrier velocity through the bottom and top electrodes (cantilever's tip), respectively and the built-in current–voltage switchable diode effect (Figure 2.10).

The influence of NiO is taken into account because of its considerable role as a buffer layer. The effect was considered in the scope of equilibrium energy band diagrams. The equilibrium energy band diagrams of rGO/NiO/Ni/Pt heterostructures are shown in Figure 2.10. In this structure, the height and width of the contact barrier between graphene, Ni and Pt are defined as differences in work functions -eφ. In the NiO contact area the widths of the contact barrier are correspondingly defined as eΔNiO - eφ. Compared with the contact barrier

between rGO, Pt and Ni the energy band bending at the NiO interface (Φ_w, ΨNiO < eφ) is much smaller due to the large work function of NiO. In addition, the ultrathin p-type NiO layer reduces the contact barrier width at the NiO/Ni interface (ΔNiO, -eφ+Ni). Therefore, with the presence of the NiO buffer layer, electrons can pass through the barrier more easily [35].

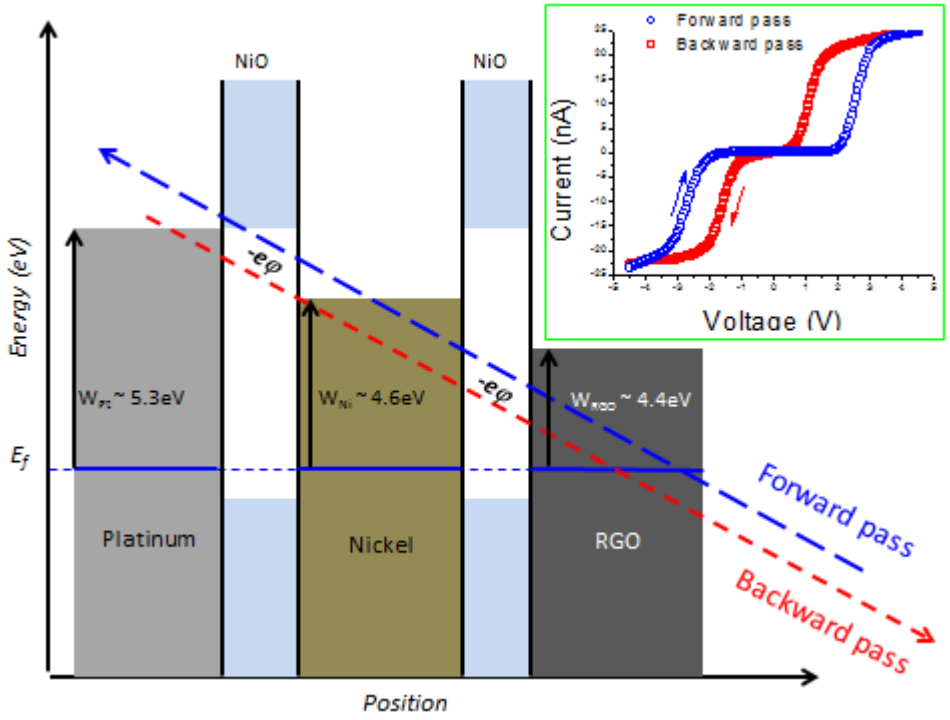

Figure 2. 10 The equilibrium energy band diagrams of rGO/Ni/Pt structure.

2.6 Conclusion

In summary, we showed a new one-step hydrothermal approach for the controlled synthesis of rGO/Ni nanocomposites using $N_2H_4.H_2O$ as a reducing agent. We observed that $N_2H_4.H_2O$ concentration is a key experimental parameter to control the size, morphology, distribution and crystalline structure of Ni particles at the GO surface. $N_2H_4.H_2O$ has a major

role in this reaction not only because it allows control of the nucleation and growth of metallic Ni NPs through the reduction of Ni ions, but also by reducing the surface of GO. The results obtained on the synthetic process showed that the increase of $N_2H_4.H_2O$ concentration in the reaction medium corresponds to an increase of Ni NPs sizes, varying from 145 to 900 nm, and also affects the Ni particles morphologies, from spherical to spiky and finally big agglomerates. For the preparation of all nanocomposites we did not use any alkaline media, despite of the previous reports on such NPs growth, indicating that the pH value can be adjusted in solution using an appropriate amount of $N_2H_4.H_2O$. For nanocomposites with spiky NPs (rGO/spiky Ni) it was observed that the increase of the reaction time promotes the growth of Ni nanothorns. The results also indicate that spiky Ni particles are composed of a core/shell structure: a metallic Ni core and a few nm thin outer layer of NiO. Furthermore, it is observed that the thickness of the NiO outer layer increases with the increase of the reaction time.

By means of spreading resistance SPM mode we have shown that spiky Ni particles implemented in the rGO matrix enhance conductivity with nonlinearity in current-voltage dependence if the output electrodes are attached. Via the equilibrium energy band, we confirmed that all the experimental structure components (Ni particles, rGO, NiO and Pt-tip) are exactly in place, even NiO plays a role of gate insulator. In general, this structure works like a graphene-based transistor switch or embedded in a graphene based matrix switchable diode both of which could be very useful for graphene based embedded nanoelectronics applications.

2.7 Bibliography

[1] K.S. Novoselov, A.K. Geim, S.V. Morozov, D. Jiang, Y. Zhang, S.V. Dubonos, I.V. Grigorieva and A.A. Firsov, "Electric field effect in atomically thin carbon films. *Science*," vol. 306, pp. 666-669, 2004.

[2] S. Ghosh, I. Calizo, D. Teweldebrhan, E.P. Pokatilov, D.L. Nika, A.A. Balandin, W. Bao, F. Miao and C.N. Lau, "Extremely high thermal conductivity of graphene: Prospects for thermal management applications in nanoelectronic circuits," *Appl. Phys. Lett.* vol. 92, no. 15, pp. 151911-151913, 2008.

[3] A.K. Geim, "Graphene: Status and Prospects," *Science*, vol. 324, no. 5934 pp. 1530-1534, 2009.

[4] K.S. Novoselov, V.I. Fal'ko, L. Colombo, P.R. Gellert, M.G. Schwab and K. Kim, "A roadmap for graphene," *Nature*, vol. 490, no.7419, pp. 192-200, 2012.

[5] C. Lee, X.D. Wei, J.W. Kysar and J. Hone, "Measurement of the elastic properties and intrinsic strength of monolayer graphene," *Science*, vol. 321, no. 5887, pp. 385-388, 2008.

[6] Q. Li, N. Mahmood, J. Zhu, Y. Hou and S. Sun, "Graphene and its composites with nanoparticles for electrochemical energy applications," *Nano Today*, vol. 9, no. 5, pp. 668-683, 2014.

[7] H. Wang, H.S. Casalongue, Y. Liang and H. Dai, "$Ni(OH)_2$ Nanoplates Grown on Graphene as Advanced Electrochemical Pseudocapacitor Materials," *Journal of the Am. Chem. Soc.*, vol. 132, no. 21, pp. 7472-7477, 2010.

[8] H. Yin, C. Zhang, F. Liu and Y. Hou, "Hybrid of Iron Nitride and Nitrogen-Doped Graphene Aerogel as Synergistic Catalyst for Oxygen Reduction Reaction," *Adv. Funct. Mater*., vol. 24, no. 20, pp. 2930-2937, 2014.

[9] H. Jabeen, V. Chandra, S. Jung, J.W. Lee, K.S. Kim and S. Bin Kim, "Enhanced Cr(VI) removal using iron nanoparticle decorated graphene," *Nanoscale*, vol. 3, no. 9, pp. 3583-3585, 2011.

[10] Z. Ren, N. Meng, K. Shehzad, Y. Xu, S.X. Qu, B. Yu and J.K. Luo, "Mechanical properties of nickel-graphene composites synthesized by electrochemical deposition," *Nanotechnology*, vol. 26, no. 6, pp. 065706, 2015.

[11] Y.J. Chen, Q.S. Wang, C.L. Zhu, P. Gao, Q.Y. Ouyang, T.S. Wang, Y. Ma and C.W. Sun, "Graphene/porous cobalt nanocomposite and its noticeable electrochemical hydrogen storage ability at room temperature," *J. Mater. Chem.*, vol. 22, no. 13 pp. 5924-5927, 2012.

[12] G.Q. Chen, F.L. Wang, F. Liu and X. Zhang, "One-pot preparation of Ni-graphene hybrids with enhanced catalytic performance," *Appl. Surf. Sci.*, vol. 316, pp. 568-574, 2014.

[13] M.H. Choi, Y.J. Min, G.H. Gwak, S.M. Paek and J.M. Oh, "A nanostructured Ni/graphene hybrid for enhanced electrochemical hydrogen storage," *J. Alloy. Compd*., vol. 610, pp. 231-235, 2014.

[14] K. Gotoh, T. Kinumoto, E. Fujii, A. Yamamoto, H. Hashimoto, T. Ohkubo, A. Itadani, Y. Kuroda and H. Ishida, "Exfoliated graphene sheets decorated with metal/metal oxide nanoparticles: Simple preparation from cation exchanged graphite oxide," *Carbon*, vol. 49, no. 4, pp. 1118-1125, 2011.

[15] K. Bhowmik, A. Mukherjee, M.K. Mishra and G. De, "Stable Ni Nanoparticle-Reduced Graphene Oxide Composites for the Reduction of Highly Toxic Aqueous Cr(VI) at Room Temperature," *Langmuir*, vol. 30, no. 11, pp. 3209-3216, 2014.

[16] G. Goncalves, P.A.A.P. Marques, C.M. Granadeiro, H.I.S. Nogueira, M.K. Singh and J. Gracio, "Surface Modification of Graphene Nanosheets with Gold Nanoparticles: The Role of Oxygen Moieties at Graphene Surface on Gold Nucleation and Growth," *Chem. Mater*., vol. 21, no. 20, pp. 4796-4802, 2009.

[17] Z. Li, Y. Su, Y. Liu, J. Wang, H. Geng, P. Sharma and Y. Zhang, "Controlled one-step synthesis of spiky polycrystalline nickel nanowires with enhanced magnetic properties," *CrystEngComm*, vol. 16, no.36, pp. 8442-8448, 2014.

[18] L.Y. Bai, F.L. Yuan and Q. Tang, "Synthesis of nickel nanoparticles with uniform size via a modified hydrazine reduction route," *Mater. Lett*., vol. 62, no.15, pp. 2267-2270, 2008.

[19] B. Li, H. Cao, J. Yin, Y.A. Wu and J.H. Warner, "Synthesis and separation of dyes via Ni@reduced graphene oxide nanostructures*," J. Mater. Chem*., vol. 22, no. 5, pp.1876-1883, 2012.

[20] Z. Wang, Y. Hu, W. Yang, M. Zhou and X. Hu, "Facile One-Step Microwave-Assisted Route towards Ni Nanospheres/Reduced Graphene Oxide Hybrids for Non-Enzymatic Glucose Sensing," *Sensors*, vol. 12, no. 4, pp. 4860-4869, 2012.

[21] Z. Ji, X. Shen, G. Zhu, H. Zhou and A. Yuan, "Reduced graphene oxide/nickel nanocomposites: facile synthesis, magnetic and catalytic properties," *J. Mater. Chem.*, vol. 22, no. 8, pp.3471-3477, 2012.

[22] B.J. Li, H.Q. Cao, J.F. Yin, Y.M.A. Wu and J.H. Warner, "Synthesis and separation of dyes via Ni@reduced graphene oxide nanostructures," *J. Mater. Chem*., vol. 22, no.5 pp.1876-1883, 2012.

[23] J.J. Wang, H. Pang, J.Z. Yin, L.N. Guan, Q.Y. Lu and F. Gao, "Controlled fabrication and property studies of nickel hydroxide and nickel oxide nanostructures," *CrystEngComm*, vol. 12, no.5, pp. 1404-1409, 2010.

[24] G.X. Zhu, X.W. Wei and S. Jiang, "A facile route to carbon-coated nickel-based metal nanoparticles," *J. Mater. Chem*., vol. 17, no. 22, pp. 2301-2306, 2007.

[25] Y.D. Li, L.Q. Li, H.W. Liao and H.R. Wang, "Preparation of pure nickel, cobalt, nickel-cobalt and nickel-copper alloys by hydrothermal reduction," *J. Mater. Chem*., vol. 9, no. 10, pp. 2675-2677, 1999.

[26] X. Ni, Q. Zhao, Y. Zhang and H. Zheng, "Reticular nickel microwires with assembled nanostructures: Synthesis, magnetism and catalysis for the growth of carbon nanotubes," *Euro. J. Inorg. Chem*., no. 3, pp. 422-428, 2007.

[27] G. Goncalves, M. Vila, I. Bdikin, A. de Andres, N. Emami, R.A.S. Ferreira, L.D. Carlos, J. Gracio and P.A.A.P. Marques, "Breakdown into nanoscale of graphene oxide: Confined hot spot atomic reduction and fragmentation," *Sci. Rep*., 4, pp. 6735, 2014.

[28] A. Mathew, N. Munichandraiah and G.M. Rao, "Synthesis and magnetic studies of flower-like nickel nanocones," *Mater. Sci. Eng: B*, vol. 158, no. 1-3, pp. 7-12, 2009.

[29] Z. Libor and Q. Zhang, "The synthesis of nickel nanoparticles with controlled morphology and SiO_2/Ni core-shell structures". *Mater. Chem. Phys*., vol. 114, no. 2-3, pp. 902-907, 2009.

[30] S. Park, J. An, J.R. Potts, A. Velamakanni, S. Murali and R.S. Ruoff, "Hydrazine-reduction of graphite- and graphene oxide," *Carbon*, vol. 49, no. 9, pp. 3019-3023, 2011.

[31] G.F. Cai, J.P. Tu, J. Zhang, Y.J. Mai, Y. Lu, C.D. Gu and X.L. Wang, "An efficient route to a porous NiO/reduced graphene oxide hybrid film with highly improved electrochromic properties," *Nanoscale*, vol. 4, no. 18, pp. 5724-5730, 2012.

[32] NIST X-ray Photoelectron Spectroscopy Database, Version 4.1, National Institute of Standards and Technology, Gaithersburg, 2012, http://srdata.nist.gov/xps/.

[33] C. Wang, K.J. Jin, Z.T. Xu, L. Wang, C. Ge, H.B. Lu, H.Z. Guo, M. He and G.Z. Yang, "Switchable diode effect and ferroelectric resistive switching in epitaxial $BiFeO_3$ thin films," *Appl. Phys. Lett*., vol. 98, no. 19, pp. 192901, 2011.

[34] G.D. Rodrigues, P. Zelenovskiy, K. Romanyuk, S. Luchkin, Y. Kopelevich and A. Kholkin, "Strong piezoelectricity in single-layer graphene deposited on SiO_2 grating substrates," *Nat. Comm*., vol. 6, pp. 7572, 2015.

[35] C.S. Lee, Y.J. Lin and C.T. Lee, "Investigation of oxidation mechanism for ohmic formation in Ni/Au contacts to p-type GaN layers," *Appl. Phys. Lett*., vol. 79, no. 23, pp. 3815-3817, 2001.

[36] Y.Y. Zhang, X. Li, L.C. Wang, X.Y. Yi, D.H. Wu, H.W. Zhu and G.H. Wang, "Enhanced light emission of GaN-based diodes with a NiOx/graphene hybrid electrode," *Nanoscale*, vol. 4, no. 19, pp. 5852-5855, 2012.

[37] W.P. Maszara, Z. Krivokapic, P. King, J.S. Goo and M.R. Lin, "Transistors with dual work function metal gates by single full silicidation (FUSI) of polysilicon gates," International Electron Devices 2002 Meeting, Technical Digest, 367-370, 2002.

[38] M.D. Irwin, J.D. Servaites, D.B. Buchholz, B.J. Leever, J. Liu, J.D. Emery, M. Zhang, J.H. Song, M.F. Durstock, A.J. Freeman, "Structural and Electrical Functionality of NiO Interfacial Films in Bulk Heterojunction Organic Solar Cells," *Chem. Mater*.,vol. 23, no. 8, pp. 2218-2226, 2011.

A.1 Supplementary material of chapter 2

Figure A.1.1 shows FTIR spectra of GO, G/Ni3, G/Ni4 and G/Ni5 nanocomposites. GO profile pattern represents a complete oxidation of graphite. The broad band at high frequency (2800-3600) cm^{-1} and also a band at 2360 cm^{-1} related to vibration of OH group. Adsorption bands in 1722 cm^{-1}, 1620 cm^{-1} and 1044 cm^{-1} confirmed the vibration of C=O (in COOH), C=C and C-O groups respectively. In rGO/Ni FTIR spectrum there are two weak peaks at 1558 cm^{-1} and 1176 cm^{-1}. The former is related to C-O vibration band and the later one is related to graphene sheets vibration. The rest of oxygen functional groups do not exist anymore according to the reduction of GO[1].

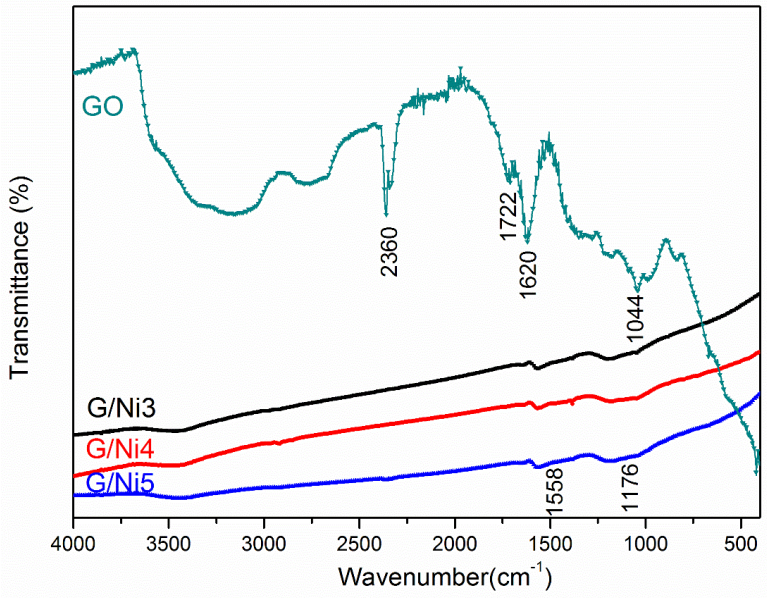

FigureA.1.1 FTIR spectra of GO, G/Ni3, G/Ni4 and G/Ni5.

High-angle annular dark-field scanning transmission electron microscopy (HAADF-STEM) of G/Ni5 nanocomposite with corresponding elemental information in the core of a Ni particle and in a single nanothorn are shown in Figures A.1.2 and A.1.3, respectively. This

information indicated that the core and the nanothorn of Ni particle composed of about 99% metallic Ni and around 1 % oxygen. This confirmed a very thin oxidation layer covering the Ni particles both around the cores and the nanothorns.

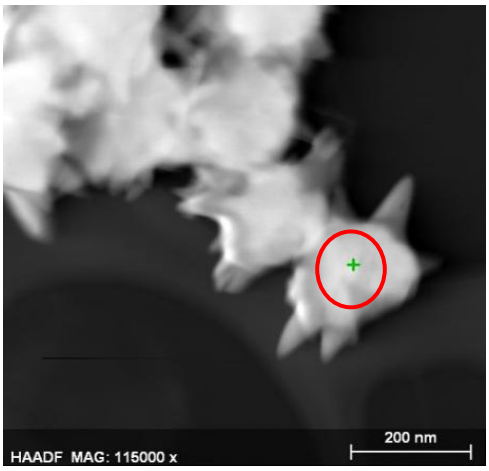

FigureA.1.2 High-angle annular dark-field scanning transmission electron microscopy of G/Ni5 nanocomposite and corresponding elemental information at selected area of Ni core.

Elements	Series	Net	[wt.%]	norm.wt.%]	[norm.at.%]	Error in wt.%(3 sigma).
Oxygen	K-series	5062	1.14954	1.14954	4.091551	0.202793
Nickel	K-series	1846671	98.85046	98.85046	95.90845	21.144
		Sum:	100	100	100	

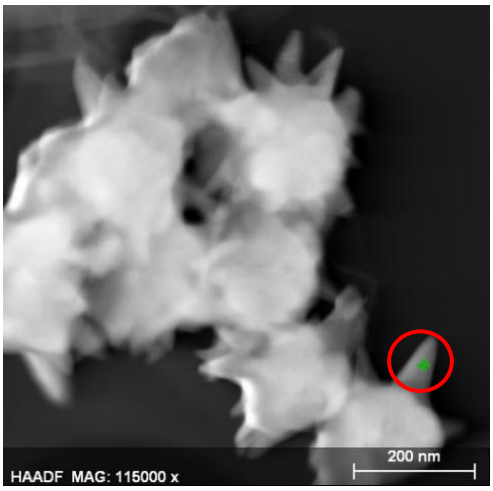

FigureA.1.3 High-angle annular dark-field scanning transmission electron microscopy of G/Ni5 nanocomposite and corresponding elemental information at selected area of one single nanothorn.

Elements	Series	Net	[wt.%]	norm.wt.%]	[norm.at.%]	Error in wt.%(3 sigma).
Oxygen	K-series	703	0.749622	0.749622	2.69604	0.189628
Nickel	K-series	394874	99.25038	99.25038	97.30396	21.23402
		Sum:	100	100	100	

[1] Z. Ji, G. Zhu, X. Shen, H. Zhou, C. Wu and M. Wang "Reduced graphene oxide supported FePt alloy nanoparticles with high electrocatalytic performance for methanol oxidation," *New J. Chem.*, vol. 36, no. 9, pp. 1774-1780, 2012.

Chapter 3

Solvothermal synthesis of Ni/rGO nanocomposite: from nickel nanoclusters to homogeneously distributed discrete nickel nanoparticles

3.1 Scope

Here we present a two-step synthesis protocol based on a solvothermal method supplemented by a thermal treatment under H_2 atmosphere to decorate reduced graphene oxide (rGO) with nanosized nickel nanoparticles (Ni NPs).

The control of the size of Ni NPs to values less than 10 nm and of their density at the surface of Ni/rGO nanocomposite was successfully achieved by the control of the reaction time. The obtained results showed that, at the initial stage of the solvothermal process, the GO surface is saturated by the formation of Ni nanoclusters. With the increase of the reaction time it was observed that the adjacent nanoclusters are able to coalesce and form monodisperse ultrafine Ni NPs at the surface of rGO nanosheets. The thermal treatment of the nanocomposites under reducing atmosphere of H_2 showed to play a crucial role for the formation of metallic Ni NPs. The electrophysical properties (work function and conductivity) of the Ni/rGO nanocomposites were founded in direct dependence on the Ni NPs size and NiO buffer layer width. We proposed a crucial role of the NiO buffer layer thickness in Pt-NiO-Ni-NiO-rGO interface changing the conductivity from metallic to Schottky contact and to p-n heterojunction making the prepared Ni/rGO nanocomposite a favorable material in the scope of nanoelectronics and lithium ion batteries.

3.2 Introduction

Graphene oxide (GO) has been widely explored as a substrate for the controlled growth of different type of NPs to develop new multifunctional nanocomposites with interesting properties able to achieve high performance on different areas of application. The high active surface area, light weight, thermal stability and high electron transport properties are remarkable features that makes graphene an extraordinary substrate for the integration with different types of NPs[1]. These extraordinary properties in combination with the singular properties of different inorganic NPs can provide a new category of nanomaterials for nanoelectronics [2], biomedical [3], energy storage [4], catalysis [5], chemical and biological sensor applications [6]. Among inorganic NPs, Ni NPs have been the focus of intense research due to its remarkable magnetic, [7, 8] conductive [9], catalytic [10] and hydrogen storage [11] properties. However, accurate control of the nanocomposite synthesis parameters is needed in order to maximize the synergistic effects of the different components and obtain a significant improvement on its final properties. Indeed the large particle size, agglomeration and non-homogeneously distributed NPs on substrate, impairs their functionalities [12].

Hydrothermal methods are the most explored approaches for the synthesis of graphene nanocomposites due to the massive and cost-effective production. Several works reported the formation of micrometric size of nickel oxide (NiO) particles via hydrothermal route for the preparation of rGO based nanocomposites [13-15]. The precise control over particles morphology was reported as an important advantage of hydrothermal synthesis process [16, 17]. Recently, we reported that the effective control of the concentration of strong reducing agent, hydrazine, in solution medium is a key factor for the reduction of cationic Ni ions and controlled growth of spiky Ni NPs on rGO surface [18]. Generally, despite the simplicity of the hydrothermal methods, it is difficult to obtain nanosized Ni with narrow particle size distribution in graphene based nanocomposites. Curiously, Zhou et al. reported a multistep methodology for synthesis of Ni/graphene nanocomposite for hydrogen storage with Ni NPs size of 10 nm, however it was reported a broad NPs size distribution [11, 19]. Literally, a few studies states that an accurate control of the concentration of Ni precursor can be the key

experimental factor for the preparation of Ni/graphene nanocomposites with very small and well distributed NPs [19, 20].

Solvothermal method is considered a more elegant approach for the synthesis of metal and metal oxide NPs and respective graphene-based nanocomposites due to the better control over the size and size distribution of NPs, morphology and crystallinity [21]. Several factors including reactant concentration, additives, pH, reaction time and temperature are involved to produce NPs with desired size and morphology [22]. In addition, solvothermal methods can have a strong impact on GO structure during the nanocomposites preparation. Nethravathi et al. observed that the reduction of GO can occur at low temperature (120 °C-200 °C) for both non-reducing (water) and reducing solvent (ethylene glycol or ethanol), however the extent of the reduction is higher in case of using the reducing solvents [23].

The use of stabilizer agents for the controlled growth of NPs is conventional in solvothermal methods. Recently, Tian el al reported a one-step production of Ni/rGO nanocomposites using ethylene glycol as a solvent and poly(N-vinyl-2-pyrrolidone) as a stabilizer. These authors observed the formation of spherical Ni NPs with an average size of 8 nm well distributed at the rGO surface, which provides excellent properties for catalysis [24]. Unprecedented work performed by Li et al. described the preparation of carbon monoliths evenly decorated with superfine Ni NPs through the formation of covalent bonds with carbon (Ni-C) by solvothermal method. The nanocomposite was synthesized using Ni nitrate as a precursor, ethanol as a solvent, ascorbic acid as a stabilizer and hydrazine as a reducing agent. After thermal treatment, the nanocomposites showed a very uniform dispersion of isolated Ni NPs with an average size of 10 nm and a very narrow size distribution [25]. A novel approach for the synthesis of Ni/graphene nanocomposites was also recently reported by Zhang et al. using pre-doped graphene with sulfur and nitrogen (N-S-G) for the functionalization with hybrid Ni tetrapyridyloxyphthalocyanine (NiTPPc) via solvothermal method. The results showed that the establishment of π-π interactions allows a homogenous coverage of the N-S-G surface with the NiTPPc nanocrystals with an average size of around 10 nm. The authors reported that the nanocomposite exhibits superior electrocatalytic activity towards the oxidation of bisphenol A, comparing with pristine NiTPPc or N-S-G [26].

In this current study, we report a new and efficient two step synthesis of nanosized and mono dispersed Ni NPs homogeneously decorated the surface of rGO nanosheets. The solvothermal treatment promotes the nucleation and growth of Ni nanoclusters at the surface of rGO through the reduction of Ni acetate in diethylene glycol. It is observed that the size of the Ni nanoclusters formed at the surface is dependent on the solvothermal reaction time and can varied from just a few nanometers until a maximum of approximately 10 nm. The subsequent thermal treatment in a reductive hydrogen atmosphere at 450 ºC, promotes the crystallization into metallic Ni NPs. Moreover, we provide an experimental confirmation of the theoretical results previously obtained by Cheng et al. dedicated to the first-principle calculation of electronic structure of the graphene/metal oxide interfaces [27]. Particularly, the Schottky barrier height (SBH) and the Schottky-Mott limit (SML) were calculated for the graphene/Ni/NiO-Ni interface which is similar to the one investigated in the current work for the Ni/rGO composites. Finally, we provide a comparison of theoretical and experimental values for the SBH, SML and work function (WF). A sufficient conductivity decreasing and WF increasing as function of the Ni NPs radius and a NiO buffer layer width were observed which are consistent with the theoretical predictions described [2, 27]. These crucial results make the Ni/rGO a favorable nanocomposite for the nanoelectronics (Shottky contact, n-p heterojunctions) and lithium ion battery (anode material) application areas. Consequently, we propose a remarkable benefit of the Pt-NiO-Ni-NiO-rGO interface as a part of embedded electronic circuit where a variation of conductivity from metallic to those characteristic of a Shottky contact or a p-n heterojunction is needed.

3.3 Material and Methods

3.3.1 Materials

Graphite powder (powder, >45 mm, ≤99.99%, Sigma-Aldrich), Diethylene glycol (≥99.0%, Sigma-Aldrich) and Nickel (II) acetate tetrahydrate (99.999%-Ni, Stream Chemicals) were purchased and used as received.

3.3.2 Synthesis of graphene oxide

GO was obtained from graphite using the modified Hummers method, usually considered as a top-down approach for the synthesis of graphene. Basically, it consists on the exfoliation of graphite into individual GO layers via oxidative process [28]. Briefly, 2 g of graphite was dispersed in a 50 mL of sulfuric acid, after that 7 g of potassium permanganate was added slowly to the reaction medium and kept aging during 2 hours. The reaction was stopped by addition of H_2O_2 (30 wt % in water). The resultant suspension was intensively washed with distilled water by filtration until solution reach neutral pH. Finally, GO solution was lyophilized and a dried powder was obtained.

3.3.3 Solvothermal synthesis of nickel/graphene oxide nanocomposites (Ni/GO)

For the synthesis of Ni/GO nanocomposites, 2 mg of Ni (II) acetate was first dissolved in 10 mL diethylene glycol (DEG) for 3 hours stirring. After that 10 mg of GO was added to the solution and sonicated during 15 minutes in order to obtain a homogeneous brownish GO dispersion in DEG. The mixture was transferred to a 25 mL Teflon autoclave and heated at 150 ºC for 1, 3, 6 and 24 hours. The resultant samples were labeled as Ni/GO1, Ni/GO3 and Ni/GO6 and Ni/GO24, respectively. After cooling down, the samples were subjected to centrifugal separation and then washed extensively with deionized water and finally freeze dried.

To investigate the effect of the reaction temperature, one sample was prepared under same experimental preparation and heating at 200 ºC for 24 hours and labeled as Ni/GO 24 (200 ºC).

3.3.4 Thermal annealing of nanocomposites under hydrogen atmosphere (Ni/rGO)

All the samples prepared by solvothermal method were heat treated in a tubular furnace at 450°C with the heating rate of 5 °C/min, under hydrogen flow of 8 mL/min during 2 h. The obtained samples were labeled as Ni/rGO1, Ni/rGO3, Ni/rGO6 and Ni/rGO24, respectively.

3.3.5. Materials Characterization

The powder X-ray diffraction (XRD) patterns of the samples were collected at room temperature in a continuous scanning mode (step 0.04°) on a powder diffractometer PANalytical Empyrean with a secondary monochromator CuKα X-radiation in the range of 5°-90°. The Raman spectra were collected using Thermo Scientific DXR smart Raman spectrometer with excitation wavelength of 532 nm with a power of 10 mW. Transmission electron microscope (TEM) and high resolution TEM (HRTEM) images were taken with FEI Tecnai G2 20 and FEI Titan^3 80-300 microscope. FTIR data were collected from KBr pellets using FTIR Bruker Tensor 27 with the resolution of 4 cm^{-1} in the range of 4000 cm^{-1} to 500 cm^{-1}. X-ray photoelectron spectroscopy (XPS) was carried out in a system equipped with SPECS Phoibos 150 and monochromatic Al Ka X-ray source. The spectra were recorded at normal emission take-off angle and with a pass-energy of 20 eV. XPS data in this study were calibrated for BE $C1s = 284.5$ eV [29]. Inductively coupled plasma optical emission spectroscopy (ICP-OES) technique was used to determine the Ni content in each synthesized nanocomposite. This measurement was carried out using an ICP-OES, Horiba Jobin-Yvon, Activa M model with forward power of 1000W, 12 L/min argon flow plasma and sheath gas 0.8 L/min equipped with Burgener MiraMist nebulizer. About 5mg of each sample were weighted and digested with 1mL HNO3 p.a. and 1mL HCl p.a. on a microwave oven system (CEM MARS 5). The samples were collected to 100 mL flasks and were filled with milli Q water.

Nanoscale characterization of the samples was carried out by using a commercial scanning probe microscope Ntegra Prima (NT-MDT) operating in semicontact and contact Atomic Force Microscopy (AFM), Kelvin Probe Force Microscopy (KPFM), Spreading Resistance (SR) and Conductive Atomic Force Microscopy (c-AFM) modes permitting the topography, surface potential distribution, conductivity and local current measurements to be measured. Pt-coated NSG03/Pt cantilevers with a resonance frequency of 100 kHz and a force constant of 4 N/m were used. KPFM technique [30] allowed to measure a work function (WF) difference between the tip and the sample according to the equation

$$V_{CPD} = \frac{W_{tip} - W_{sample}}{-e} \qquad (1)$$

where W_{tip} is a WF of the SPM tip, W_{sample} is a WF of the sample, e is the elementary charge, and V_{CPD} is the measured contact potential difference, viz. the surface potential. *AC* voltage of the second pass was 0.1 V, lifting height was 50 nm. Bias voltage applied to the samples during the SR and c-AFM measurements varied in the range of 1-10 Volts. All the scanning probe microscopy (SPM) measurements were carried out in ambient conditions at humidity of about 30%.

3.4 Results and discussion

3.4.1 Solvothermal synthesis of Ni/GO nanocomposites

The synthesis of Ni/GO nanocomposites was performed by solvothermal method using DEG as both solvent and reducing agent for controlling the Ni NPs growth on the surface of GO nanosheets. Our experimental results were conducted under mild temperature conditions (150 ºC) using different reaction times for the accurate control of the size and density of Ni NPs. The XRD analysis of the as-prepared nanocomposites does not clearly indicate the

presence of the characteristic peak of Ni crystalline phase, suggesting that, if the Ni species are present at the surface of GO, they are in the amorphous state (Figure 3.1a)). In fact, it was already reported that the use of DEG at a reaction temperature near its boiling point (244 ºC) promotes a higher reduction reaction rate and degree of crystallinity of the Ni NPs. In this study, the sample prepared at 200 ºC showed also bigger Ni particles (≈1μm) with higher crystallinity than the ones prepared at 150 ºC and randomly distributed on rGO surface. (see XRD in Figure A.2.1 and SEM in Figure A.2.2 in supplementary material section).

With respect to the Figure 3.1a), the XRD pattern of GO is also shown that presents a sharp peak at 10.1º with a calculated (Bragg equation) basal d spacing of 8.7 Å which is characteristic of (002) planes. The XRD spectrum of Ni/GO1 showed a similar peak position for GO, which indicates a low degree of reduction for short periods of solvothermal reaction time. Indeed, it was observed a significant shift and broadening of the characteristic GO peak for higher 2θ values with the increase of reaction time for samples Ni/GO3, Ni/GO6 and Ni/GO24. The appearance of XRD (002) peak for Ni/GO3, Ni/GO6 and Ni/GO24 at 22.7º, confirm the successful conversion of GO to rGO due to the high reduction of oxygen containing functional groups [31, 32]. In addition the broadening of (002) peaks indicates a short-range order in stacked graphene layers with increase of the reaction time [1]. The increasing of interplanar spacing of the samples with the reaction time might be due to the introduction of Ni species into the GO structure. Lee et al reported the synthesis of rGO/α-$Ni(OH)_2$ hybrid composites using ethylene glycol medium. In their study, it was reported that the (002) plane of GO did not shift significantly after the preparation of the different nanocomposites, although they used different experimental conditions (temperature of 180 ºC during 6h and NaOH as a reducing agent) [33].

The FTIR analysis of GO displayed high intensity bands that are attributed to several oxygen functional groups (Figure 3.1b). The broad band with a maximum at ~3450 cm^{-1} is usually attributed to -OH stretching vibrations. The characteristic stretching vibrations of C=O at 1730 cm^{-1}, C=C at 1626 cm^{-1}, C-O at 1222 cm^{-1} and C-O-C at 1057 cm^{-1} are also clearly present. The two small bands at 2930 and 2855 cm^{-1} can be assigned to the asymmetric and symmetric vibrations of CH_2 stretching, that became more evident with the increase of

reaction time due to the GO reduction [34]. FTIR spectrum of sample Ni/GO1 showed the lower decrease of the intensity of bands corresponding to the oxygen functional groups, suggesting that 1 hour of solvothermal reaction time has a small impact on the reduction of GO, which is in good agreement with the XRD data discussed before. For the samples, Ni/GO3, Ni/GO6 and Ni/GO24 the reduction of GO is much more evident. The reduction of oxygen functional groups is evidenced by the decrease of intensity of the bands at 1730, 1222 and 1053 cm^{-1} which clearly indicate the conversion into rGO. It was also observed for those samples that the C=C band shifts for lower wavelength values of 1575 cm^{-1}.

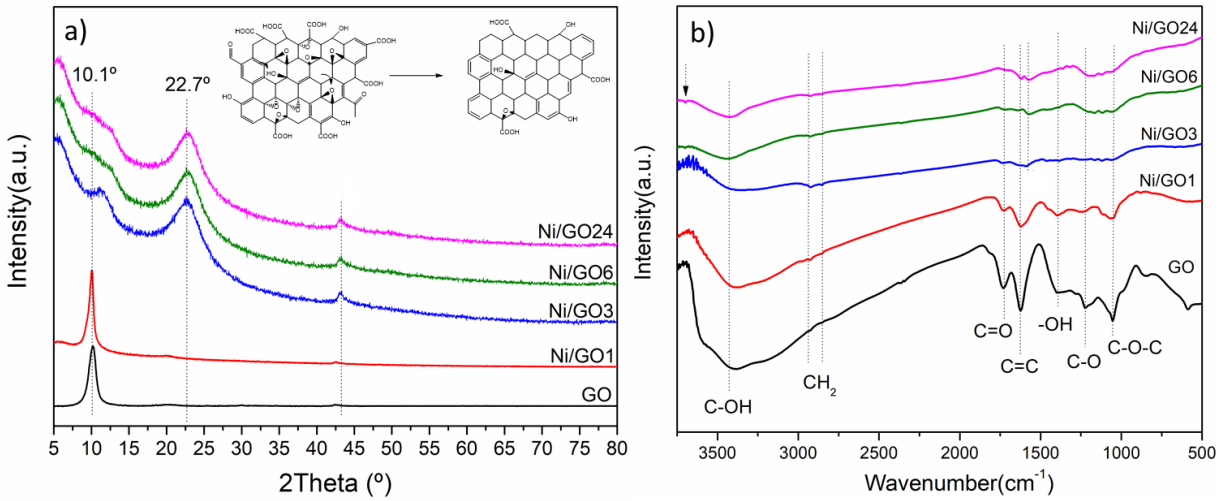

Figure 3.1 XRD profile and FTIR spectrum of Ni/GO nanocomposites synthesized using different solvothermal reaction times.

Wang et al. suggests that this shift can be attributed to the π electrons interactions in the polarizable aromatic ring being transformed into cation–π interactions [35]. Moreover, the band at 3450 cm^{-1} for Ni/GO samples was not just limited to the OH contribution, it can also be attributed to stretching vibrations of metal hydroxide ($Ni(OH)_2$) [33]. Indeed, it was observed for those samples the appearance of a new peak at 3635 cm^{-1} which can be attributed to the formation of nickel hydroxide as reported by Jeevanandam et al [36]. The appearance of two new peaks in the region 1500-1000 cm^{-1} may also suggest the presence of $Ni(OH)_2$. Niederberger et al. recently reviewed the mechanisms for the formation, growth and surface functionalization of metal oxide NPs in organic solvents [22]. In this work, several nonaqueous systems were proposed for the formation of M-OH and M-O-M bonds through

organic reactions. The Guerbet-type reaction reported, seems to be the most appropriate organic mechanism for formation of a metal hydroxide using primary alcohols as solvent. However, we believe that the mechanism for our system should not be restrict to the organic reaction proposed because the oxygen functional groups presented at GO surface play also an important role on the mechanism of nucleation and growth of Ni.

X-ray photoelectron spectroscopy (XPS) analysis was carried out to determine the chemical structure of GO and Ni/GO nanocomposites. High resolution detailed spectra of C1s and Ni2p of samples GO and Ni/GO1, Ni/GO3, Ni/GO6 and Ni/GO24 are shown respectively in Figure 3.2 a) and b). The C1s spectra show a significant decrease of the intensity of carbon containing oxygen groups (C-O) with the increase of solvothermal reaction time (Figure 3.2a)) [37]. Nevertheless, for samples with solvothermal treatment times higher than 3h the C1s spectra showed similar profile. This data suggests that 6 hours of solvothermal treatment is enough to reduce the GO. High resolution detailed spectra of Ni2p for Ni/GO samples showed the appearance of two major peaks centered at 872.9 and 855.8 eV that can be assigned to $Ni(OH)_2$ phase [38].

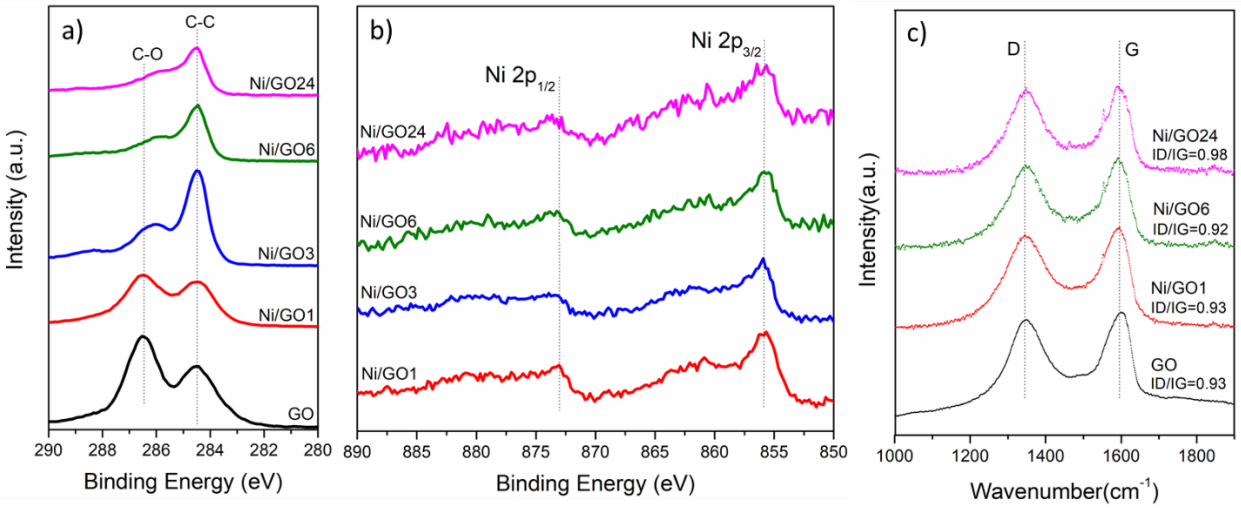

Figure 3.2 High resolution XPS of C 1s a) and Ni 2p b); Raman spectra c) for the nanocomposites Ni/GO after solvothermal treatment at different reaction times (1h, 3h, 6h and 24h).

Raman study of the nanocomposites were performed in order to access the structural changes induced by the solvothermal process. All samples showed the presence of characteristic D and G bands of the GO (Figure 3.2c)). The I_D/I_G ratio correlate with the average size of sp^2 domains with the level of disorder in graphene planes [39]. The I_D/I_G ratio calculated for GO sample was 0.93, which is very similar with the values observed for the samples after solvothermal treatment of 1h and 6h, 0.93 (Ni/GO1) and 0.92 (Ni/GO6) respectively. These results suggest that the integration of Ni species on GO surface occurs preferentially on defect regions without causing significant disturbs on the aromatic structure. However, for sample with higher reaction time (24h) it was observed a considerable increase of the I_D/I_G value to 0.98 (Ni/GO24). This pronounced increase of I_D/I_G value corresponds to the decrease of graphene domains (G band) and correspondingly increase of structural defects (D band) [40]. These results suggest an increased integration of Ni NPs into the rGO structure causing the formation of more aromatic carbon structural defects.

3.4.2 Reduction of Ni/GO nanocomposites by thermal treatment under hydrogen atmosphere

After solvothermal reaction, all samples were thermal treated under a reductive atmosphere of hydrogen at 450 ºC during 2h, in order to induce the formation of crystalline metallic Ni NPs at the surface of rGO. XRD pattern of Ni/rGO nanocomposites showed a peak at 25.0º that can be assigned to rGO layers with the interplanar spacing of 3.52 Å [41] (Figure 3.3a). The results showed a slight shift of the (002) peak for higher 2θ values when compared with the values observed for the respective samples after solvothermal treatment. These changes are caused by a more effective reduction of rGO after the thermal treatment in a reducing hydrogen atmosphere, which improve the decomposition and removal of residual oxygen groups and consequently promotes a higher rearrangement of the aromatic structure [42]. The XRD patterns of Ni/rGO1, Ni/rGO3, Ni/rGO6 and Ni/rGO24 nanocomposites also showed the clear presence of metallic Ni phase after thermal treatment under reductive hydrogen atmosphere. Three peaks at 44.43°, 51.99° and 76.31° can be attributed to (111),

(200) and (220) crystal planes of Ni NPs with fcc crystal structure (JCPDS, no. 04-0850). It was also observed a shoulder at ~43º that can be attributed to the (200) plane of NiO (JCPDS, no. 47-1049) [43]. These results can suggest that the Ni NPs are composed by a core of metallic Ni and a shell of NiO as recently reported by Wang et al [43]. However, there is also the possibility of the peak at 43º be attributed to rGO due to the re-staking process of the nanosheets [44].

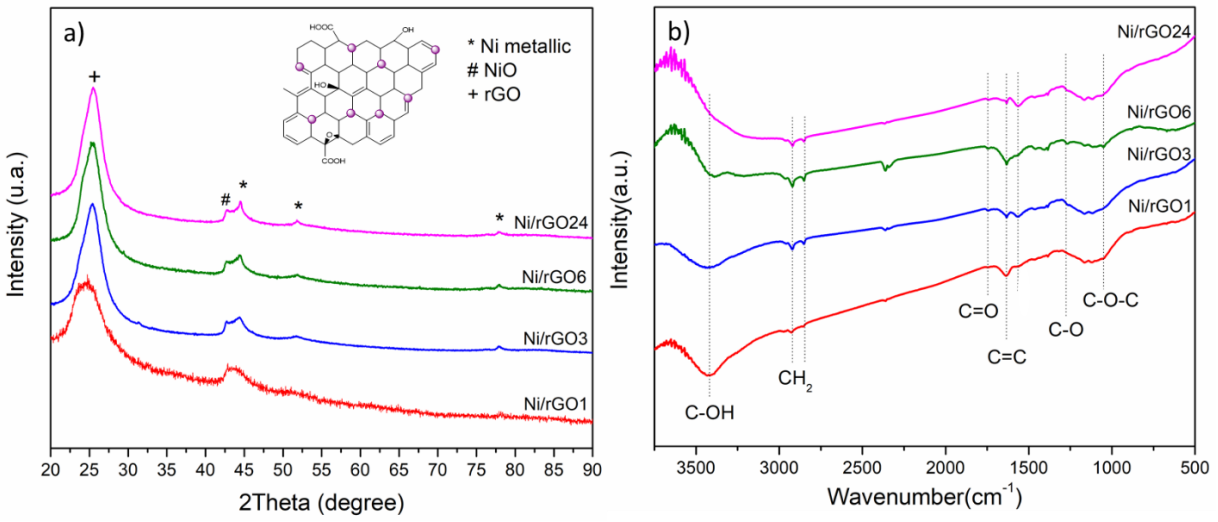

Figure 3.3 XRD patterns a) and FTIR b) of different Ni/rGO nanocomposite after thermal treatment under hydrogen at 450 ºC during 2 h (Ni/rGO).

FTIR spectra for Ni/rGO nanocomposites are shown in Figure 3.3b. The results showed that the thermal treatment used, promoted a significant reduction in the intensity of the peaks associated to oxygen functional groups, in particular for the sample Ni/rGO1. However, the results revealed that some oxygen functional groups remain on the rGO structure, such as C-OH (3420cm^{-1}), C=O (1740cm^{-1}), C-O (1270 cm^{-1}), C-O-C (1050cm^{-1}) after this reduction conditions. The peak at 1640 cm^{-1}, attributed to the skeletal ring vibrations (C=C) suffers an unusual shift for lower frequency after the reduction treatment with hydrogen. Yoon et al. reported that after hydrogenation of rGO the C=C bonds appear at region 1550 cm^{-1}. At the region of 1400-1380 cm^{-1} it is also observed the appearance of two main peaks that are usually attributed to -C-H vibrations. These results can suggest that the graphene structure can be

doped with hydrogen after thermal treatment. Furthermore, it is possible to observe an increase of the intensity of the bands corresponding to CH_2 asymmetric stretching at 2920 cm^{-1} and symmetric stretching at 2850 cm^{-1}, suggesting the possible hydrogenation of the graphene structure [45].

High resolution XPS spectra of C1s and Ni 2p from samples Ni/rGO1, Ni/rGO3, Ni/rGO6 and Ni/rGO24 heat treated with H_2 are shown in Figure 3.4. C1s spectra showed a significant reduction of oxygen functional groups of rGO when compared with the respective spectra obtained for samples before this treatment. The small shoulder at 286 eV correspondents to C-O bonds, which shows the presence of some residual oxygen functional groups on the graphene planes for all the samples after thermal treatment under H_2 atmosphere as observed by FTIR.

The high resolution Ni2p spectra exhibit two main components for all the samples. A shoulder around 853 eV that can be attributed to the metallic nickel (Ni (0)) and the peak around 855 eV is related to the oxidized Ni species (NiO) [43]. These data suggest that the surface of Ni NPs is oxidized in the form of NiO instead of $Ni(OH)_2$, as observed before the reductive thermal treatment.

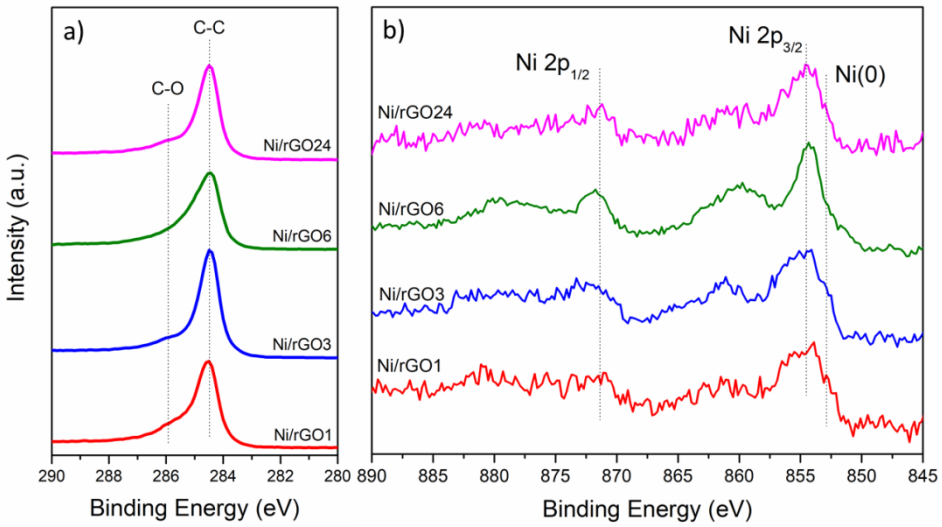

Figure 3.4 High resolution XPS of C 1s a) and Ni 2p b) for the nanocomposites Ni/rGO prepared after thermal treatment in hydrogen atmosphere at 450 ºC during 2h.

Raman studies of samples Ni/rGO1, Ni/rGO6 and Ni/rGO24 after H_2 reduction showed that I_D/I_G ratio calculated were 0.94, 0.96 and 0.99 respectively (Figure 3.5). These data are similar to the values observed before the reduction treatment, that suggest no significant structural changes on the rGO sheets during the thermal treatment.

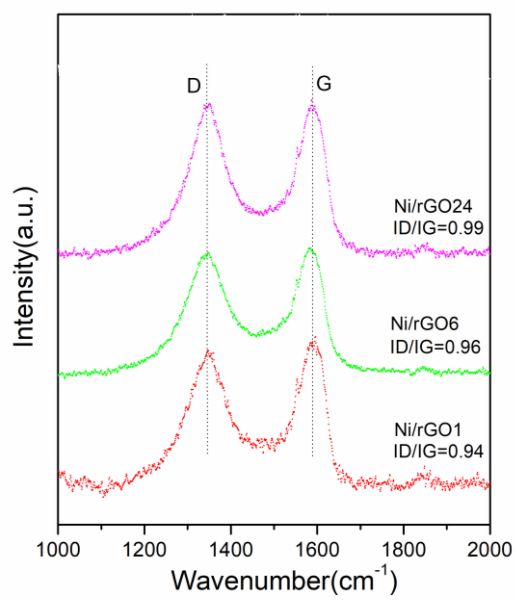

Figure 3.5 Raman spectra of different nanocomposite samples after reduction under hydrogen atmosphere at 450 ºC during 2h.

The obtained results suggested that the thermal treatment did not affect notably the structure of rGO, in contrast, it was observed that has a strong effect on the structural properties of Ni NPs on the final nanocomposites (see SEM images (Figure A.2.3) in supplementary material section). The structural analyses of the different nanocomposites after thermal annealing at 450 ºC under reducing atmosphere were examined by TEM. Figure 3.6 shows the TEM images of Ni/rGO1, Ni/rGO3, Ni/rGO6 and Ni/rGO24. For all samples, it was observed the presence of very small round shaped Ni NPs homogenously distributed on the rGO surface. In fact, samples Ni/rGO1 and Ni/rGO3 show a lower contrast between the Ni NPs and the surface of rGO nanosheets, contrarily to samples Ni/rGO6 and Ni/rGO24 which show a higher contrast. These results suggest, since the thermal treatment time is similar for all the samples, that the reaction time during the solvothermal synthesis plays an important role on the nucleation and growth of Ni nanoclusters at the rGO surface. Evidences obtained by the analyses of Ni NPs size distribution in the inset of Figure 3.6 show a quite similar size

distribution for samples Ni/rGO1 (5.9±3.2 nm), Ni/rGO3 (4.4±2.6 nm) and significant increase of NPs size for sample Ni/rGO6 (8.7±4 nm) and Ni/rGO24 (10.50±3.8). Curiously, it can be observed by TEM images that the concentration of Ni NPs at the surface of rGO sheets decrease with the increase of solvothermal reaction time. These results suggest that solvothermal synthesis of Ni/GO nanocomposites occurs through two different stages. The first stage of nucleation of Ni nanoclusters limited by the saturation of the surface of GO, afterwards, the second stage that corresponds to the growth of the Ni NPs through the coalescence of neighbor Ni nanoclusters and reduction of GO to rGO as confirmed before by XPS, FTIR and XRD.

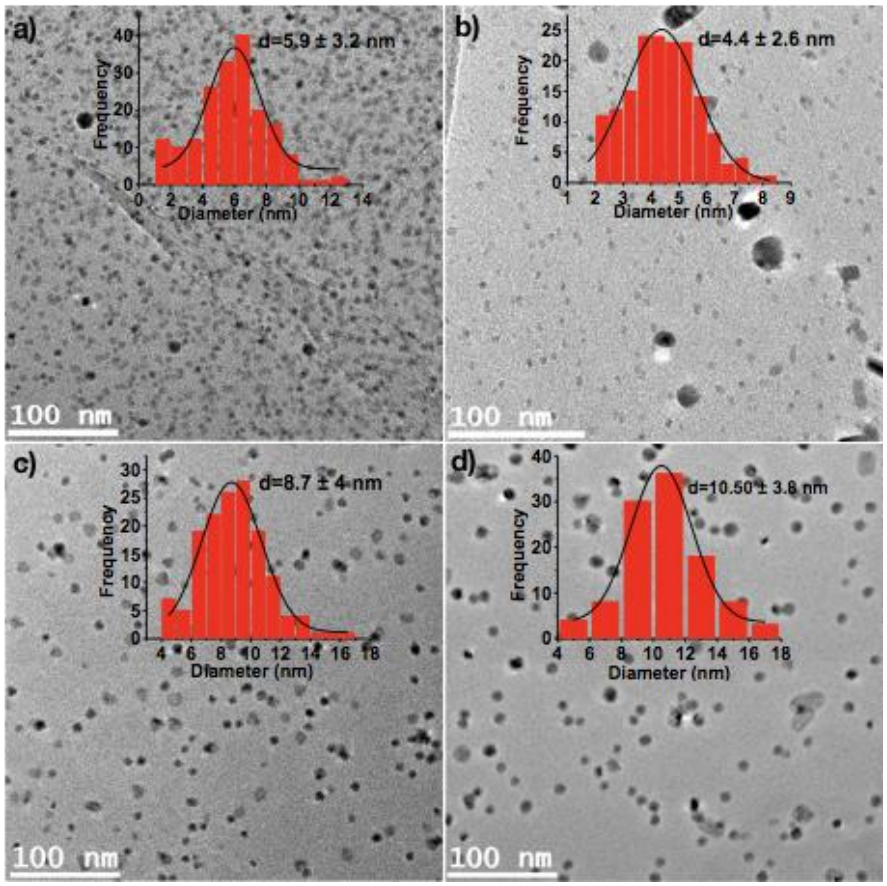

Figure 3.6 TEM images of the Ni/rGO nanocomposites after reduction under hydrogen atmosphere at 450 ºC during 2h (Ni/rGO1 a), Ni/rGO3 b), Ni/rOG6) and Ni/rGO24).

In order to further investigate the previous assumption, the topography of Ni/rGO samples was investigated by AFM (see Figure 3.7a). AFM images showed the flat surface of rGO

nanosheets with homogeneous distributed Ni NPs for all the synthesized nanocomposites. The NPs size distribution calculated using AFM data showed the average sizes of around 11.0, 11.5, 13.0 and 22.0 nm for samples Ni/rGO1, Ni/rGO3, Ni/rGO6 and Ni/rGO24, respectively (Figure 3.7b).

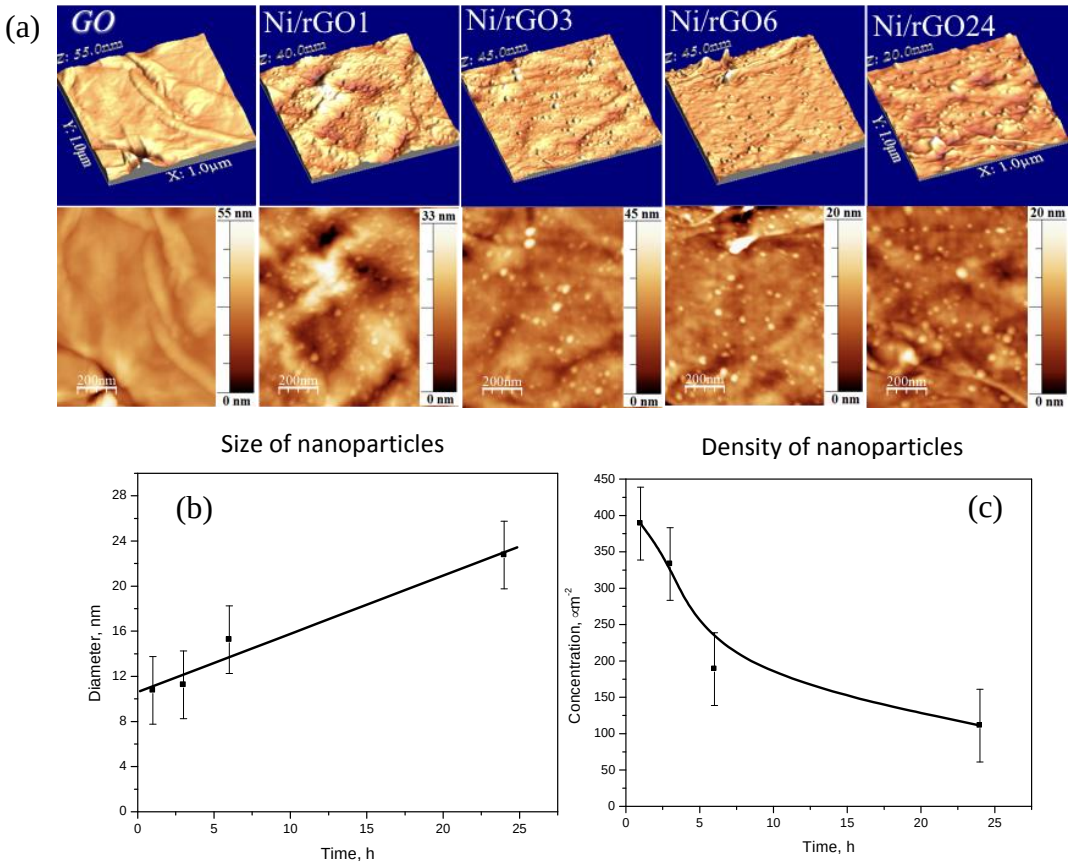

Figure 3.7 a) AFM images of the GO and Ni/rGO nanocomposites after thermal annealing under hydrogen atmosphere at 450 ºC during 2h, b) Ni NPs size distribution and c) density of NPs at the surface of the different nanocomposites.

Although the size distribution of Ni NPs at the surface of rGO obtained by AFM measurements didn't correspond exactly to the values obtained by the TEM analysis, they followed the same increasing trend according to the increase of solvothermal reaction time. The deviation from the real size of NPs reflect the limitation associated with the size of AFM tip apex radius. Interestingly, the calculations of the density of the Ni NPs at the surface of rGO (Figure 3.7c) showed a significant decrease with the increase of solvothermal reaction

time. These data are in good agreement with those observed by TEM, where it was suggested that the growth of the Ni NPs over time occurs predominantly by the coalescence of smaller Ni NPs at the surface of rGO nanosheets.

The schematic representation in Figure 3.8, proposed that for the short solvothermal reaction times (1h) a primary heterogeneous nucleation of Ni species occurs at GO surface, resultant from the Ni precursor decomposition and establishment of interactions with the oxygen functional groups at GO surface [46]. In fact, the precise nature of the species involved in this stage is not completely clear due to high diversity of oxygen functional groups available at GO surface. With the increase of the solvothermal reaction time, in particular for samples 3h, 6h and 24h, it is possible to observe by TEM the continuous growth of Ni NPs, probably by the possible coalescence of the neighbor primary nanoclusters. Furthermore, it was also observed that after the coalescence of the primary nanoclusters into NPs, no more primary nanoclusters can be formed at the free surface of rGO for samples 3h, 6 and 24 h. In order to confirm this behavior, the quantification of the Ni for the samples prepared under different reaction times was determined by ICP. The results obtained showed the following quantity of Ni for samples: Ni/rGO1 (8.0 %m/m), Ni/rGO3 (3.0 %m/m), Ni/rGO6 (2.8 %m/m) and Ni/rGO24 (2.8 %m/m). In fact, it can be confirmed that after 1h of reaction time it was obtained the Ni saturation of GO surface (higher concentration of Ni). Curiously, it was observed a marked decrease in concentration of Ni for reaction times $\geq$ 6 hours (2.8 %m/m) rather than a constant concentration of Ni over all the reaction time. These results suggested that the quantity of Ni at the surface of GO is related with the level of the reduction of GO. As discussed before, according to the XPS results, the reduction equilibrium of GO occurs for 6h solvothermal treatment and for the same reaction time it is now observed a constant concentration of Ni (2.8 %m/m) for nanocomposites.

This behavior (schematized in Figure 3.8) indicates that the oxygenated surface of GO (Figure 3.8a) plays an important role on the nucleation and anchorage of primary nanoclusters, (green spheres Figure 3.8b), probably some of the primary clusters can coalesce during solvothermal reaction time to form Ni NPs at rGO surface (blue spheres Figure 3.8c). In the meantime, and simultaneously, some of these primary nanoclusters can be released from the

GO surface due to the removal of oxygen anchorage sites during the reduction process (green spheres Figure 3.8c). Increasing the reaction time up to 6h continually increasing the size of NPs (red spheres Figure 3.8d) and finally after 24h the bigger NPs with lower coverage density are formed (yellow spheres in Figure 3.8e) from coalescence of smaller ones (red spheres in Figure 3.8e) on rGO surface (pathways of smaller nanoparticles movement is shown in red on rGO).

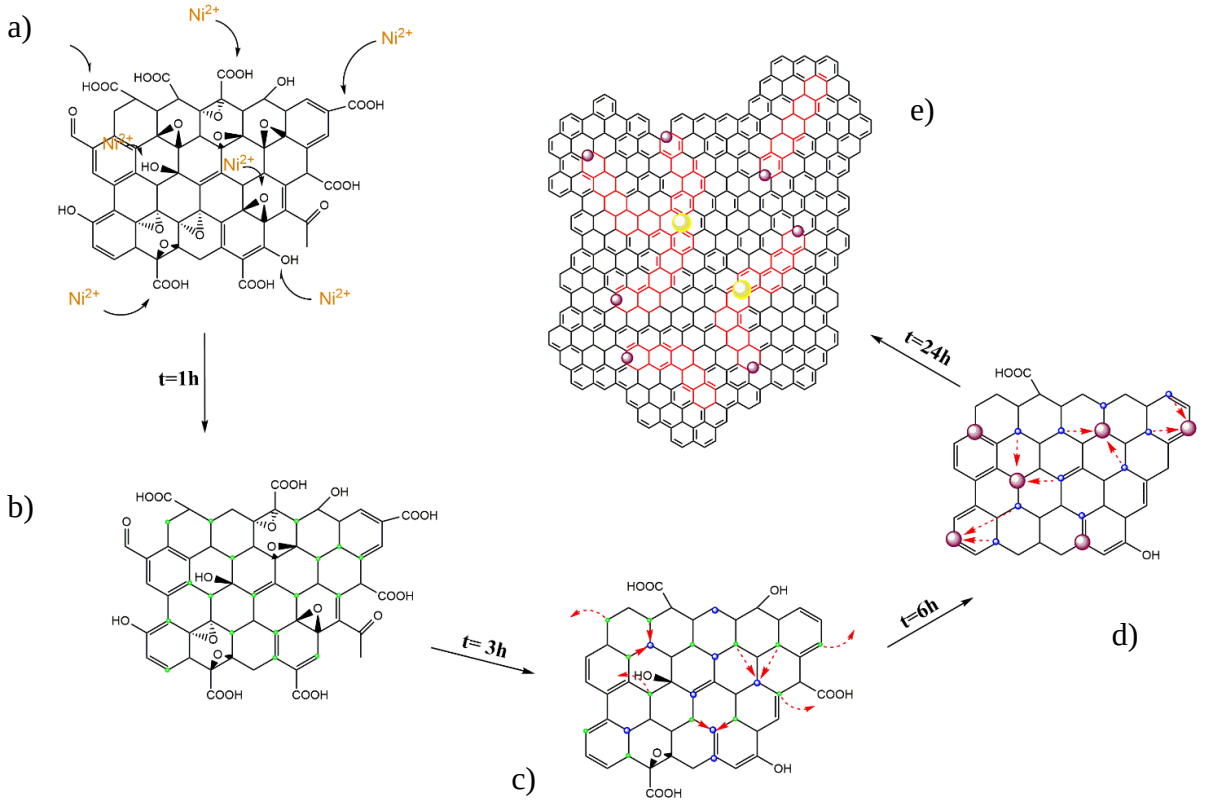

Figure 3.8 Schematic representation of nucleation and growth of Ni NPs at GO surface (not to scale): Solvothermal treatment of GO in DEG using nickel acetate as a precursor during t=1h, t=3h, t=6h and t=24h. After solvothermal synthesis, all the Ni/GO nanocomposites were thermal treated under hydrogen atmosphere at 450 ºC during 2h in order to form metallic Ni NPs.

The combination of these two phenomena can explain the constant decrease of the density of primary Ni nanoclusters and the constant growth of Ni NPs over the solvothermal reaction time.

The structural surface of the Ni/rGO nanocomposites heat treated with H_2 was further investigated by HRTEM. The HRTEM images of the nanocomposites Ni/rGO1, Ni/rGO3, Ni/rGO6 and Ni/rGO24 are shown in Figure 3.9. For all the Ni NPs investigated on the

different nanocomposites we observed the marked lattice fringes corresponding to the crystal planes, Ni(111) with a interplanar distance of approximately 0.2 nm and the NiO(111) with interplanar distance of approximately 0.24 nm [43]. These results suggest the formation of core-shell structure of Ni/NiO at the surface of rGO for all the samples after thermal treatment under hydrogen atmosphere. In fact, the results obtained suggest that the formation of NiO shell is more pronounced for the samples with higher reaction times. Moreover, HRTEM image of sample Ni/rGO24 showed the coalescence between two Ni/NiO NPs at the surface of rGO nanosheets (blue dot-line). Recently Li et al. reported an in situ atomic-scale observation of coalescence driven nucleation and growth at liquid/solid interfaces of Bi/$SrBi_2Ta_2O_9$ [47]. These results reinforce our predictions that suggest the decrease of the density of Ni NPs on the surface of rGO occurs due to the coalescence of the neighboring nanoclusters to larger NPs.

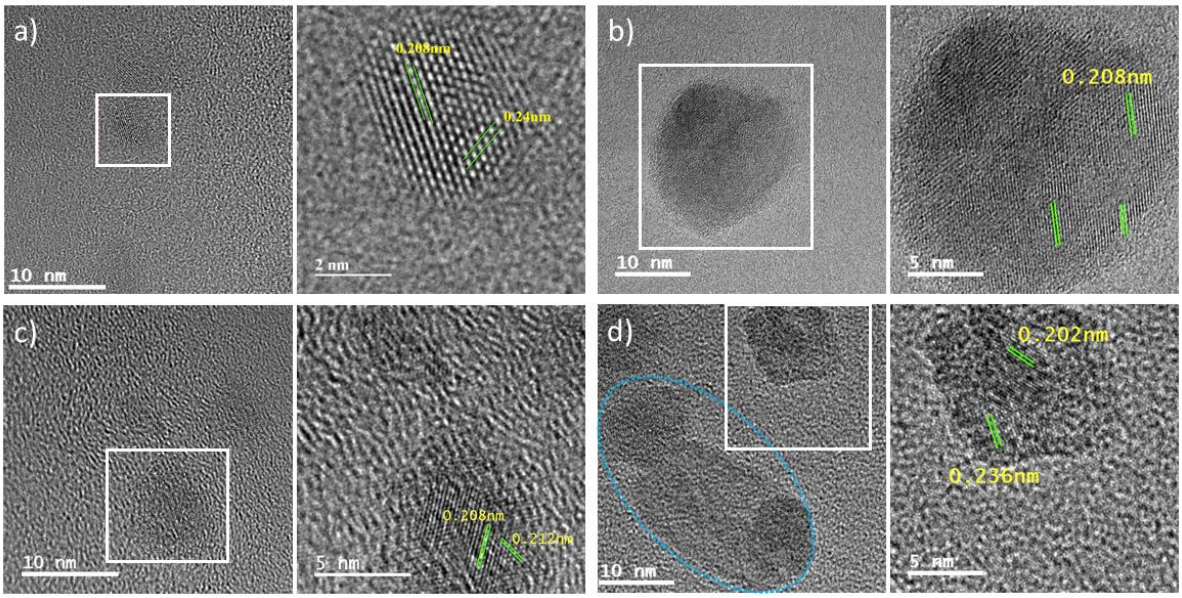

Figure3.9 HRTEM images of the nanocomposites Ni/rGO1 a), Ni/rGO3 b), Ni/rGO6 c) and Ni/rGO24 d). The blue dot-line shows the coalescence between two Ni/NiO NPs on rGO.

3.5 SPM measurements of Ni/rGO nanocomposites

Kelvin Probe Force Microscopy (KPFM) carried out for the reference rGO sample shows a homogeneous potential distribution corresponding to the work function of ~ *4.7±0.4* eV (Figure 3.10a)). The value is consistent with the previously reported data (Table 3.1).

KPFM responses measured on the surface of the Ni/rGO nanocomposites suggest a distribution of the electric potential. The Ni NPs appeared as dark dots with a lower V_{CPD} signal (higher WF) as compared to the rGO matrix (Figure 3.10). Being measured at the very local scale (~2 x 2 μm), the sample Ni/rGO1 demonstrates a uniform KPFM response (Figure 3.10 (b)). For the 1h sample this kind of behavior could be linked with an effect of doping of the rGO matrix with Ni ions without formation of the NPs and/or nanoclusters. On the contrary, the samples Ni/rGO3, Ni/rGO6 and Ni/rGO24 show a random distribution of the NPs at the local scale (Figure 3.10 (c-e)). The results correlate well with the TEM data (Figure 3.6), even though the size of the particles cannot be determined precisely due to the large tip apex radius (~ 25 nm) and huge impact of electrostatic interaction between the tip and Ni/rGO composite surface. It has been pointed out that increasing the heating time (from 1 to 24 hours) gives rise to increase of both the Ni NPs size and NiO layer thickness. The latter plays an important role in the interaction between the Ni NPs via a changing the electrostatic force from attractive to repulsive [18]. This assumption fully correlates with the V_{CPD} values (Figure 3.10 (b-e)) which decreasing with increasing of the Ni NPs diameter and NiO width.

The Ni/rGO3 and Ni/rGO6 samples show similar KPFM responses from the Ni NPs distributed in the rGO matrix (Figure 3.10 (c, d)). However, the difference of 3 and 6 hour's reactions causes the variation of Ni NPs types where the big particles could be formed from the aggregation of the smaller ones. Probably, due to this effect, the distribution of the Ni NPs into rGO matrix for the Ni/rGO3 and Ni/rGO6 samples are obviously different. At the same number of scans, an additional KPFM phase which corresponds to the work function of graphene was measured in these samples. This phase appears as a strong background, especially in the Ni/rGO6 sample. The pattern of this background is close to that characterizing the NPs distribution. We suppose that one of the possible reasons underlying

the appearance of such a background could be due to the formation of graphene NPs during the heating (annealing) of rGO matrix accompanying the Ni/rGO3 and Ni/rGO6 samples fabrication. Additional KPFM measurements performed at different second pass heights (10-100 nm) and integral current amplifying (0.1-1 nA) confirm the dissimilar nature of the Ni and background nanoparticle signals. In contrast, the Ni/rGO24 sample shows a clear distribution of the individual Ni NPs with lower density due to the change of electrostatic forces to the repulsive (the size of the NPs shown in Figure 3.10 (e) correlates with the TEM data presented in Figure 3.6).

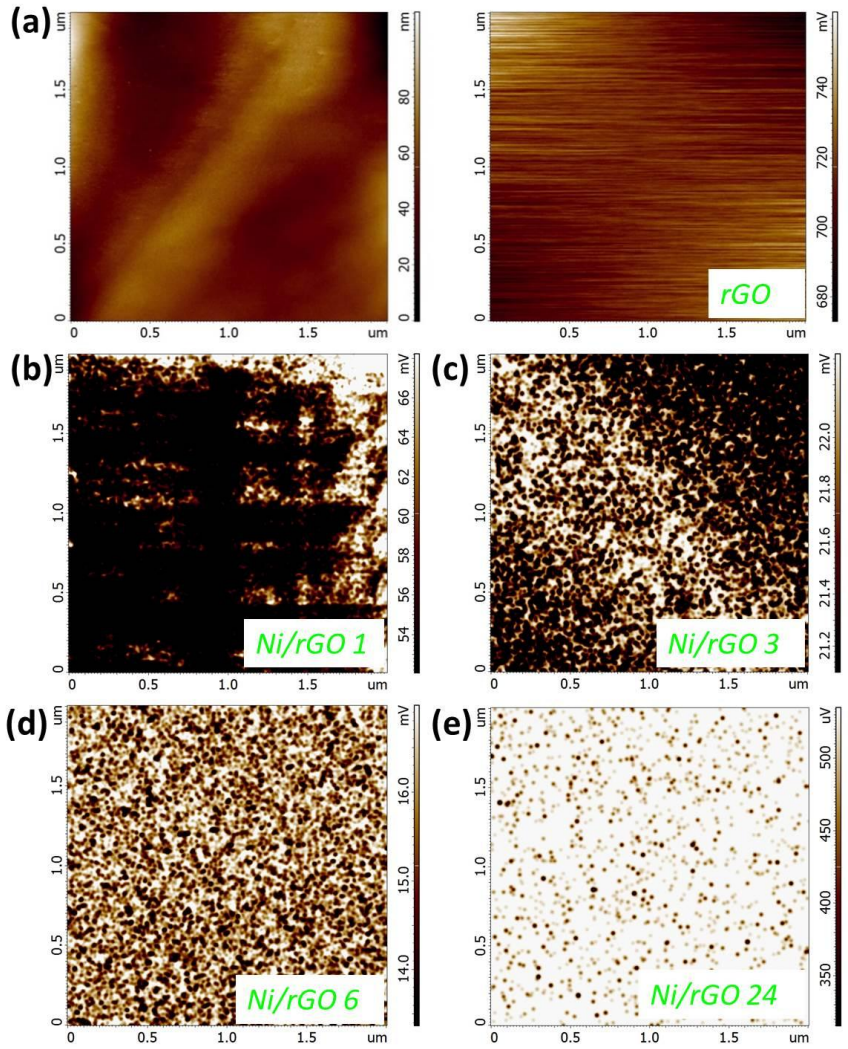

Figure 3.10 Topography (left) and corresponding KPFM response (right) of (a) reference rGO sample; the KPFM responses of Ni/rGO1 (b) 3 (c), 6 (d) and 24 (e) composites.

Table 3.1 Recommended work functions for polycrystalline materials [48]

Material (polycrystalline)	***Work function (eV)***
Pt	*5.5 ± 0.4*
Graphite	*4.60±0.34*
rGO	*4.30±0.2*
Ni	*5.2±0.2*

The variation in the V_{CPD} *(WF)* of the nanocomposites should be associated with a difference in the NiO shell width. The crucial role of the buffering NiO shell in electro-physical behavior of the Ni/rGO nanocomposite has been previously shown in our previous work[18]. Our results suggested that the increase of Ni NPs size causes the increase in the NiO layer width, thus changing the conductivity of the Ni NPs in the rGO matrix and tuning the dielectric permittivity of the Ni/rGO nanocomposites. These results have been predicted in the theoretical work reported by Cheng et al. [27] devoted to the calculation of Schottky Barrier Height (SBH) and Schottky-Mott (S-M) limit of the interface between graphene (GR), Ni and NiO layers. The reported values for SBH and S-M were -0.414 eV and -1.023 eV, respectively. The positive charge doping in NiO layer was predicted to take place over the depth of about 1.2 Å, which is consistent with the 0.609 eV difference between SBH and S-M [27]. This correlates with the KPFM data obtained on the Ni/rGO composites (Figure 3.10 (b - e)).

The surface roughness studied during the contact Spreading Resistance (SR) measurements was found to be around 10 nm. The SPM topography is characterized by the smoothed surface morphology specific to all the Ni/rGO samples (the topographies recorded in the semicontact mode and presented in Figure 3.10 (a, b) coincides with that captured in the contact mode). The roughness does not influence the measured current distribution (Figure 3.10 (a), Figure 3.11 (e)). In general, the SR signal represents a real mapping of the sample conductivity which, for the Ni/rGO (1, 3, 6) nanocomposites, demonstrates a very similar

behavior (Figure 3.11 (a-c)). The surface of these composites is composed of the almost uniformly conductive and insulating regions. This behavior of conductivity could be explained by a trend of Ni NPs towards compact packing (probably due to a strong electrostatic attractive force between the NPs) forming the conductive chains and planes (blue arrow in Figure 3.11 (c, f)). The insulating regions could be explained as appearing due to the deterioration of the rGO matrix induced by Ni NP rearrangement (red arrow in Figure 3.11 (c, f)). The SR mapping of the Ni/rGO24 composite differs from that characteristic of the 1, 3, 6 samples: corresponding measurements show conductivity pattern combining the responses from individual and grouped Ni NPs distributed in rGO matrix (Figure 3.11 (d)). These data are fully consistent with the KPFM results (Figure 3.10 (e)), thus reaffirming the suggestion regarding the great influence of electrostatic repulsive forces between the NPs on the conductivity of the Ni/rGO24 nanocomposite. Finally, the SR signal of the reference rGO sample corresponds to the almost insulating behavior and can be measured only at 10 V (Figure 3.11 (e)). These data completely confirm a huge impact of Ni NPs to the highly increase of the rGO matrix conductivity.

The c-AFM measurements were done at the most conductive parts of the Ni/rGO nanocomposites and the reference (rGO) sample (Figure 3.12 (a) compares the currents registered at ± 3 V). The current–voltage dependence obtained for the rGO sample shows a standard nonlinear p-type semiconductor behavior (Figure 3.12 (b)). The I–V dependence of the Ni/rGO1 sample demonstrates a typical Ohmic behavior with two distinct regions: 0 ± 25 nA (0 ± 0.05 V) and ± 25 nA ± 50 nA (± 0.05 V ± 3 V), respectively. In this measurement, the microscope apparatus saturation current was achieved at ± 3 V (50 nA). This type of I–V curve is associated with a metallic conductivity of doped rGO matrix [49]. The staircase current-voltage behavior is explained by the Coulomb blockade effect describing by the cooperative quantum tunneling of electrons across Ni NPs.

The forward and backward current-voltage dependences obtained for the Ni/rGO (3, 6, 24) nanocomposites show an obvious diode-like rectifying I–V characteristic (Figure 3.12 (d-f)). It can be seen that during the measuring cycle the diodes polarity can be switched in the range of 0.5-4 V.

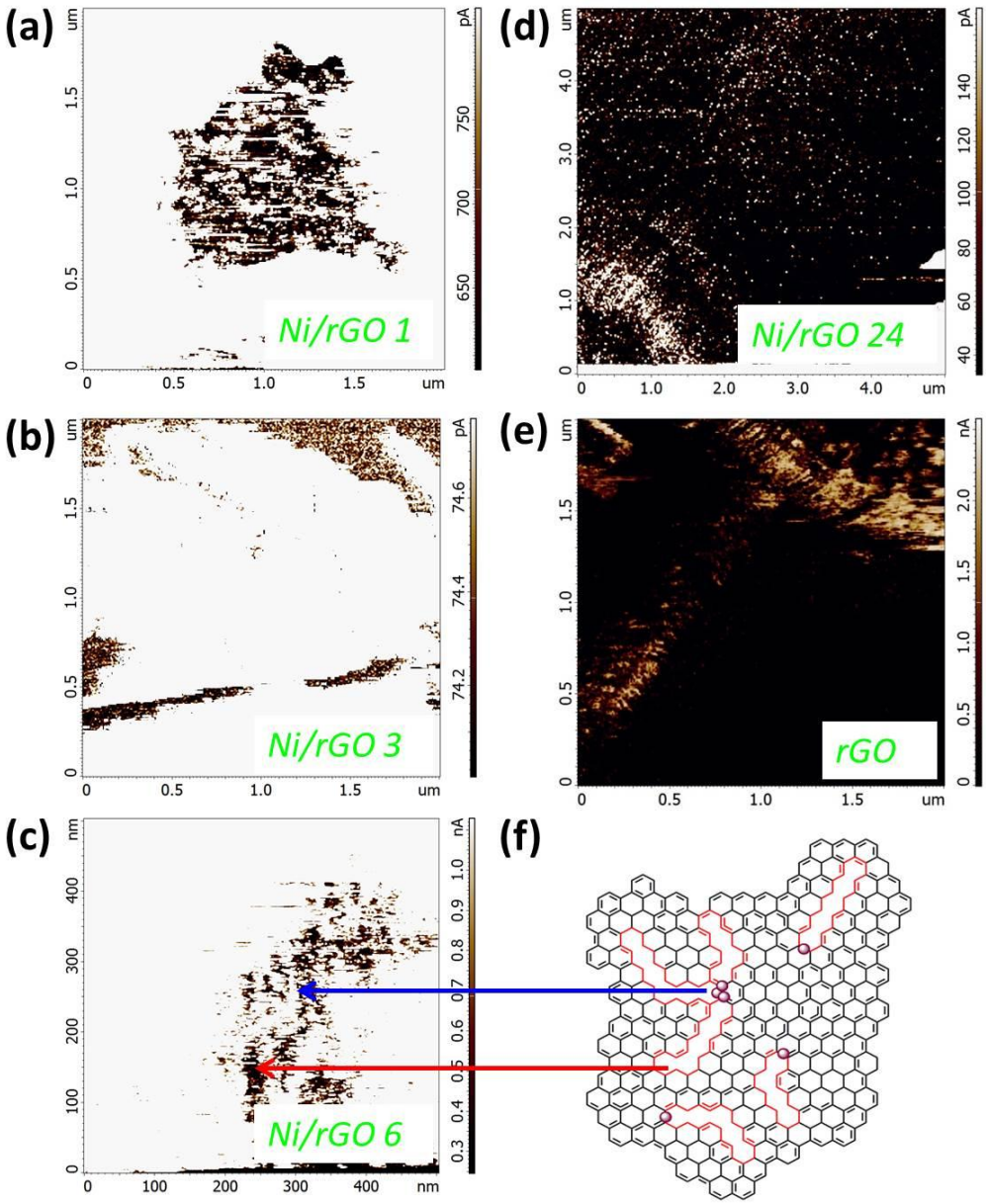

Figure 3.11 The SR signal measured in the Ni/rGO 1 (a), 3 (b), 6 (c), 24 (d) at 1 V and rGO (e) at 10 V; f) schematic representation of the deterioration of the rGO matrix induced by Ni NP rearrangement.

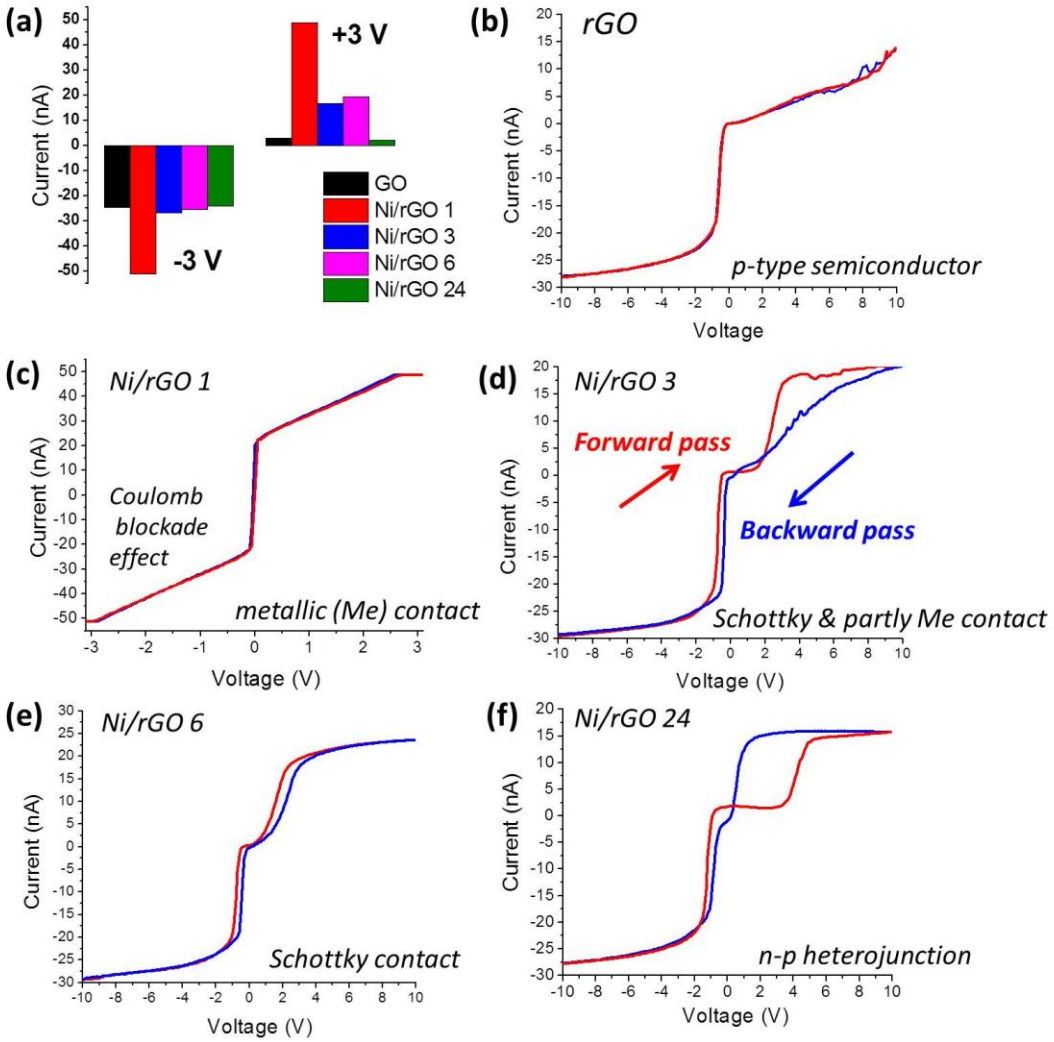

Figure 3.12 a) A comparison of the currents registered in Ni/rGO and rGO samples at ± 3 V; current-voltage behavior of the rGO (b), Ni/rGO1 (c), 3 (d), 6 (e) and 24 (f) samples.

Based on the analysis of the I-V curve (Figure 3.12), the switchable diode behavior in the Ni/rGO (3, 6, 24) samples can be explained by the interaction between Ni NP, NiO shell and rGO matrix and modulation of diode barriers at both bottom and top (cantilever's tip) electrodes. In particular, the Ni/rGO3 sample demonstrates the Ohmic behavior for the backward pass (Figure. 11(d)), which probably reflects some residual metallic coupling between Ni NPs. The increase of NiO width causes the typical Schottky-like I–V characteristic in the Ni/rGO6 sample (Figure 3.12 (e) and schematized in Figure 3.13) and n-p

heterojunction behavior in the Ni/rGO24 sample (Figure 3.12 (f) and schematized in Figure 3.13). In terms of the n-p heterojunction, the interface Pt-NiO plays a role of n-type area and the interface rGO-NiO plays a role of p-type area. Both, the n-type and p-type areas are connected via the Ni NP: Pt-NiO-**Ni**-NiO-rGO (Figure 3.13). These results support the theoretical predictions recently described by Cheng et al [27]. Moreover, our assumption is consistent with the KPFM measurements of the Ni/rGO24 nanocomposite showing that the broadening of the NiO shell causes the increase of the work function (Figure 3.10 (b - e)) and decrease of the conductivity (Figure 3.12 (a)).

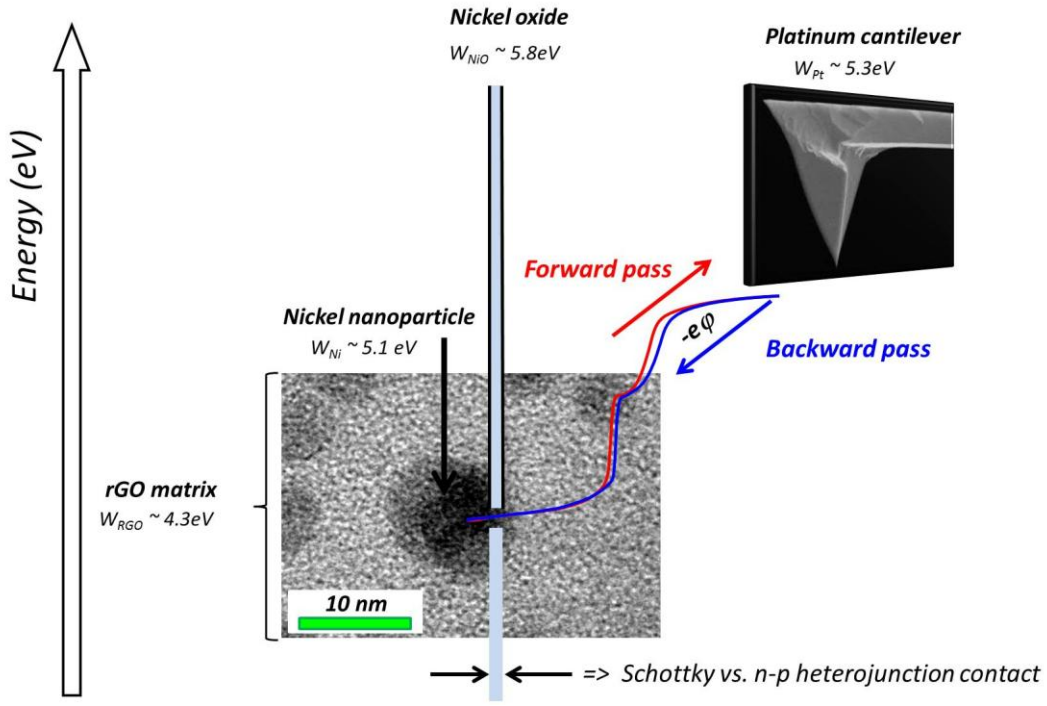

Figure 3.13 The schematic view of the energy diagram organized in the Ni/rGO nanocomposites and the effect caused by the NiO buffer layer.

3.6 Conclusions

In summary, we reported solvothermally fabrication of reduced graphene oxide decorated with Ni from nanocluster to fine discrete NPs homogeneously distributed on the surface of rGO. Four different reaction time 1h, 3h, 6h and 24h were used in solvothermal synthesis. Further reduction in hydrogen atmosphere caused the formation of metallic Ni nanocluster and Ni NPs on the rGO surface.

It was found that simply controlling the reaction time in solvothermal process dictate the size and size distribution of the particles at the final stage. The role of hydrogen reduction has been assumed to reduce the nanocomposite to form metallic Ni. This treatment had strong influence for further reduction of GO only for those samples that were solvothermally heat treated in short reaction time (1h and 3h).

The potential advantage of this proposed method is to design different matrix of Ni/rGO exhibiting different electronic functionalities. As it was shown by electrophysical measurements the work function and conductivity were founded in direct dependence on the Ni NPs size, NiO buffer layer width and Ni NPs concentration. This allows manipulating the conductivity of Pt-NiO-Ni-NiO-rGO interface from metallic with quantum Coulomb blockade effect (Ni/rGO1) to Schottky (Ni/rGO6) towards to n-p heterojunction behavior (Ni/rGO24) making the prepared Ni/rGO nanocomposite a favorable material for nanoelectronics applications.

3.7 Bibliography

[1] M. Khan, M.N. Tahir, S.F. Adil, H.U. Khan, M.R.H. Siddiqui, A.A. Al-warthan and W. Tremel, "Graphene based metal and metal oxide nanocomposites: synthesis, properties and their applications," *J. Mater. Chem. A*, vol. 3, no. 37, pp. 18753–18808, 2015.

[2] C. Chen, W. Cai, M. Long, B. Zhou, Y. Wu, D. Wu and Y. Feng, "Synthesis of Visible-Light Responsive Graphene Oxide/TiO2 Composites with p/n Heterojunction", *ACS Nano*, vol. 4, no. 11, pp. 6425-6432, 2010.

[3] K. Yang, L. Feng, X. Shi, Z. Liu, "Nano-graphene in biomedicine: theranostic applications", *Chem. Soc. Rev*, vol. 42, no. 2, pp. 530-547, 2013.

[4] L. Fenghua, S. Jiangfeng, Y. Huafeng, G. Shiyu, Z. Qixian, H. Dongxue, I. Ari, N. Li, "One-step synthesis of graphene / SnO_2 nanocomposites and its application in electrochemical supercapacitors," *Nanotechnology*, vol. 20, no. 45, pp. 455602, 2009.

[5] L. Shang, T. Bian, B. Zhang, D. Zhang, L.-Z. Wu, C.-H. Tung, Y. Yin, T. Zhang, "Graphene-Supported Ultrafine Metal Nanoparticles Encapsulated by Mesoporous Silica: Robust Catalysts for Oxidation and Reduction Reactions," *Angew. Chem. Int. Ed*, vol. 53, no. 1, pp. 250-254, 2014.

[6] I.V. Lightcap, T.H. Kosel, P.V. Kamat, "Anchoring Semiconductor and Metal Nanoparticles on a Two-Dimensional Catalyst Mat. Storing and Shuttling Electrons with Reduced Graphene Oxide," *Nano Lett.*, vol. 10, no. 2, pp. 577-583, 2010.

[7] D.-H. Chen, C.-H. Hsieh, "Synthesis of nickel nanoparticles in aqueous cationic surfactant solutions," *J. Mater. Chem.*, vol. 12, no. 8, pp. 2412-2415, 2002.

[8] S.-H. Wu, D.-H. Chen, "Synthesis and characterization of nickel nanoparticles by hydrazine reduction in ethylene glycol," *J. Colloid. Interface Sci.*, vol. 259, no. 2, pp. 282-286, 2003.

[9] F. Bidault, D.J.L. Brett, P.H. Middleton, N. Abson, N.P. Brandon, "A new application for nickel foam in alkaline fuel cells," *Int. J. of Hydrogen Energy*, vol. 34, no. 16, pp. 6799-6808, 2009.

[10] W. Zhang, Y. Li, X. Zeng, S. Peng, "Synergetic effect of metal nickel and graphene as a cocatalyst for enhanced photocatalytic hydrogen evolution via dye sensitization," Sci. Rep., vol. 5 pp.10589, 2015.

[11] C. Zhou, J.A. Szpunar, X. Cui, "Synthesis of Ni/Graphene Nanocomposite for Hydrogen Storage," *ACS Appl. Mater. Interfaces*., vol. 8, no. 24, pp. 15232-15241, 2016.

[12] G. Demazeau, "Review. Solvothermal Processes: Definition, Key Factors Governing the Involved Chemical Reactions and New Trends," *Z. Naturforsch B*, pp. 999, 2010.

[13] P. Cao, L. Wang, Y. Xu, Y. Fu, X. Ma, "Facile hydrothermal synthesis of mesoporous nickel oxide/reduced graphene oxide composites for high performance electrochemical supercapacitor," *Electrochim. Acta*., vol. 157, pp. 359-368, 2015.

[14] I.R.M. Kottegoda, N.H. Idris, L. Lu, J.-Z. Wang, H.-K. Liu, "Synthesis and characterization of graphene–nickel oxide nanostructures for fast charge–discharge application," *Electrochim. Acta*., vol. 56, no. 16, pp. 5815-5822, 2011.

[15] B. Li, H. Cao, J. Yin, Y.A. Wu, J.H. Warner, "Synthesis and separation of dyes via Ni@reduced graphene oxide nanostructures," *J. Mater. Chem*., vol. 22, no. 5, pp. 1876-1883, 2012.

[16] X. Feng, J. Zhou, L. Wang, Y. Li, Z. Huang, S. Chen, Y. Ma, L. Wang, X. Yan, "Synthesis of shape-controlled NiO-graphene nanocomposites with enhanced supercapacitive properties," *New J. Chem*, vol. 39, no. 5, pp. 4026-4034, 2015.

[17] X. Liu, W. Liu, M. Ko, M. Park, M.G. Kim, P. Oh, S. Chae, S. Park, A. Casimir, G. Wu and J. Cho, "Metal (Ni, Co)-Metal Oxides/Graphene Nanocomposites as Multifunctional Electrocatalysts," *Adv. Funct. Mater*., vol. 25, no. 36, pp. 5799-5808, 2015.

[18] M. Salimian, M. Ivanov, F.L. Deepak, D.Y. Petrovykh, I. Bdikin, M. Ferro, A. Kholkin, E. Titus and G. Goncalves, "Synthesis and characterization of reduced graphene oxide/spiky nickel nanocomposite for nanoelectronic applications," *J. Mater. Chem. C*., vol. 3, no. 43, pp. 11516-11523, 2015.

[19] Z. Ji, X. Shen, G. Zhu, H. Zhou and A. Yuan, "Reduced graphene oxide/nickel nanocomposites: facile synthesis, magnetic and catalytic properties," *J. Mater. Chem*., of Materials Chemistry, vol. 22, no. 8, pp. 3471-3477, 2012.

[20] S. Mandal and S.K. Saha, "Ni/graphene/Ni nanostructures for spintronic applications," *Nanoscale*., vol. 4, no. 3, pp. 986-990, 2012.

[21] J. Li, Q. Wu and J. Wu, "Synthesis of Nanoparticles via Solvothermal and Hydrothermal Methods, Springer International Publishing," Cham, Switzerland; Oak Ridge National Laboratory (ORNL), Oak Ridge, TN (United States) 2015.

[22] R. Deshmukh and M. Niederberger, "Mechanistic Aspects in the Formation, Growth and Surface Functionalization of Metal Oxide Nanoparticles in Organic Solvents," *Chem. Euro. J*., vol. 23, no. 36, pp. 8542-8570, 2017.

[23] C. Nethravathi, M. Rajamathi, "Chemically modified graphene sheets produced by the solvothermal reduction of colloidal dispersions of graphite oxide," *Carbon*, vol. 46, no. 14, pp. 1994-1998, 2008.

[24] Y. Tian, Y. Liu, F. Pang, F. Wang and X. Zhang, "Green synthesis of nanostructured Ni-reduced graphene oxide hybrids and their application for catalytic reduction of 4-nitrophenol," *Colloids and Surfaces A: Physicochem. Eng. Aspects*., vol. 464, pp. 96-103, 2015.

[25] N. Li, M. Cao and C. Hu, "A simple approach to spherical nickel-carbon monoliths as light-weight microwave absorbers," *J. Mater. Chem*., vol. 22, no. 35 pp. 18426-18432, 2012.

[26] B. Zhang, Y. Wang, X. Dai, D. Liu and X. He, "A nitrogen and sulfur co-doped graphene-supported nickel tetrapyridyloxyphthalocyanine hybrid fabricated by a solvothermal method and its application for the detection of bisphenol A," *RSC Adv*., vol. 5, no. 103, pp. 84457-84464, 2015.

[27] K. Cheng, N. Han, Y. Su, J. Zhang and J. Zhao, "Schottky barrier at graphene/metal oxide interfaces: insight from first-principles calculations," *Sci. Rep*., vol. 7, pp. 41771, 2017.

[28] G. Goncalves, P.A.A.P. Marques, C.M. Granadeiro, H.I.S. Nogueira, M.K. Singh and J. Grácio, "Surface Modification of Graphene Nanosheets with Gold Nanoparticles: The Role of Oxygen Moieties at Graphene Surface on Gold Nucleation and Growth," *Chem. Mater*., vol. 21, no. 20, pp. 4796-4802, 2009.

[29] N.I. Kovtyukhova, Y. Wang, A. Berkdemir, R. Cruz-Silva, M. Terrones, V.H. Crespi and T.E. Mallouk, "Non-oxidative intercalation and exfoliation of graphite by Brønsted acids," *Nat Chem*., vol. 6, no. 11, pp. 957-963, 2014.

[30] S. Kalinin and A. Gruverman, "Scanning Probe Microscopy: Electrical and Electromechanical Phenomena at the Nanoscale," vol. I, Springer, New York, 2006.

[31] W. Fan, Q. Lai, Q. Zhang and Y. Wang, "Nanocomposites of TiO_2 and Reduced Graphene Oxide as Efficient Photocatalysts for Hydrogen Evolution," *J. Phys. Chem. C*., vol. 115, no. 21, pp. 10694-10701, 2011.

[32] R.N. Muthu, S. Rajashabala and R. Kannan, "Facile synthesis and characterization of a reduced graphene oxide/halloysite nanotubes/hexagonal boron nitride (RGO/HNT/h-BN) hybrid nanocomposite and its potential application in hydrogen storage," *RSC Adv*., vol. 6, no. 82, pp. 79072-79084, 2016.

[33] J.W. Lee, T. Ahn, D. Soundararajan, J.M. Ko and J.-D. Kim, Non-aqueous approach to the preparation of reduced graphene oxide/ [small alpha]-Ni(OH)2 hybrid composites and their high capacitance behavior," *Chem. Commun*., vol. 47, no. 22, pp. 6305-6307, 2011.

[34] G. Gonçalves, M. Vila, I. Bdikin, A. de Andrés, N. Emami, R.A.S. Ferreira, L.D. Carlos, J. Grácio and P.A.A.P. Marques, "Breakdown into nanoscale of graphene oxide: Confined hot spot atomic reduction and fragmentation," *Sci. Rep*., vol. 4, pp. 6735, 2014.

[35] J. Wang, S. Liang, L. Ma, S. Ding, X. Yu, L. Zhou and Q. Wang, "One-pot synthesis of CdS-reduced graphene oxide 3D composites with enhanced photocatalytic properties," CrystEngComm., vol. 16, no. 3, pp. 399-405, 2014.

[36] P. Jeevanandam, Y. Koltypin and A. Gedanken, "Synthesis of Nanosized α-Nickel Hydroxide by a Sonochemical Method," *Nano Lett*., vol. 1, no. 5, pp. 263-266, 2001.

[37] S. Stankovich, D.A. Dikin, R.D. Piner, K.A. Kohlhaas, A. Kleinhammes, Y. Jia, Y. Wu, S.T. Nguyen and R.S. Ruoff, "Synthesis of graphene-based nanosheets via chemical reduction of exfoliated graphite oxide," *Carbon*, vol. 45, no. 7, pp. 1558-1565, 2007.

[38] Y. Zhu, C. Cao, S. Tao, W. Chu, Z. Wu and Y. Li, "Ultrathin Nickel Hydroxide and Oxide Nanosheets: Synthesis, Characterizations and Excellent Supercapacitor Performances," *Sci. Rep*., vol. 4, pp. 5787, 2014.

[39] A.C. Ferrari and D.M. Basko, "Raman spectroscopy as a versatile tool for studying the properties of graphene," *Nat. Nano*., vol. 8, no. 4, pp. 235-246, 2013.

[40] Y. Liu, R. Wang and X. Yan, "Synergistic Effect between Ultra-Small Nickel Hydroxide Nanoparticles and Reduced Graphene Oxide sheets for the Application in High-Performance Asymmetric Supercapacitor," *Sci. Rep*., vol. 5, pp. 11095, 2015.

[41] Y. Si and E.T. Samulski, "Exfoliated Graphene Separated by Platinum Nanoparticles," *Chem. Mater*., vol. 20, no. 21, pp. 6792-6797, 2008.

[42] Y. Chen, Z. Huang, H. Zhang, Y. Chen, Z. Cheng, Y. Zhong, Y. Ye and X. Lei, "Synthesis of the graphene/nickel oxide composite and its electrochemical performance for supercapacitors," *Int. J. Hydrogen Energy*., vol. 39, no. 28, pp. 16171-16178, 2014.

[43] J. Wang, D. Teschner, Y. Yao, X. Huang, M. Willinger, L. Shao and R. Schlogl, "Fabrication of nanoscale NiO/Ni heterostructures as electrocatalysts for efficient methanol oxidation," *J. Mater. Chem. A*., vol. 5, no. 20, pp. 9946-9951, 2017.

[44] N.A. Mohd Zaid and N.H. Idris, "Enhanced Capacitance of Hybrid Layered Graphene/Nickel Nanocomposite for Supercapacitors," *Sci.Rep*., vol. 6, pp. 32082, 2016.

[45] Y. Xia, Y. Xiong, B. Lim and S.E. Skrabalak, "Shape-Controlled Synthesis of Metal Nanocrystals: Simple Chemistry Meets Complex Physics?" *Angew. Chem. Int. Ed*., vol. 48, pp.60-103, 2009.

[46] D. Yoon, K.Y. Chung, W. Chang, S.M. Kim, M.J. Lee, Z. Lee and J. Kim, "Hydrogen-Enriched Reduced Graphene Oxide with Enhanced Electrochemical Performance in Lithium Ion Batteries," *Chem. Mater*., vol. 27, no. 1, pp. 266-275, 2015.

[47] J. Li, Z. Wang and F.L. Deepak, "In Situ Atomic-Scale Observation of Droplet Coalescence Driven Nucleation and Growth at Liquid/Solid Interfaces," *ACS Nano*, vol.11, no. 6, pp. 5590-5597, 2017.

[48] S.Y. Luchkin, K. Romanyuk, M. Ivanov and A.L. Kholkin, "Li transport in fresh and aged LiMn cathodes via electrochemical strain microscopy," *J. Appl. Phys*., vol.118, no. 7, pp. 072016, 2015.

[49] W. Park, J. Hu, L.A. Jauregui, X. Ruan and Y.P. Chen, "Electrical and thermal conductivities of reduced graphene oxide/Polystyrene composites," *Appl. Phys.Lett*., vol. 104, no. 11, pp. 113101, 2014.

A.2 Supplementary material of chapter 3

XRD pattern of Ni-GO sample that solvothermally synthesized under the condition of (200 °C, 24h) is shown in Figure A.2.1. The broadened band at around 23° is related to the rGO [1]. Three peaks at 44.7°, 52° and 76.5° corresponding to (111), (200) and (220) of Ni planes in fcc crystal structure [2] showed the formation of metallic Ni in solvothermal treatment at the temperature of 200 °C.

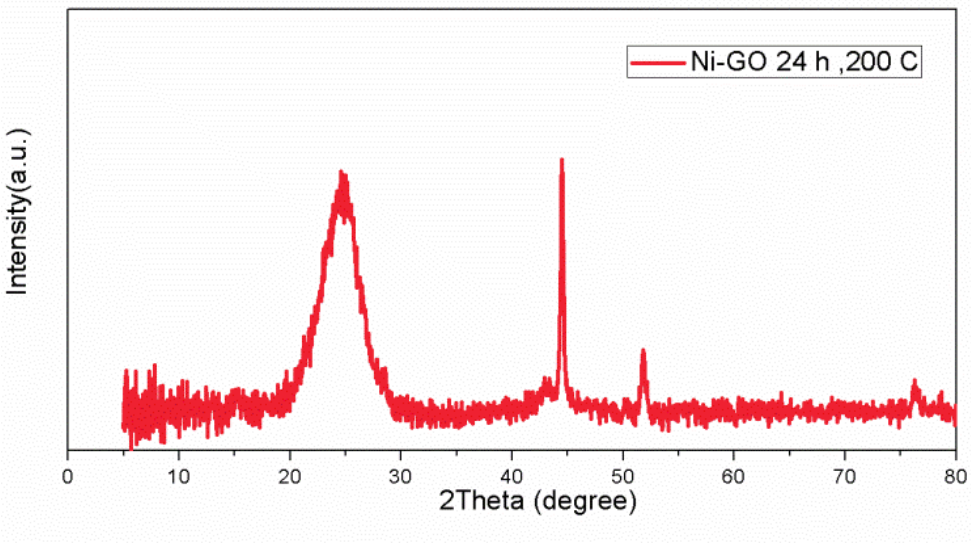

Figure A.2.1 XRD spectra of sample Ni-GO 24 synthesized by solvothermal method at 200 °C.

Different scales of SEM images (Figure A.2.2) of Ni-GO that prepared by solvothermal method at 200 ºC for 24h reaction time showing the presence of Ni particles with the size of around 1µm randomly distributed on the surface of rGO. Comparing this images with the SEM images (see Figure A.2.3) obtained from sample Ni/rGO24 which prepared in two steps solvothermal (150 ºC, 24h) and hydrogen reduction treatment (450 ºC, 2h) showed the successful two steps synthesis for decoration of rGO with nanosized Ni NPs.

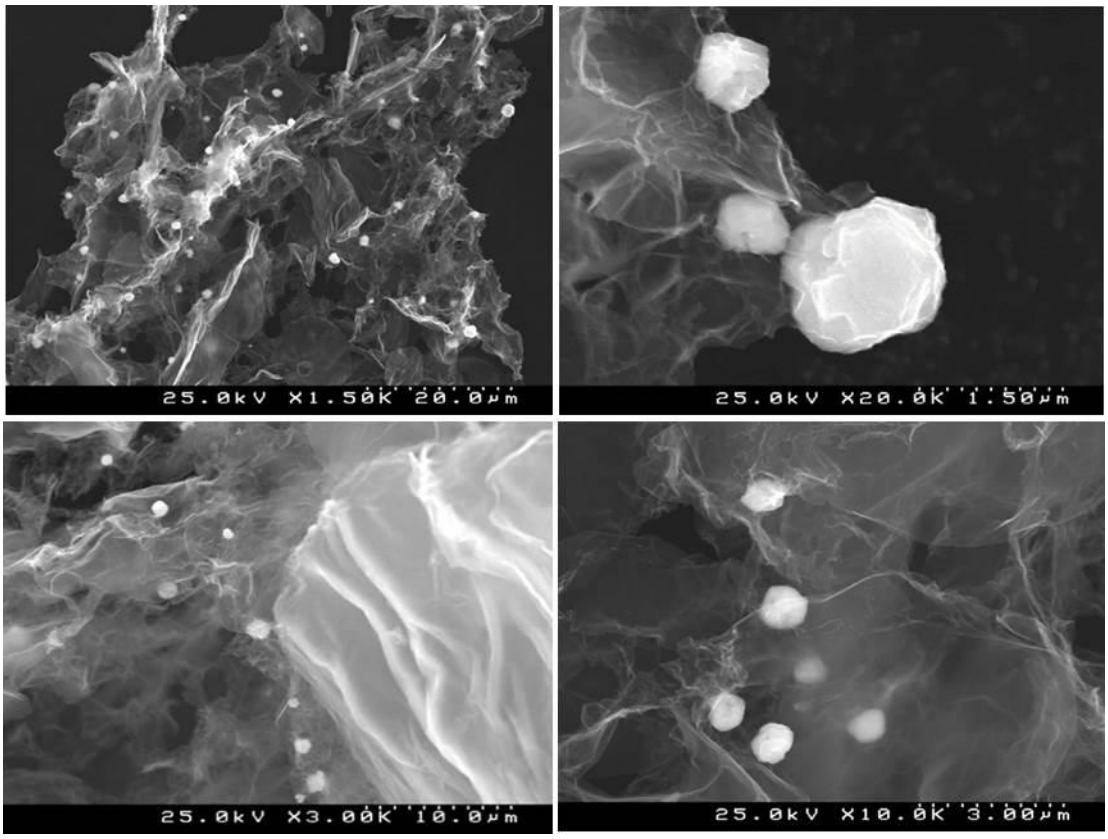

Figure A.2.2 SEM images of sample Ni-GO 24 prepared by solvothermal method at 200 °C, 24h).

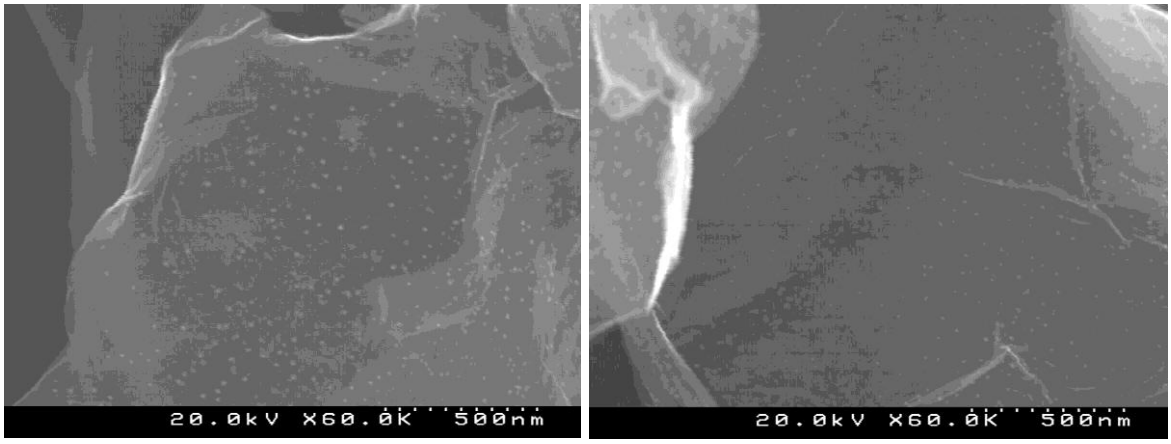

Figure A.2.3 SEM images of sample Ni/rGO24 prepared by two steps: solvothermal (150 ºC, 24h) and hydrogen reduction treatment (450 ºC, 2h).

[1] Park, Sungjin, Jinho An, Jeffrey R. Potts, Aruna Velamakanni, Shanthi Murali, and Rodney S. Ruoff. "Hydrazine-reduction of graphite-and graphene oxide," *Carbon*, vol. 49, no. 9, pp. 3019-3023, 2011.

[2] Zhu, Guo-Xing, Xian-Wen Wei, and Shan Jiang. "A facile route to carbon-coated nickel-based metal nanoparticles." *Journal of Materials Chemistry*, vol. 17, no. 22, pp. 2301-2306, 2007.

Chapter 4
Structural changes of Ni/rGO nanocomposites by thermal annealing

4.1 Scope

The Ni/rGO (3, 6 and 24) nanocomposites reported in chapter 3 were heat treated under reducing atmosphere of hydrogen (H_2) at 450 ºC. The aim of this treatment was to investigate the thermal stability or possible structural changes of these nanocomposites regarding their future potential application in the area of heterogeneous catalysis. The obtained results showed the good structural stability of Ni/rGO nanocomposites during 2 hours of thermal treatment with remaining of well dispersed of Ni NPs on rGO surface. An intense heating treatment on Ni/rGO24 nanocomposite under inert atmosphere of argon (Ar) at 900 ºC during 2 hours was performed in order to complete reduction of NiO shell to metallic Ni. This sample containing pure metallic Ni NPs was further treated under the same thermal annealing condition (in H_2 atmosphere and at 450 °C) and characterized. After intense thermal treatment in Ar, it was observed that the NPs were completely reduced to metallic Ni. However, during this treatment the NPs migrated at the rGO surface through the etching process and formed Ni aggregates leaving trenches behind on the rGO network. The further heat treated of this sample under H_2 at 450 °C promoted the formation of more trenches on rGO.

4.2 Introduction

Highly dispersed metal or metal oxide NPs on thermally stable supports can be used for heterogeneous catalytic reactions [1]. The two-dimensional graphene structure offers a high potential as a catalyst support for metal and metal oxide NPs [2] due to its high specific surface area, high thermal and electrical conductivity and low mass transfer phenomena. Catalytic reactions normally operate under medium temperature (from 100 ºC to 400 ºC) to high temperature (> 400 ºC) consequently the thermal stability of the deposited NPs is an important parameter that needs to be controlled [1]. During these catalytic reactions involving temperature, the increase of particles size via sintering can occurs, leading to reduce the surface area of particles and impairs their catalytic activity. So, the design of well dispersed NPs on substrate with anti-sintering properties is highly demanding [3]. In this regard, the stability of NPs on substrate under reaction temperature is an important factor that should be taken in to account for fabrication of catalyst materials.

On the other hand, new findings reveals that the existence of foreign atoms on graphene can manipulate the graphene structure [4]. It was indicated that the different metal atoms of Cu, Pt and Au can have different interactions with graphene structure. For Pt atoms, it was reported the ability to etch the graphene layer while in case of Cu atoms it was observed the ability of mending it. However, for Au atoms neither etching nor mending effects were reported on graphene structure.

Etching of graphitic structure by transition metal NPs through the catalytic hydrogenation of carbon has been reported as an interesting way for fabrication of nanopatterned graphene [5]. In this method, transition metals NPs like Ni or Fe are introduced on the graphene sheets. After thermal treatment at high temperatures of 700 ºC to 900 ºC under hydrogen atmosphere, these NPs cause the catalytic reaction between hydrogen and carbon producing methane gas. This process creates channels, pits and islands on graphene surface which can change the electronic properties of graphene [6]. Controlled cutting of graphene can creates nanoribbons with a desired size, shape and defined crystallographic edge showing different electronic properties that can be applicable in future electronic integrated devices [7] .For example, Wei L. Wang et al [8] applied benzenoid graph theory and first-principles calculations to

investigate the magnetic properties of arbitrarily shaped finite graphene flakes. It was shown that the spin of each flake is depending on its shape suggesting an avenue to nanoscale spintronic through the sculpting of graphene fragments.

The etching process occurs preferably on the smooth surface of carbon while the pitting process frequently happens on the defective surface. In fact, the prevalence of these processes can be dictated by NPs size. Usually, it was observed that the formation of pits occurs in the case of bigger NPs size, while the etching is a product of smaller ones[9]. S. Datta demonstrated the etching of few layer graphene on SiO_2/Si substrate by thermally activated Fe NPs [10]. Few layer graphene (FLG) with a proper amount of $Fe(NO_3)_3H_2O$ solution was spin coated on SiO_2/Si substrate, afterward transferred to furnace and heated at 900 °C under H_2/Ar flow during 45 minutes. At this temperature, Fe NPs (15nm) were formed and diffused along the SiO_2 and graphene surface and etched the few layer graphene on the substrate. It was explained that these etched trenches were oriented with the crystal lattice of graphene. The etching mechanism of few layers graphene is similar to the hydrogenation mechanism of bulk carbon which was reported before by A. Tomita [11]. In that work, the catalytic activities of transition metals (Fe, Co, Ni, Rh) in hydrogenation process of graphite was investigated. It was revealed the formation of channels, both with irregular shape or with preferred orientation in basal planes of graphite are made by the catalyst particles.

The size of NPs is an important factor to design the etch on the graphene surface. According to Lijie. Ci [12] the width of channels made by nanosized Ni (1nm - 40nm) under Ar/H_2 flow and at high temperature (750 ºC -1100 ºC) is comparable with the NP size. Moreover, the size of NPs dictate the edge structure of etches. It was observed that the narrower channel made by the smaller Ni NPs (< 10 nm) created a zigzag edge while the bigger ones (> 10 nm) creates the armchair edges. These different shapes determine the electronic properties of the final material. Nanoribbons with zigzag edge shows metallic behavior while with armchair edge, they are semi-conductive or semi-metallic [13]. Besides, etching of graphene by non-metallic NPs was also reported [14]. Libo et al. prepared few layer graphene (FLG) on Si/SiO_2 substrate and thermally treated under H_2 atmosphere at 850-1100 ºC. The formation of SiO_x NPs with various sizes, mostly less than 30 nm and several trenches

on FLG were observed. It was shown that the SiO_x NPs can tailor few FLG into regular pieces with smooth edges. The results suggested that the tailoring of graphene lattice occurs by the motion of SiO_x NPs along the graphene lattice and the tailored trenches exhibit high selectivity of the crystallographic orientation, similar to the behavior reported for metallic NPs. In addition, it was reported that under the same experimental conditions of heating and in the absence of SiO_x NPs no trenches were formed.

Catalytic etching of monolayer of graphene decorated with zinc oxide NPs which was thermal treated at 250 °C under Ar atmosphere has been also reported [6]. The authors repeated the thermal treatment for several times in order to investigate the evolution of etched channels on the graphene surface. It was explained that the etching process occurs by gasification of graphene through the solid-state reaction of ZnO + C => Zn + CO. XPS data showed the presence of both Zn and ZnO binding energies which revealed the involvement of NPs in graphene etching process. Moreover, Raman analysis showed the increase of defects after several heating treatments that confirmed the promotion of etched channel by repeating the heat treatment.

The concept of cutting graphitic materials using metallic NPs is not new. In 2006, Wang et al. introduced a new approach for cutting multi walled carbon nanotubes (MWCNT) based on the solid state reaction between NiO NPs and carbon [15]. To achieve this, the NiO NPs were deposited on MWCNT and then heated under Ar atmosphere at 900 ºC for 2h. It was shown that at this temperature NiO reduced to Ni by consumption of carbon from MWCNT (NiO + C => Ni + CO) and this caused the cutting of nanotubes to form smaller ones.

Here we investigated the structural changes of Ni and rGO in Ni/rGO nanocomposites by heat treatment under reducing and inert atmosphere (H_2 and Ar) and different temperatures (450 ºC and 900 ºC). The results suggest that the thermal treatment at 450 °C under reducing atmosphere doesn't promote significant structural changes in Ni/rGO nanocomposites. On the contrary, the thermal treatment at 900 °C under Ar atmosphere caused the complete elimination of oxide shell of Ni NPs in Ni/rGO nanocomposites, however anisotropic etching of the few layers of rGO sheets by Ni catalyst and formation of Ni aggregates were observed.

4.3 Experimental section

4.3.1 Thermal annealing treatment of Ni/rGO nanocomposites

The Ni/rGO3, Ni/rGO6 and Ni/rGO24 nanocomposites that their preparation and characterization were explained in previous chapter were now heat treated in a tube furnace at 450 °C with the heating rate of 5 °C/min under hydrogen flow of 8 mL/min during 2 h and labeled as Ni/rGO3-H_2, Ni/rGO6-H_2 and Ni/rGO24-H_2 respectively.

Sample Ni/rGO24 was heat treated in a tube furnace at 900 ºC with the heating rate of 5 ºC/min under Ar flow of 10 mL/min during 2h and was labeled as Ni/rGO24-Ar. This later sample was kept in the furnace and further heated in H_2 atmosphere at 450 °C under the same conditions referred before for this gas and labeled as Ni/rGO24-Ar-H_2. All the experimental conditions used are summarized in Table 4.1.

Table 4.1 Experimental conditions used for the thermal treatment of the nanocomposites Ni/rGO3, Ni/rGO6 and Ni/rGO24.

sample	Heat treatment conditions
Ni/rGO3-H_2	Ni/rGO3 annealed under H_2 at 450 ºC during 2 h
Ni/rGO6-H_2	Ni/rGO6 annealed under H_2 at 450 ºC during 2 h
Ni/rGO24-H_2	Ni/rGO24 annealed under H_2 at 450 ºC during 2 h
Ni/rGO24-Ar	Ni/rGO24 annealed under Ar at 900 ºC during 2 h
Ni/rGO24-Ar-H_2	Ni/rGO24 annealed firstly under Ar at 900 ºC during 2 h and then under H_2 at 450 ºC during 2 h

4.3.2 Characterization

Raman spectra were collected in a Thermo Scientific DXR smart Raman spectrometer with excitation wavelength of 532 nm with the maximum power of 10 mW. Transmission electron microscope (TEM) images were taken with FEI Tecnai G2 20 microscope. FTIR spectra were collected using KBr pellet technique with FTIR BRUKER TENSOR 27 with the resolution of 4 cm^{-1} in the range of 4000 cm^{-1} to 350 cm^{-1}. X-ray photoelectron spectroscopy (XPS) measurements were carried out on a PHI 5600 CI spectrometer (Physical Electronics) equipped with a hemispherical analyzer operated at pass energy of 29 eV. Monochromated Al K_α radiation (at 350 W) was used. Base pressure of the system was around 2 $x10^{-8}$ Pa. The Ar ions (Ar^+) of 3.5 keV with the rate of 0.05 nm/s was used. A transfer system (Physical Electronics) was used to guarantee transport from the glove-box in Ar atmosphere without exposing the samples to the ambient air.

4.4 Results and discussion

4.4.1 Structural study of samples Ni/rGO3-H_2, Ni/rGO6-H_2 and Ni/rGO24-H_2

The first studies were performed in order to access the effect of the thermal treatment under H_2 atmosphere on treated Ni/rGO3-H_2, Ni/rGO6-H_2 and Ni/rGO24-H_2 nanocomposites. FTIR and Raman spectra of the nanocomposites after annealing under (450 ºC, H_2, 2 h) are shown in Figure 4.1 (a) and (b) respectively. FTIR results showed the presence of a band at around 1570 cm^{-1} that can be related to the in plane skeletal vibration of hexagonal aromatic ring in graphene [16]. It was reported the presence of a band in the range of 1585-1565 cm^{-1} can be assigned to the reduction of GO. Moreover, the bands observed in the range of 1640-1620 cm^{-1} are generally attributed to the hydroxyl groups, however they can be overlapped with C=C vibration of aromatic carbon [17], [18]. The presence of C-O and C-O-C groups

indicate these oxygen functional groups are thermally stable at this heating condition and were not completely eliminated. Raman spectra showed the presence of the characteristic G and D bands of rGO. The calculated I_D/I_G were 0.94 ,0.98 and 0.96 for the nanocomposites Ni/rGO3-H_2, Ni/rGO6-H_2 and Ni/rGO24-H_2 respectively.

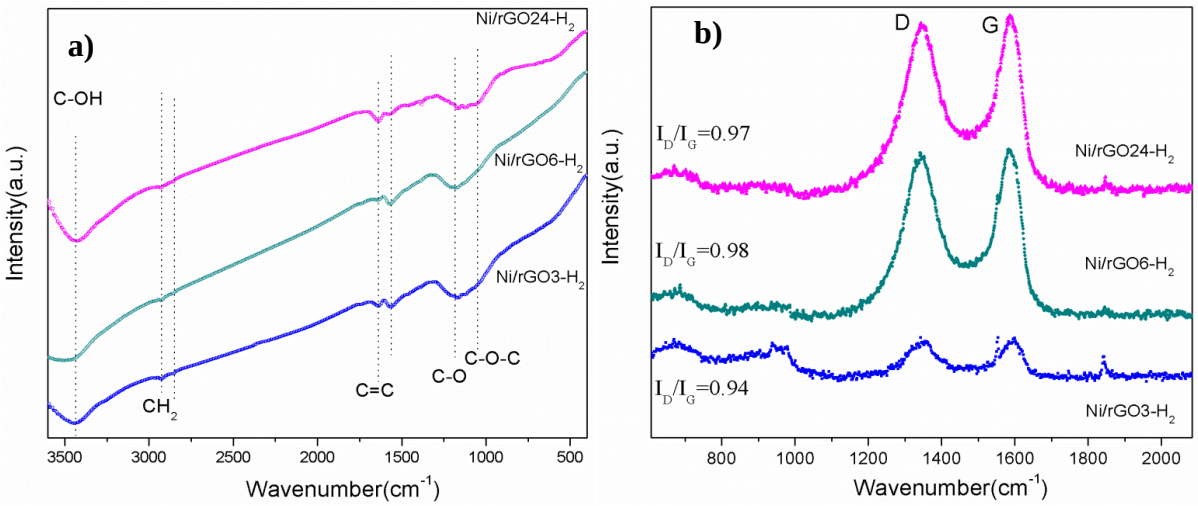

Figure 4.1 FTIR (a) and Raman (b) spectra of the three nanocomposites after annealing at 450 ºC in H_2 during 2h.

These I_D/I_G values are similar to the I_D/I_G obtained values before annealing reported in chapter 3, which can suggest that no significant structural changes on the rGO sheets occurred during annealing in H_2 atmosphere. The values of I_D/I_G reported for sample Ni/rGO6 and Ni/rGO24 in chapter 3 are 0.96 and 0.99 respectively.

XPS spectra of C1s and Ni2p3 for the different nanocomposites are shown in Figure 4.2 a) and b) respectively. The peak of C1s of rGO is similar for all samples, showing mainly a sharp peak at 284.5 eV corresponding to the C=C/C-C covalent bonds and the presence of small shoulder of C1s peak at higher binding energy (around 286.5) revealed the existence of some oxygen functional groups in all samples [16]. These results indicate that the annealing treatment at 450 °C under H_2 didn't promote further oxygen reduction, which is in consistent with our FTIR and Raman results. These results showed that after a second thermal treatment of rGO, a similar XPS profile to the first thermal treatment (chapter 3) was observed, that

suggest the thermal stability of rGO at 450 °C under H_2 atmosphere. Regarding Ni analysis, two peaks at 853 eV and 855.4 eV can be ascribed to Ni($2p_{3/2}$) of metallic Ni and Ni($2p_{3/2}$) of NiO respectively, which indicates that Ni is in both metallic and oxide phase in all samples that can be related to the Ni/NiO core-shell structure as was suggested in the previous chapter.

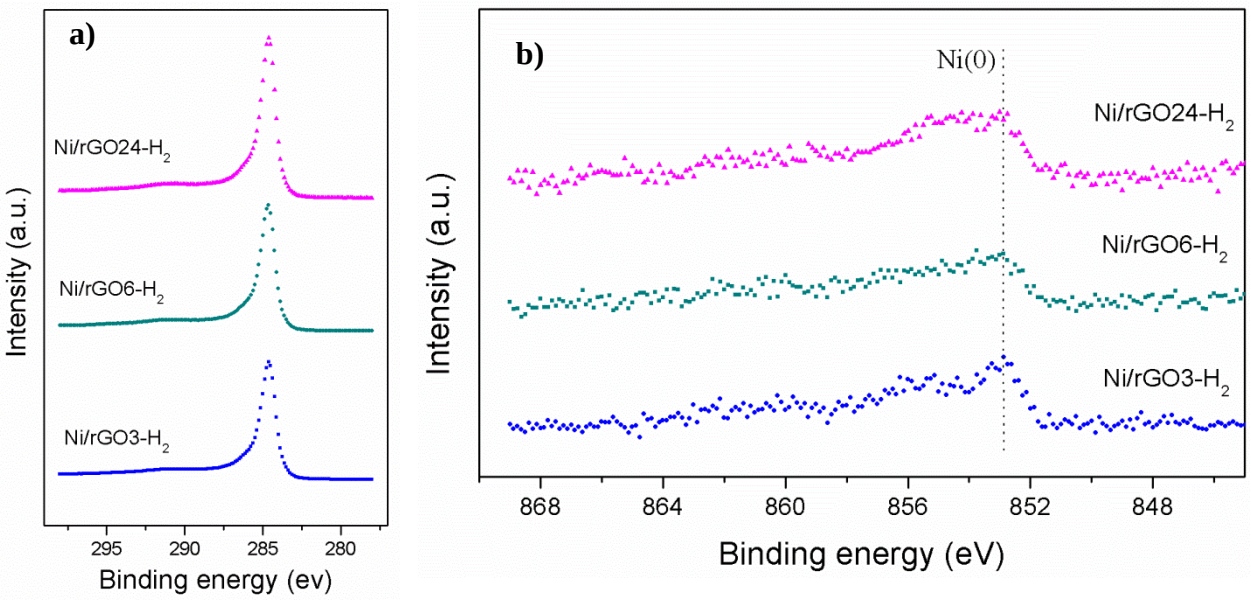

Figure 4.2 XPS C1s (a) and Ni2p3 (b) spectra of nanocomposites annealed under H_2 atmosphere at 450 º C for 2 hours.

The Table 4.2 represents the calculated relative atomic concentration of each element (C, O and Ni) in the different nanocomposites from the XPS data. The obtained C/O ratio for samples Ni/rGO3-H_2, Ni/rGO6-H_2 and Ni/rGO24-H_2 are 21.4, 22 and 23.5 respectively, which showed a comparable degree of oxygen reduction of rGO for all samples. In this case, the concentration of Ni in the samples is similar. This can be related with the superficial analysis nature made by XPS that cannot be compared with the previous Ni content results obtained from ICP analysis for the same samples discussed in chapter 3, which was a bulk analysis.

Table 4.2 Atomic concentration for C, N, O and Ni of the nanocomposites after annealing at 450 ºC in H_2 during 2h.

Samples	C1s (concentration at.%)	N1s (concentration at.%)	O1s (concentration at. %)	Ni2p3 (concentration at.%)	C/O ratio
Ni/rGO3-H_2	95.15	0.30	4.44	0.11	21.4
Ni/rGO6-H_2	95.45	0.12	4.33	0.10	22
Ni/rGO24-H_2	95.59	0.26	4.06	0.10	23.5

During the XPS analysis, Ar^+ sputtering was applied to the Ni/rGO6-H_2 and Ni/rGO24-H_2 samples surface to remove/diminish the shell of Ni NPs and analyze the depth profile. The XPS spectra of these samples after Ar^+ sputtering are shown in Figure 4.3. The obtained data showed the appearance of a sharp peak at around 853 eV for both samples which can be assigned to Ni2p3 of metallic Ni. Due to the high reactivity of Ni towards the oxygen, it is difficult to explain the origin of this oxide shell around Ni core, which can be formed during the synthesis and/or after, by the air exposure. To clarify this point, further XPS studies were performed on reference samples of Ni and NiO (commercially obtained). The XPS for Ni and NiO were collected before and after Ar^+ sputtering. In order to investigate re-oxidation of Ni, sputtered Ni sample was kept in the lab exposed to the air for 1.5 h and further analyzed by XPS (Figure 4.4).

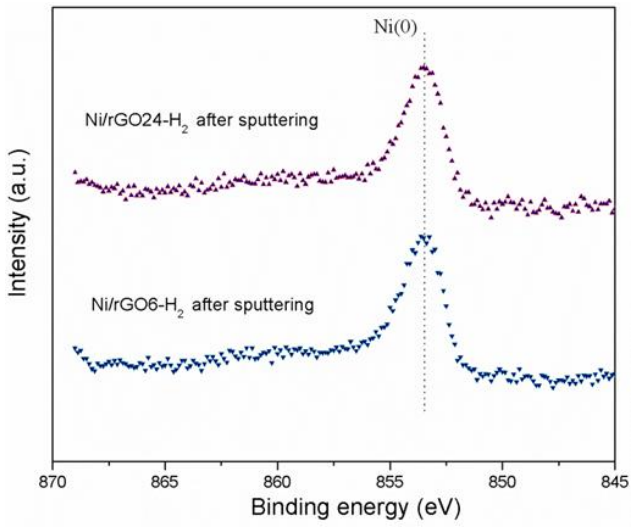

Figure 4.3 XPS spectra of Ni/rGO6-H_2 and Ni/rGO24-H_2 after Ar^+ sputtering

The spectrum of Ar^+ sputtered Ni after exposing to air showed the appearance of the NiO peak confirming the fast surface oxidation of Ni and is comparable with previous XPS results (Figure 3.4). Comparing the XPS spectra of samples Ni/rGO3-H_2, Ni/rGO6-H_2 and Ni/rGO24-H_2 before Ar^+ sputtering and after Ar^+ sputtering (Figure 4.3) with reference spectra suggested that the Ni NPs are composed of a metallic core and an outer oxidized shell.

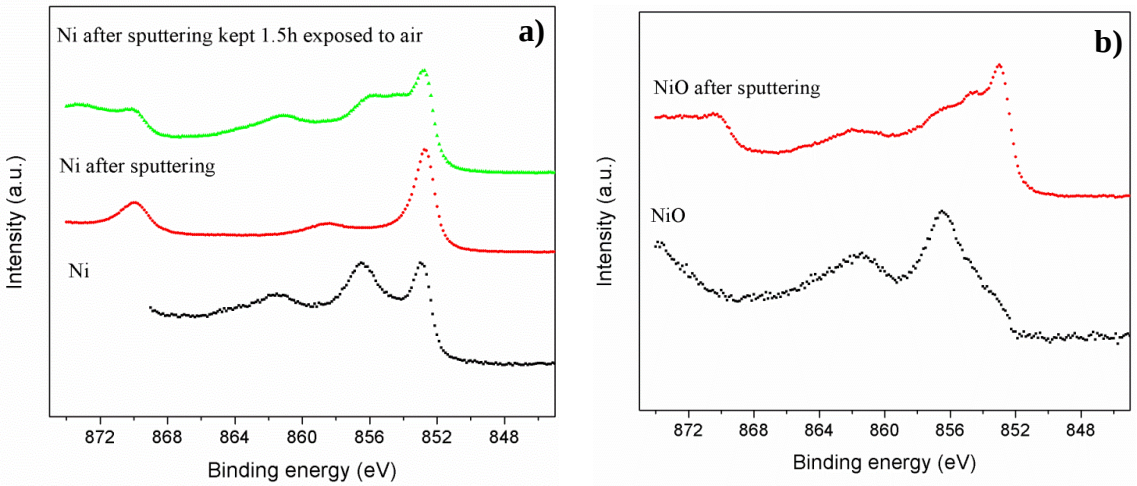

Figure 4.4 XPS reference spectra of (a) Ni before Ar^+ sputtering, after Ar^+ sputtering, and after the sputtered sample was exposing to the air (for 1.5 h), NiO (b) before and after Ar^+ sputtering

To observe the effect of thermal treatment on Ni NPs in Ni/rGO nanocomposites the TEM study was carried out for sample Ni/rGO6-H_2, (see Figure 4.5). It can be seen that Ni NPs were still well distributed on rGO surface and were not sintered during 2 h heating at 450 °C under H_2 atmosphere. These results suggested that this nanocomposite can be favorable to use in heterogeneous catalysis which needs to be operated up to 450 °C. However, the existence of few trenches on rGO can be observed indicating the rGO underwent some catalytic etching process. Catalytic etching of graphene with NPs was reported to be occurred under H_2, oxygen and water vapor environments. The etching mechanism suggested to be related with the presence of metal NPs attached to the defects of graphite and step edges. At high temperature, the oxidizing or reducing agents attached to the metal NPs react and form atomic H_2 or oxygen which are released and diffused to the surface of graphene and react with carbon atoms located at the edges and desorbed in the form of CO, CO_2 or CH_4. Metal NPs move on through the graphene surface and create the trenches [19]. As it can be seen in Figure 4.5 (red circles), the

etched channel width is comparable with the particles size. The low propagation of channels might be due to the small size of the NPs. It was reported that in hydrogenation of graphite by Ni particles the channel propagation rate increases by increasing the particle size [20].

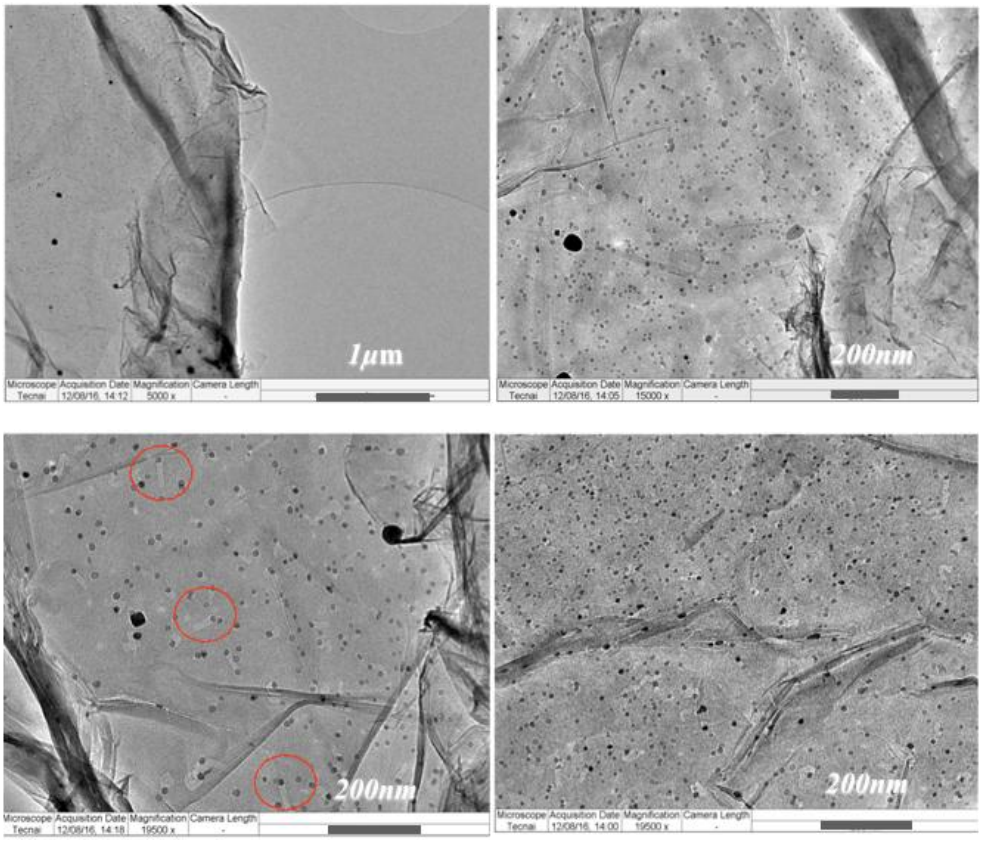

Figure 4. 5 TEM images of Ni/rGO6-H_2 indicating well dispersed Ni NPs and a few trenches made by catalytic etching of rGO. red circles show the dimension of trenches are comparable with the NPs size.

C. W. Keep [21] studied the catalyzed hydrogenation of graphite by Ni particles. In this study graphite was coated with Ni and heated under H_2 atmosphere. The nucleation of round shaped Ni particles in the size range of (10-25 nm) from Ni film occurred at the temperature between 825-925K.The size of the particles were increased by increasing the temperature and at around 975 K those particles that were in contact to edge or step edge started creating the channel along the basal plane. It was showed that the channel propagation rate is temperature dependent and was increased by increasing the temperature.

4.4.2 Morphology and structural study of samples Ni/rGO24-Ar and Ni/rGO24-Ar-H_2

TEM images of Ni/rGO24-Ar are shown in Figure 4.6. It can be seen that the intense thermal treatment at 900 °C caused the increase of Ni NPs size (Figure 4.6 a) most probably due to the migration of NPs (Figure 4.6 b) on the surface of rGO, coalescence and formation of large aggregates with the maximum final size of around 150 nm leaving many trenches at the rGO surface. Recently, the etching of graphene with Ni NPs was explained as "Pacman" mechanism by Qiu et al [22]. It was suggested that this mechanism is dependent on the close contact between graphene and Ni NPs and also their size. The occurrence of the anisotropic channels was explained as due to the specific active sites of the catalysts (Ni NPs). A catalyst with irregular shapes (see Figure 4.6 c and the magnified image in 4.6 d) contains more active sites and as a result, it doesn't continue the constant channel direction. The bigger particles are more complicated in shapes, having more facets and consequently more active sites, which results in an increase of the probability for the formation of bending channels on the rGO surface[11].

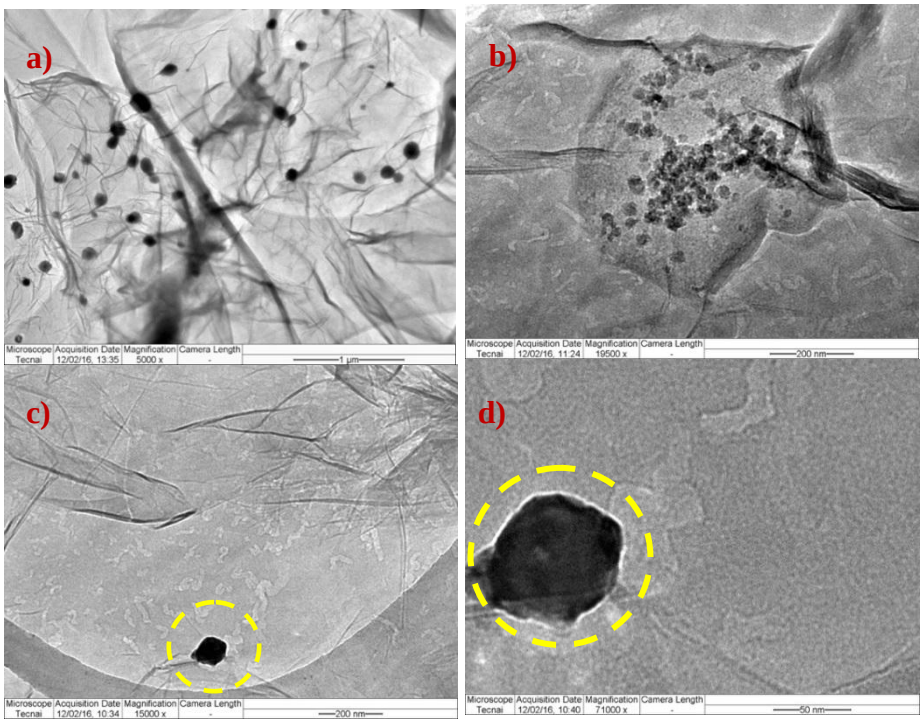

Figure 4.6 TEM images of a) distribution of Ni in Ni/rGO24-Ar b) migrated Ni NPs on rGO to form aggregates c) formation of trenches and bigger size of Ni by coalescence of Ni NPs, d) a single NP.

The mechanism of etching of rGO by Ni NPs under Ar atmosphere at 900 °C can be explained as the same mechanism reported by X. Wang [15], in which the reduction of NiO to Ni occurs by consumption of carbon atoms and creating the trenches on rGO surface. TEM images of sample Ni/rGO24-Ar-H_2 which was firstly treated in Ar and then in H_2 are shown in Figure 4.7. It can be seen that Ni NPs are randomly distributed on the highly-etched surface of rGO (see Figure 4.7 a and b). The existence of random trenches on rGO rather than crystallographic oriented etching might be due to the structure of rGO which contains several oxygen groups and defects. HRTEM image of Ni NPs interacted on rGO surface is shown in Figure 4.7 c.

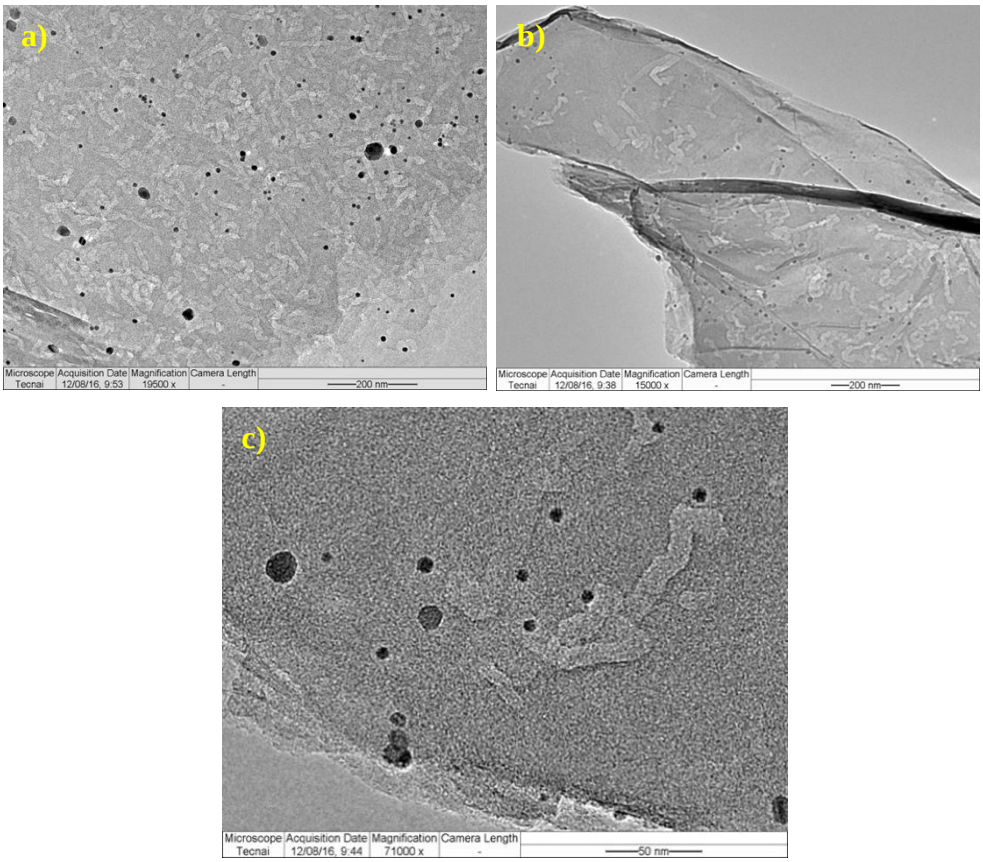

Figure 4.7 TEM images (a, b) of Ni/rGO24-Ar-H_2 showing randomly distributed of Ni and the accumulation of trenches on rGO c) HRTEM of etched rGO by Ni NPs.

In order to obtain further structural details of the etched samples, complementary FTIR, Raman and XPS measurement were performed.

Figure 4.8 (a) shows the FTIR spectra of samples Ni/rGO24-Ar and Ni/rGO24-Ar-H_2. It is possible to observe that the intensity of all bands related to the oxygen functional groups decreased significantly, when compared with FTIR of Ni/rGO24-H_2, (see Figure 4.1a) which was treated under H_2 at 450 °C revealing the higher extent of rGO reduction at higher temperature of 900 °C. The presence of the band at 1640 cm^{-1} which was attributed to C=C showed that after intense thermal annealing the aromatic structure of graphene was not destroyed. The Raman spectra in Figure 4.8 (b) showed a significant increase of the I_D/I_G ratio to 1.1 and 1.4 for Ni/rGO24-Ar and Ni/rGO24-Ar-H_2 respectively. The increase of I_D/I_G value after thermal annealing suggest the introduction of more defects which might arises through the etching process [6]. It was reported that the origin of D band of Raman spectrum in single layer graphene after etching process can be due to the presence of edges caused by etching process or due to the defects caused by high temperature treatment [7]. It is worth noting that the value of I_D/I_G is not representative of degree of oxidation or reduction since the increase of this value can be caused by varied factors such as edges, charge puddles and other defects [23]. The higher value of I_D/I_G for Ni/rGO24-Ar-H_2 might accompanied this idea that increasing the number of edges during annealing in Ar introduced more active carbons through the formation of edges resulting higher catalytic hydrogenation of rGO and formation of more trenches during H_2 annealing. It was reported that the carbon atoms located on the edges are more active than those on basal plane [10].

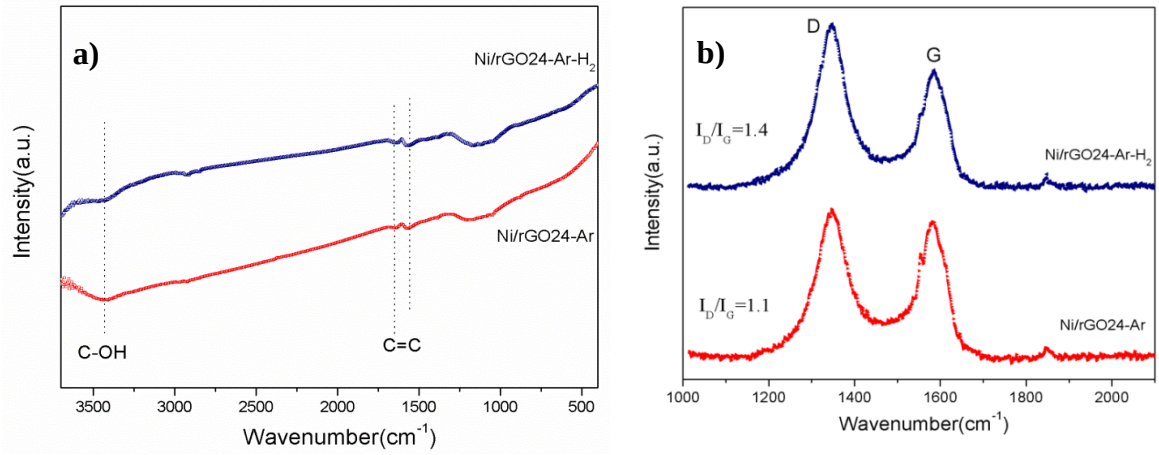

Figure 4.8 FTIR (a) and Raman (b) spectra of etched Ni/rGO24-Ar and Ni/rGO24-Ar-H_2 samples.

XPS spectra of C1s and Ni2p3 of Ni/rGO24-Ar and Ni/rGO24-Ar-H_2 are shown in Figure 4.9 (a) and (b), respectively. The appearance of a sharp peak for C1s at 284.4 eV showed the high reduction level of the rGO in the nanocomposites. In case of Ni it was observed the presence of two peaks at 853 eV and at 871 eV which can attribute to $Ni2p_{3/2}$ and $Ni2p_{1/2}$. This results confirm effective reduction to metallic Ni and complete elimination of NiO shell [24].

Table 4.3 showed the atomic percentage of C, O and Ni for Ni/rGO24-Ar and Ni/rGO24-Ar-H_2. The C/O ratio for Ni/rGO24-Ar and Ni/rGO24-Ar-H_2 are 63.7 and 44.8 respectively. This difference can be due to the higher consumption of carbon atoms for sample Ni/rGO24-Ar-H_2 than Ni/rGO24-Ar through the etching process and formation of more trenches which is in consistent with the Raman results.

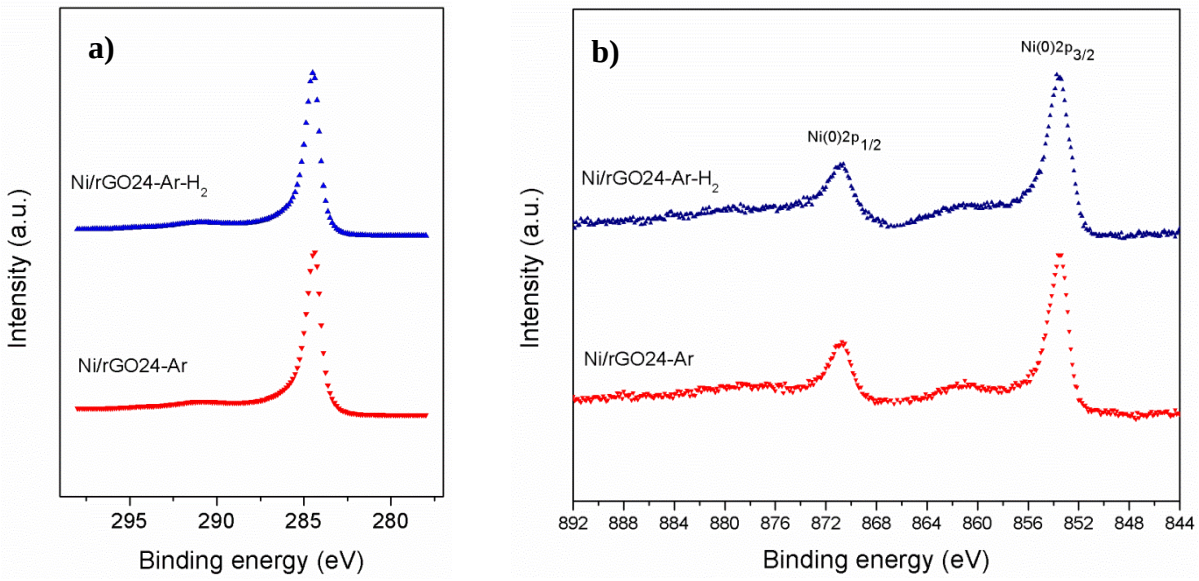

Figure 4.9 XPS C1s (a) and Ni2p3 (b) spectra of Ni/rGO24-Ar and Ni/rGO24-Ar-H_2 after heat treatment under Ar and H_2.

Table 4.3 Atomic concentration of samples Ni/rGO24-Ar and Ni/rGO24-Ar-H_2 after heat treatment at 900 ºC under Ar.

Samples	C1s (concentration at.%)	O1s (concentration at.%)	Ni2p3 (concentration at.%)	C/O ratio
Ni/rGO24-Ar	98.19	1.54	0.26	63.7
Ni/rGO24-Ar-H_2	97.62	2.18	0.21	44.8

4.5 Conclusion

In conclusion, we studied the stability of Ni/rGO nanocomposites under H_2 reducing atmosphere at 450 °C. Three samples, Ni/rGO3, Ni/rGO6, Ni/rGO24 prepared by solvothermal method were heat treated during 2 h and characterized. The FTIR and Raman results showed a good degree of stability for all samples. XPS analysis showed that the Ni NPs have core /shell structure of Ni and NiO respectively.

Sample Ni/rGO24 was heat treated at high temperature of 900 °C under Ar for 2 h for complete reduction of NiO shell of NPs and further heat treated under H_2 at 450 °C for 2 h. It was shown that thermal treatment under inert atmosphere of Ar at 900 °C is capable for complete elimination of NiO shell from the particles.

Under this condition, the migration and aggregation of Ni NPs and etching of rGO were observed. At this stage FTIR and Raman results showed the higher degree of reduction of the oxygen groups and appearance of more defects on rGO. XPS data revealed the complete reduction of NiO to metallic Ni. The further annealing in H_2 atmosphere caused the formation of more defects. This can be due to the formation of trenches which introduce more active carbon on edges and undergoes catalytic hydrogenation of carbon on rGO surface.

To bring the catalytic cutting of graphene to the application, it needs more studies and investigation in other to fully understand the mechanism behind this interesting phenomenon and also needs more efforts to find a way to precisely patterning the graphene in order to be applicable in electronic areas of application.

4.6 Bibliography

[1] I. Janowska *et al.*, "High temperature stability of platinum nanoparticles on few-layer graphene investigated by In Situ high resolution transmission electron microscopy," *Nano Res.*, vol. 4, no. 5, pp. 511–521, 2011.

[2] S. O. Moussa, L. S. Panchakarla, M. Q. Ho, and M. S. El-Shall, "Graphene-supported, iron-based nanoparticles for catalytic production of liquid hydrocarbons from synthesis gas: The role of the graphene support in comparison with carbon nanotubes," *ACS Catal.*, vol. 4, no. 2, pp. 535–545, 2014.

[3] S. Li and J. Gong, "Strategies for improving the performance and stability of Ni-based catalysts for reforming reactions," *Chem. Soc. Rev.*, vol. 43, no. 21, pp. 7245–7256, 2014.

[4] E. Kano, A. Hashimoto, and M. Takeguchi, "Opposite effects of Cu and Pt atoms on graphene edges," *Appl. Phys. Express*, vol. 10, no. 2, 2017.

[5] L. P. Biró, P. Nemes-Incze, and P. Lambin, "Graphene: nanoscale processing and recent applications," *Nanoscale*, vol. 4, no. 6, pp. 1824–1839, 2012.

[6] J. E. Jin *et al.*, "Catalytic etching of monolayer graphene at low temperature via carbon oxidation," *Phys. Chem. Chem. Phys.*, vol. 18, no. 1, pp. 101–109, 2016.

[7] L. C. Campos, V. R. Manfrinato, J. D. Sanchez-Yamagishi, J. Kong, and P. Jarillo-Herrero, "Anisotropic etching and nanoribbon formation in single-layer graphene," *Nano Lett.*, vol. 9, no. 7, pp. 2600–2604, 2009.

[8] W. L. Wang, S. Meng, and E. Kaxiras, "Graphene NanoFlakes with large spin," *Nano Lett.*, vol. 8, no. 1, pp. 244–245, 2008.

[9] E. O. Pentsak, E. G. Gordeev, and V. P. Ananikov, "Noninnocent nature of carbon support in metal/carbon catalysts: Etching/pitting vs nanotube growth under microwave irradiation," *ACS Catal.*, vol. 4, no. 11, pp. 3806–3814, 2014.

[10] S. S. Datta, D. R. Strachan, S. M. Khamis, and A. T. C. Johnson, "Crystallographic etching of few-layer graphene," *Nano Lett.*, vol. 8, no. 7, pp. 1912–1915, 2008.

[11] A. Tomita and Y. Tamai, "Optical microscopic study on the catalytic hydrogenation of graphite," *J. Phys. Chem.*, vol. 78, no. 22, pp. 2254–2258, 1974.

[12] L. Ci *et al.*, "Controlled nanocutting of graphene," *Nano Res.*, vol. 1, no. 2, pp. 116–122, 2008.

[13] A. L. Elias *et al.*, "Longitudinal cutting of pure and doped carbon nanotubes to form graphitic nanoribbons using metal clusters as nanoscalpels," *Nano Lett.*, vol. 10, no. 2,

pp. 366–372, 2010.

[14] G. Libo, W. Ren, B. Liu, Z. S. Wu, C. Jiang, and H. M. Cheng, “Crystallographic tailoring of graphene by nonmetal SiOx nanoparticles,” *J. Am. Chem. Soc.*, vol. 131, no. 39, pp. 13934–13936, 2009.

[15] X. X. Wang, J. N. Wang, L. F. Su, and J. J. Niu, “Cutting of multi-walled carbon nanotubes by solid-state reaction,” *J. Mater. Chem.*, vol. 16, no. 43, p. 4231, 2006.

[16] M. E. Uddin, N. H. Kim, T. Kuila, S. H. Lee, D. Hui, and J. H. Lee, “Preparation of reduced graphene oxide-NiFe2O4 nanocomposites for the electrocatalytic oxidation of hydrazine,” *Compos. Part B Eng.*, vol. 79, pp. 649–659, 2015.

[17] V. Ţucureanu, A. Matei, and A. M. Avram, “FTIR Spectroscopy for Carbon Family Study,” *Crit. Rev. Anal. Chem.*, vol. 46, no. 6, pp. 502–520, 2016.

[18] P. Dash, T. Dash, T. K. Rout, A. K. Sahu, S. K. Biswal, and B. K. Mishra, “Preparation of graphene oxide by dry planetary ball milling process from natural graphite,” *RSC Adv.*, vol. 6, no. 15, pp. 12657–12668, 2016.

[19] N. Tamura, T. Tomai, N. Oka, and I. Honma, “Capacity improvement of the carbon-based electrochemical capacitor by zigzag-edge introduced graphene,” *Appl. Surf. Sci.*, vol. 428, pp. 986–989, 2018.

[20] A. Tomita and Y. Tamai, “Optical microscopic study on the catalytic hydrogenation of graphite,” *J. Phys. Chem.*, vol. 78, no. 22, pp. 2254–2258, 1974.

[21] C. W. Keep, S. Terry, and M. Wells, “Studies of the nickel-catalyzed hydrogenation of graphite,” *J. Catal.*, vol. 66, no. 2, pp. 451–462, 1980.

[22] Z. Qiu, L. Song, J. Zhao, Z. Li, and J. Yang, “The Nanoparticle Size Effect in Graphene Cutting: A ‘Pac-Man’ Mechanism,” *Angew. Chemie Int. Ed.*, vol. 55, no. 34, pp. 9918–9921, 2016.

[23] W. Li, J. Liu, and C. Yan, “Reduced graphene oxide with tunable C/O ratio and its activity towards vanadium redox pairs for an all vanadium redox flow battery,” *Carbon N. Y.*, vol. 55, pp. 313–320, 2013.

[24] C. Liu *et al.*, “Nanostructure-induced colored TiO 2 array photoelectrodes with full solar spectrum harvesting,” *J. Mater. Chem. A*, vol. 5, no. 7, pp. 3145–3151, 2017.

Chapter 5
Conclusions and future work

5.1 Conclusion Outlines

In this thesis two different approaches for the synthesis of Ni NPs decorated rGO surface, Ni/rGO under different experimental conditions, hydrothermal and solvothermal, are documented. In each experimental approach, the control of various reaction parameters was found to be strongly essential on the final structure of the nanocomposites which in turn affects their properties. In this regard, several conclusions can be drawn from this thesis as listed below.

Regarding the hydrothermal method:

- Using the hydrothermal methodology, the size, morphology, crystalline structure and distribution of the Ni NPs on rGO surface can be controlled by the hydrazine hydrate (N_2H_4) concentration in the reaction solution. In this method, there is no need to use stabilizing agents or alkaline media which shows that this proposed method is a straightforward approach and easy to be implemented.
- The increase of N_2H_4 concentration leads to an increase of the size of the metallic Ni NPs on rGO surface. The Ni/rGO nanocomposite containing the well distributed metallic Ni NPs with the smallest particles' size of 145 nm was obtained using 0.17 mol/L N_2H_4. Ni/rGO nanocomposite with spiky Ni NPs (300 nm) with Ni/NiO core-shell structure was obtained using 0.83 mol/L N_2H_4 in reaction solution. The growth of nanothorns in this structure was controlled by the reaction time. Increasing the reaction time leads to increase the size of these nanothorns.
- The current-voltage (I-V) characteristic of spiky Ni/rGO nanocomposite showed nonlinear and highly reproducible current hysteresis behavior indicating a large resistive switching which can be described as the switchable diode effect. It was shown that the outer shell of NiO around the Ni NPs is acting as a buffer layer which should be taken in to account for equilibrium energy band diagram. I-V characteristic of rGO showed nonlinearity similar to Schottky effect without any hysteresis behavior which suggested the Ni NPs are mainly responsible for switchable diode effect of this nanocomposite.

Regarding the solvothermal method:

- This method allows obtaining smaller Ni NPs at rGO surface, typically less than 10 nm. The optimized reaction parameters allow to control the size and size distribution of Ni NPs in Ni/rGO nanocomposites as well as the degree of GO reduction by only controlling the reaction time. The increase of the reaction time leads to an increase of the size of Ni NPs and concomitantly to the decrease of the density of NPs on rGO surface. A heat treatment under H_2 atmosphere at 450 ºC was crucial for formation of metallic Ni NPs after the solvothermal reaction.
- I-V characteristics of solvothermally synthesized Ni/rGO nanocomposites showed switchable diode effect for the samples were obtained during 3, 6 and 24 h reaction time. This behavior was due to the interaction of Ni/NiO core-shell structure in rGO matrix and cantilever's tip as electrodes. I-V characteristic of Ni/rGO nanocomposite that was obtained during 1 h reaction time showed the ohmic behavior. For this sample, the current saturation was achieved at ± 3V (50nm). These results confirmed that electrophysical properties are dependent to the structure of Ni/rGO nanocomposites.
- Higher temperature heating treatment of Ni/rGO under Ar atmosphere (900 ºC) caused the migration of Ni NPs on rGO and formation of anisotropic trenches through the etching of rGO nanostructure.

5.2 Future work

At this moment, the chemical mechanism that can describe the formation of the highly monodisperse Ni NPs at the surface of GO by solvothermal method is not yet fully understood. Several characterization techniques are now being considered in order to obtain valuable information for clarification of the structural changes observed over the different reaction time. In fact, the strategy consists on the establishment of a correlation between the Ni morphology/contents with the degree of reduction of GO during the different phases of the

synthesis. However, the very promising electronic properties already observed for the current obtained Ni/rGO nanocomposites synthesized by the hydrothermal and solvothermal methods, allows that these materials can now be explored for several applications. Currently, the potential application of Ni/rGO nanocomposite is under investigation for the assembly with biomolecules for the development of new nanobiomaterials for harvesting energy. Study the effect of integration of rGO/spiky Ni NPs in to the self-assembled diphenylalanine (FF) peptide microtubes' structure is ongoing work which has been conducted at the Physics department, University of Aveiro. This work is motivated by the recent results of professor Kholkin's group [M. Ivanov *et al.*, "High Resolution piezoresponse Force Microscopy Study of Self-Assembled Peptide Nanotubes," *MRS Adv.*, vol. 2, no. 2, pp. 63–69, 2017]. According to their obtained results the introduction of rGO to peptide microtubes, significantly modifying the piezoelectric properties with the appearance of radial (vertical) piezoresponse that was confirmed via PFM analysis.

Moreover, nanosized Ni/rGO nanocomposite can be a favorable candidate for enhancement of hydrogen adsorption through the spillover mechanism in solid state hydrogen storage application. Spillover is a transport of active species generated on one substance (activator) to another (receptor) that would not normally adsorb it. Yang et al [L. Wang and R. T. Yang, "New sorbents for hydrogen storage by hydrogen spillover - a review," *Energy Environ. Sci.*, vol. 1, no. 2, pp. 268–279, Jul. 2008.] showed that metal support interaction is the key for the spillover. He proposed the Bridge-building technique (making contact between metal, support and receptor by carbon precursor such as glucose) for enhancement of hydrogen adsorption capacity on the receptor. Our work suggests that by well integration of Ni/rGO nanocomposite to the hydrogen adsorbent materials (receptor) rGO can act as a bridge-building material between activator and receptor as well as the support for metal particles.